The University Of Sheffield.

Developing Raman sorting and imaging techniques to characterise and differentiate unculturable microbial single cells

M. Li

A thesis submitted to The University of Sheffield for the degree of

Doctor of Philosophy

2012

Developing Raman sorting and imaging techniques to characterise and differentiate unculturable microbial single cells

Mengqiu Li

Department of Civil and Structural Engineering

A thesis submitted to The University of Sheffield for the degree of

Doctor of Philosophy

November 2012

Declaration

The author declares that this thesis is his own work and that other sources of information have been clearly cited and acknowledged.

Signature:

Date:

Abstract

Unculturable microorganisms are a major challenge facing researchers in environmental microbiology, and Raman spectroscopy has emerged as a novel technique in this field as it is able to analyse single microbial cells without cultivation. It has been combined with stable isotope probing (SIP) to identify the ecological functions of unculturable microorganisms. However, Raman signal from microorganisms is usually weak and taking single-cell Raman spectra is timing consuming. The interpretation of microorganisms' Raman spectra is also difficult due to their complexity.

This thesis aims to improve Raman spectroscopic techniques for environmental microbiology research. Resonance Raman (RR) spectroscopy and surface enhanced Raman scattering (SERS) were employed to enhance single-cell Raman spectra. RR spectroscopy was combined with SIP to rapidly image natural photosynthetic microorganisms and reveal their CO_2 fixation activities at single-cell level. Single photosynthetic microorganisms with only 10 % difference in their ^{13}C content can be rapidly differentiated using RR spectroscopy in a non-destructive manner. Two potentially suitable methods to synthesise SERS-active nanoparticles for labelling the surface of microorganisms were investigated. These two methods both labelled single microorganisms to a satisfactory level as shown by electron microscopy images, but more work is needed to study the resultant SERS spectra. A novel quantitative spectral marker, the thymine Raman band, was identified during the investigation of using Raman spectroscopy to track

carbon flow in a model food chain. This new spectral marker shows intriguingly different isotopic shift behaviour from the well documented phenylalanine Raman band. This difference was studied and brought to light a previously omitted aspect of Raman spectroscopy: the isotopic shift of Raman bands may reveal the biochemical pathways. With enhanced Raman signal, high-throughput Raman activated cell sorting (RACS) became possible and this thesis proves the concept that the combination of RR spectroscopy and microfluidic devices can rapidly profile photosynthetic microbial communities and potentially sort cells based on their *in situ* activities. This thesis also extended the Raman-SIP method to nitrogen and found that single-cell Raman spectra can quantify ^{15}N-uptake in single bacterium using multivariate analysis.

The studies included in this thesis revolve around the application of Raman spectroscopy in environmental microbiology. They strengthened and expanded the existing Raman-SIP method and opened the door to the development of important new techniques such as high-throughput RACS systems.

List of publication

Papers

1) Li M., Xu J., Romero-Gonzalez M., Banwart S.A. and Huang W.E. (2012). Single cell Raman spectroscopy for cell sorting and imaging. *Current Opinion in Biotechnology* (impact factor=8.5) 23 (1): 56-63.

2) Li M., Canniffe D.P., Jackson P.J., Davison P.A., FitzGerald S., Dickman M.J., Burgess J.G., Hunter C.N. and Huang W.E. (2012). Rapid Resonance Raman micro-spectroscopy to probe carbon dioxide fixation by single cells in microbial communities. *ISME Journal* (impact factor=6.2) 6: 875-885.

3) Li M., Huang W.E., Gibson C.M., Fowler P.W. and Jousset A. (2012). Monitoring carbon flow in a food chain model and revealing metabolic pathways using stable isotope probing and Raman spectroscopy. Submitted to *Analytical Chemistry*

4) Li M., Ashok P.C., Dholakia K. and Huang W.E. (2011). Raman activated cell counting for profiling carbon dioxide fixing microorganisms. *Journal of Physical Chemistry A* (impact factor=2.7) in press, DOI: 10.1021/jp212619n.

5) Li M., Boardman D.G. and Huang W.E. (2011). Single-cell Raman sorting. *Methods in Molecular Biology* (book chapter) in press.

6) Huang W.E., Li M., Jarvis R.M., Goodacre R. and Banwart S.A. (2010). Shining light on the microbial world: the application of Raman

microspectroscopy. *Advances in Applied Microbiology* (impact factor=3.9) 70: 153-186.

Presentations and posters

1) Rapid resonance Raman micro-spectroscopy to probe carbon dioxide fixation in microbial single cells

Oral presentation given in the 14th European Conference on the Spectroscopy of Biological Molecules, Coimbra, Portugal (September 2011)

2) Single-cell Raman Spectroscopy

Oral presentation given in the Kroto-Krebs symposium, Sheffield, UK (November 2010)

Table of contents

List of figures

List of tables

Glossary

AFM: atomic force microscopy/microscope

Ca-DPA: Ca-dipicolinic acid

CARS: Coherent anti-Stokes Raman scattering/spectroscopy

CCD: charge-coupled device

CHO cell: Chinese hamster ovary cell

CLS: classical least squares

CVA: canonical variate analysis

Da: Dalton, the unified atomic mass unit

dATP: deoxyadenosine triphosphate

dCTP: deoxycytidine triphosphate

dGTP: deoxyguanosine triphosphate

DNA: deoxyribonucleic acid

dNTP: deoxyribonucleotide

dTMP: deoxythymidylate

dTTP: deoxythymidine triphosphate

dUMP: deoxyuridylate

E4P: erythrose 4-phosphate

EDX: energy-dispersive X-ray spectroscopy

FACS: fluorescence activated cell sorting

FISH: fluorescence in situ hybridization

FWHM: full width at half maximum

G6P: glucose 6-phosphate

HIV: human immunodeficiency virus

HPLC: high-performance liquid chromatography

laser: light amplification by stimulated emission of radiation

LB: lysogeny broth

LH: light-harvesting

LSPR: localised surface plasmon resonance

MA: methylated amines

MM: minimal medium

MMA: minimal medium-agar

MS: mass spectrometry

NA: numerical aperture

NMR: nuclear magnetic resonance

NP: nanoparticle

PCA: principal component analysis

PC-CVA: principal component-canonical variate analysis

PCR: polymerase chain reaction

PDMS: polydimethylsiloxane

PEP: phosphoenolpyruvate

PLSR: partial least squares regression

RACS: Raman activated cell sorting

RCF: relative centrifugal force

RNA: ribonucleic acid

ROI: region of interest

RPM: revolutions per minute

RR: resonance Raman

rRNA: ribosomal RNA

SCRR: single-cell resonance Raman

SCRS: single-cell Raman spectra/spectrum/spectroscopy

SEHRS: surface enhanced hyper Raman scattering/spectroscopy

SEM: scanning electron microscopy/microscope

SERRS: surface enhanced resonance Raman scattering/spectroscopy

SERS: surface enhanced Raman scattering/spectroscopy

SIMS: secondary ion mass spectrometry

SIP: stable isotope probing

SRS: stimulated Raman scattering/spectroscopy

TEM: transmission electron microscopy/microscope

TERS: tip enhanced Raman scattering/spectroscopy

TMM: trimethylamine monooxygenase

UHQ: ultrahigh quality

UV: ultraviolet

v/v: volume/volume

Chapter 1: Introduction

1.1 Background

Unculturable microorganisms, which account for about 99 % of organisms in microbial communities, have been an unsolved issue in environmental microbiology for decades [1-8]. These previously overlooked organisms also play vital roles in some human infection and diseases [9, 10]. The strong need for research tools that circumvent traditional cultivation steps led to the development of top-down methods such as metagenomics and bottom-up methods such as single-cell techniques. Raman spectroscopy, an important technique in bottom-up methods, has been used to analyse the identity, physiological status, phenotype and ecological function of single microbial cells (see below). This thesis focuses on the application Raman spectroscopy to characterise, image and potentially sort unculturable microbial single cells. These are the main areas where Raman spectroscopy may contribute to unculturable microorganism research, but there are still difficulties in the implementation. Novel techniques and results from this thesis may help resolve these difficulties and provide researchers powerful tools to study and understand unculturable microorganisms cell by cell. They may also serve as the stepping stones for a new generation of techniques to come.

1.1.1 Unculturable microorganisms and single-cell research

Microbiological techniques based on the growth of microorganisms and bulk measurement of them provided scientists intriguing insights into the invisible microbial world. The knowledge of microorganisms also led to the development of many vital medicines and helped boost the modern biotechnology industry. However, our entire collection of isolated microbial species is just a tip of the iceberg. There is increasing evidence showing that less than 1% of microorganisms in natural and contaminated environments will grow in commonly used laboratory growth media [1-8]. A number of factors can contribute to the microorganisms' inability to grow and divide in growth media, which include unsuitable concentration of compounds in the media, some species' need for co-metabolism, disturbance to the signalling molecules and persister cells [11, 12]. There have been some studies to grow previously unculturable microorganisms with modified media and techniques [11], therefore 'as-yet-cultivated microorganisms' may be a more precise term for these microorganisms.

Considering the extremely large number of microbial species and the difficulty in finding a growth technique for any of them, in order to gain an unbiased and global view of microbial communities, it is more appropriate and efficient to employ culture-independent methods to study environmental microorganisms.

Some techniques derived from molecular biology are commonly used to study the microbial world without growing microorganisms. The existence

of the uncultured majority of microorganisms was, in fact, confirmed by the sequencing results of extracted microbial community DNA. The analysis of the collective genome sequence, i.e. metagenomics, is a good method to study unculturable microorganisms. Sequencing and analysing the combined genomes of a microbial community was made possible by the development of high-throughput DNA sequencing techniques [13]. Metagenomics has been used successfully in many different types of microbial communities to analyse different parts of genomes, such as the 16S rRNA genes and functional genes; and it revealed the existence of previously unknown microbial species and genes, such as antibiotics resistance genes and pollutants degradation genes [14, 15]. Some novel biosynthetic products were discovered using metagenomics [16, 17]. One should note that DNA sequences, once 'cut' into short segments, may not be easily restored again, for example, a sequence cut into single base pairs cannot be restored due to the complete loss of information. A metagenome can be sequenced in segments and 'stitched' back into a statistically favoured result, with a level of uncertainty. Therefore, there are still some major challenges facing metagenomics techniques [13, 17, 18]: 1) the difficulty in reconstructing complete genomes from metagenome sequences due to the uncertainties; 2) despite its name, many metagenomics studies randomly sequence a small fraction of the whole metagenome, sequencing and analysing every DNA fragment of the whole community are still very difficult; 3) assembling short reads into longer 'contigs' is not error-proof because there may be more than one solution to assemble the segments

which may lead to errors during the reconstruction of the original community; 4) linking the ecological function to a species is still difficult because fractions of potential functional genes may be found in a metagenome but which taxonomic group they belong to may not be easily identifiable. 'Targeted metagenomics' have been employed by researchers to selectively reduce the size of DNA pool and produce more 'concise' sequencing results [19]. There are a number of ways to reduce the size of DNA pool; and using stable isotope probing (SIP) method before sequencing is one of the efficient routes leading to the targeted results that researchers are interested in [19]. Clearly, in these 'targeted metagenomics' methods, there is a need for sample selection and sample size reduction. Raman spectroscopy and the still-developing (Raman activated cell sorting) RACS system can analyse and sort single microbial cells, are therefore suitable for this purpose.

However, Raman spectroscopy offers much more than just a preliminary screening tool for metagenomics or other molecular biology techniques. Single-cell Raman spectroscopy is now widely accessible to researchers thanks to commercially available confocal Raman microscopes. Raman spectra can serve as the signature or indicator of a single cell's species, phenotypic features, physiological status, biochemical pathways (as shown in Chapter 5) and even as a quantitative marker for CO_2 fixation [20-22]. Single-cell whole-genome amplification kits are commercially available. Therefore, a Raman activated cell sorting (RACS) system that characterises and isolates single cells may resolve many problems facing metagenomics

as described above. Since genetic materials of single cells are not mixed in a RACS system, ecological functions and functional genes can be linked to single cells' taxonomic identities, providing a more definite and in-depth understanding of microbial communities. Raman spectroscopy is a unique bottom-up method targeting single cells who play 'central roles' in all ecosystems [11]. It combined several key features together: single-cell level resolution, non-destructive measurement and the ease of use.

1.1.2 Raman spectroscopy, Raman red-shift, resonance Raman spectroscopy and surface enhanced Raman scattering

Vibrational spectroscopy provides information on the chemical composition and molecular structure of a sample. Many vibrational spectroscopic techniques are non-invasive and capable of imaging live cells [23]. They are widely used in life science [20, 24, 25]. Commonly used vibrational spectroscopic techniques can be usually categorised into two groups: infrared spectroscopy and Raman spectroscopy. Infrared spectroscopy measures the absorption of a broad-band infrared light by the sample; whilst Raman spectroscopy measures the inelastically scattered laser light by the sample.

Physicist Chandrasekhara Venkata Raman was one of the scientists who experimentally proved the existence of the predicted inelastic scattering of photons. This effect was hence named after Raman and he was awarded a Nobel Prize in Physics in 1930. Raman spectroscopy became a standard

technique for analysing molecular structure and chemical composition decades later thanks to the development of laser.

Comparing with infrared spectroscopy, Raman spectroscopy is superior in the following aspects: 1) Raman spectra usually contain sharper and more distinguishable bands enabling easier identification of chemical compounds in cells; 2) Raman spectroscopy can use probing lasers in the visible range where water absorption is weak, therefore can tolerate relatively large water content that usually presents in biological samples; 3) widely available confocal Raman microscopes have a spatial resolution on the micrometer level, which enables easy and rapid hyperspectral imaging of single microbial cells; 4) Raman spectroscopy can be combined with many other techniques, such as fluorescent *in situ* hybridisation (FISH), optical tweezers, atomic force microscope (AFM) and microfluidic devices to become powerful research tools [22, 26-28].

Raman spectra arise from the quantum nature of the molecular vibration. A simple example is the one-dimensional stretching motion of a diatomic molecule following Hooke's law. The Hamiltonian operator for this system is [29]:

$$H = -\frac{\hbar^2}{2m_{eff}}\frac{d^2}{dx^2} + \frac{kx^2}{2} \qquad \text{Equation 1}$$

Where,

$$\hbar = reduced\ Planck's\ constant$$

$$m_{eff} = \frac{m_1 m_2}{m_1 + m_2}$$

$$m_1, m_2 = the\ mass\ of\ two\ atoms\ of\ this\ molecule, respectively$$

$$x = the\ displacement\ of\ atoms$$

$$k = force\ constant\ in\ Hooke's\ law$$

It takes the same form of the Hamiltonian operator for a single-particle harmonic oscillator, and m_{eff} is the effective mass of the two atoms.

And we substitute it into the time-independent Schrödinger equation:

$$H\psi = E\psi \qquad \text{Equation 2}$$

And the wavefunction is known to take the form [29]:

$$\psi_v(y) = N_v H_v(y) e^{-y^2/2} \qquad \text{Equation 3}$$

Where,

$$y = \frac{x}{\alpha}$$

$$\alpha = \left(\frac{\hbar^2}{m_{eff} k}\right)^{1/4}$$

$N_\nu = Normalisation\ constant\ at\ \nu$

$\nu = 0, 1, 2, 3, \ldots$

$H_\nu(y) = Hermite\ polynominal\ at\ \nu$

If we substitute the wavefunction (Equation 3) and Hermite's differentiation equation into Equation 2, it is revealed that the energy constant *E* is quantized into 'energy levels':

$$E_\nu = \left(\nu + \frac{1}{2}\right)\hbar\left(\frac{k}{m_{eff}}\right)^{1/2} \qquad \text{Equation 4}$$

Where,

$\nu = 0, 1, 2, 3, \ldots$

The lowest permitted energy level where $\nu = 0$ is called the ground state. Here we express the energy gap between any two energy levels by the wavenumber of a photon:

$$\sigma = \frac{1}{2\pi c}\left(\frac{k}{m_{eff}}\right)^{1/2} \qquad \text{Equation 5}$$

Where,

$$c = speed\ of\ light\ in\ vacuum$$

The gross selection rule for a molecular vibrational mode to be Raman-active (detectable in Raman spectroscopy) is that the polarisability must change during vibration; the specific selection rule is that $\Delta v = \pm 1$ [29, 30]. Polarisability (α) represents the rate of change of the molecule's induced electric dipole moment (P) as a result of electromagnetic radiation (E):

$$P = \alpha E$$

If the polarisability changes in a molecular vibrational mode, and this mode makes a transition of $\Delta v = \pm 1$ accompanied by energy exchange with the incident electromagnetic radiation, it is possible to detect this transition by applying laser light to the sample and detecting scattered light that has a different wavelength from the laser. This procedure is Raman spectroscopy. The wavenumber of a Raman band, usually used as the x-axis in Raman spectra, is expressed in Equation 5. Figure 1.1 is the energy diagram of Raman scattering. The net process is that a molecule absorbs some of the incident photon's energy and makes a transition of $\Delta v = +1$ (Stokes Raman scattering) or releases energy to the photo during the transition of $\Delta v = -1$ (anti-Stokes Raman scattering). At room temperature, most molecules are at the ground state according to Boltzmann distribution, thus Stokes scattering signal is stronger than that of anti-Stokes.

From Equation 5, we can see that in the transition $\nu = 0 \rightarrow 1$, the wavenumber will decrease if m_{eff} is increased. It is an important property of molecular energy levels and it is utilised throughout this thesis under the term 'Raman red-shift' or 'red-shift'. It is the basis of combining Raman spectroscopy with stable isotope probing (SIP). As microbiologist are often interested in the fate of carbon and nitrogen in a microbial community, substrates synthesised from heavy stable isotopes carbon-13 (^{13}C) and nitrogen-15 (^{15}N) are fed to the community and organisms that incorporate the those substrates are labelled by stable isotopes. These procedures are referred to as SIP. Although Equation 5 only represents the energy levels of a simple harmonic vibrational mode, it is experimentally proved by this thesis and many cited articles that many far more complex molecules undergo the same red-shift toward lower wavenumber in SIP experiments. To make an illustration, one can imagine that as the mass of a vibrational system becomes larger, the energy levels become closer to each other (Raman red-shift) and eventually collapse and disappear when the system grows to a macroscopic object that obeys Newton's laws.

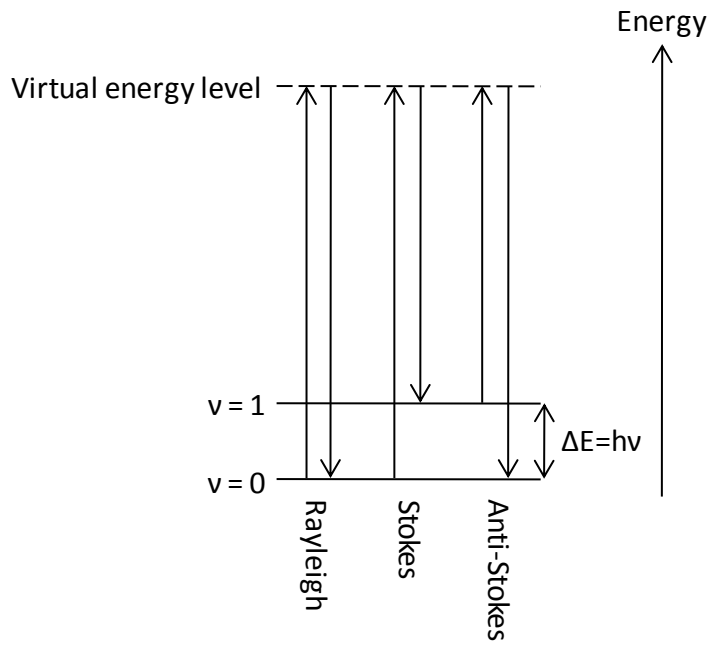

Figure 1.1 Energy diagram of Rayleigh scattering, Stokes Raman scattering and anti-Stokes Raman scattering.

The interaction between molecules and incident photons that generates Raman signal is a rare event. Normal Raman scattering, or spontaneous Raman scattering, happens about once in every 10^6 - 10^8 photons and the majority of photons undergo Rayleigh scattering (Figure 1.1). Raman spectroscopy and its combination with SIP have been widely used in chemistry where samples are usually prepared in relatively large quantities and high concentrations. However, in microbiology studies that focus on single microbial cells, Raman scattering's weak nature means that a single-cell Raman spectrum takes about 10 s to collect. In order to improve its analysing throughput and analytical selectivity, Raman signal enhancement mechanisms, such as resonance Raman (RR) scattering and surface enhanced Raman scattering (SERS), are used to enhance the Raman signal from certain molecules in samples.

Like the energy levels of atoms shown in Equation 5, electrons in a molecule have energy levels and can make transitions between them. It is observed that Raman signal intensity of some molecules can be greatly increased by up to 10^6 times when the incident laser wavelength falls into a molecular absorption band and the electrons absorb the photon energy to make a transition (resonant condition). Theories of the RR enhancement will not be present here because this thesis mainly focuses on its application and these theories are complicated. In summary, the intensity of a certain Raman band can be expressed in several terms adding together, of which the A-term represents the electronic transition that is independent from the nucleus and the B-term represents the electronic transition that is dependent on the motion of nucleus. Any increase in the A-term or B-term leads to the enhancement of the signal. Under resonant condition, total symmetric molecules can gain enhancement through the A-term whilst other molecules may gain enhancement through the B-term [28, 30, 31]. The key to achieve resonance Raman scattering is choosing the suitable laser wavelength to excite the electronic transitions of a RR-active compound. RR spectroscopy can greatly enhance the signal from RR-active molecules therefore shortens the spectrum acquisition time and enables the selective measurement of the RR-active molecules within a complex sample.

The SERS effect was discovered in the 1970s and hence became a popular research topic in ultra-low concentration detection including the measurement of biological molecules and single microbial cells. SERS has been shown to be able to detect single molecules, indicating an

enhancement factor of about 10^{10} - 10^{14} [32-36]. As discussed in Chapter 2, the SERS effect takes place in the vicinity of noble metal nano-structures, and there are a number of methods to prepare such materials and place samples on them. The mechanism of SERS enhancement is still a subject of debate, but it is agreed that SERS can result from the increased local electromagnetic field, and/or increased molecular polarisability due to the charge transfer between the metal and the sample [37, 38]. Electromagnetic enhancement is the main contributor to the SERS effect. The increased electromagnetic field on the surface of noble metal nano-structures results from a phenomenon termed localised surface plasmon resonance (LSPR). LSPR is the coherent oscillation of the conduction electrons on the surface of metal nanoparticles, metal surface with nanometre sized patterns, etc. LSPR is excited by the electromagnetic radiation with a resonant wavelength, which depends on a number of factors including the size of the nanoparticles/nano-pattern and their chemical environment. For gold or silver nanoparticles, which are widely used as SERS-active substrates, the resonant wavelengths usually fall within the infrared-visible range.

1.1.3 Application of Raman spectroscopy in microbiology and microbial ecology

As described above, the frequencies (wavenumbers) of bands in Raman spectra are specific to each different molecular vibrational mode. Therefore, a Raman spectrum can serve as the fingerprint of molecules. The rich information contained in the spectra offers a unique opportunity to look into

the microorganisms' identities, physiological status, phenotypic changes and ecological functions.

Microorganisms of different species have different Raman spectra due to their different biochemical composition. Thus Raman spectra are used to differentiate microbial species [39-48]; and even closely related strains [40, 49].

Since Raman spectra reflect the chemical composition of the measured cells, and the chemical composition may change during the growth, in response to environmental changes or vary cell-by-cell due to different gene expression, it is possible to use Raman spectroscopy to monitor the phenotypic change caused by different metabolic activities in different growth stages [44, 50, 51]. Phenotypic change caused by different environmental conditions is also detectable by Raman spectroscopy [45, 52]. Similarly, Raman spectroscopy is also used to observe phenotypic variation caused by stochastic gene expression [53].

A Raman signal enhancement mechanism, RR, as mentioned above, has been used in life science for decades [54]. RR only enhances the Raman signal from RR-active compounds or RR-active sites, e.g. charge transfer in metalloproteins, chlorophylls, carotenoids and nucleic acids (nucleic acids usually require UV laser). It has wide application in biochemical and biophysical research but it is limited by its selective nature. In environmental microbiology, a method that detects all microorganisms is

preferable. Chapter 3 shows the combination of RR spectroscopy and SIP may have great potential in environmental microbiology.

Another Raman signal enhancement mechanism, SERS, has been used in microbiology as a method to enhance Raman signal. Literature review on the application of SERS in microbiology is placed in Chapter 4.

Naturally weak Raman signal is not the only difficulty facing Raman spectroscopists. Data analysis in Raman spectroscopy is another challenge especially for biologists. As mentioned above, Raman spectra tend to contain large number of bands. However, such rich information can only become advantageous once researchers can identify these bands and assign them to the molecular vibrational modes. One can find free or commercially available Raman data bases for pure chemicals. But they can only assist in studying simple biological molecules or systems. When the sample's content is too complicated, one may find that a Raman band can belong to many different molecules that may exist in the sample. Two groups of methods have been used by researchers to tackle the problem in Raman data analysis: multivariate analysis and stable isotope probing (SIP). Suitable multivariate analysis can extract information buried in the vast data set in Raman spectroscopy [20]. Multivariate analysis uses statistical models to find variance in Raman spectra which can be correlated to know difference, treatments, trend, etc. SIP can simplify the data analysis in Raman spectroscopy because the Raman red-shift of stable isotope labelled samples unambiguously indicates that the shifted band is associated with the labelled element, e.g. ^{13}C or ^{15}N.

1.2 Objectives and thesis structure

Vibrational spectroscopy has aided biologists to study many biological systems. However, as a relatively newly emerged technique for environmental microbiologists, Raman spectroscopy has yet reached its potential in this field. The overall aim of this Ph.D. project is to develop Raman spectroscopy-based techniques further and expand their applications in environmental microbiology. There are five specific objectives in this research project:

1) Using RR spectroscopy to improve the signal-to-noise ratio of Raman spectra and reduce the spectrum acquisition time.
2) Using SERS to improve the signal-to-noise ratio of Raman spectra and reduce the spectrum acquisition time.
3) Investigating further into the application of ^{13}C-Raman-SIP techniques, including tracking carbon flow in food chains and possible theoretical explanation of the different red-shift behaviour of different Raman bands.
4) Developing an automatic cell sorting platform, Raman activated cell sorting (RACS) system, by integrating a confocal Raman microscope with a microfluidic device and flow controlling components.
5) Investigate possible Raman spectroscopy-based method to quantify ^{15}N-incorporation at single-cell level.

The structure of this thesis:

Chapter 1 serves as the introduction to this thesis which includes basic information about Raman spectroscopy, environmental microbiology and a brief introduction of the application of Raman spectroscopy in microbiology. More specific literature review and background information are given by the introduction sections in each chapter that follows.

Chapter 2 is the literature review for recent development in the application of Raman spectroscopy in environmental microbiology. Chapter 2 was converted into a paper and published:

Li M., Xu J., Romero-Gonzalez M., Banwart S. A. and Huang W. E. (2012). Single cell Raman spectroscopy for cell sorting and imaging. *Current Opinion in Biotechnology* 23 (1): 56-63.

Chapter 3 addresses the problem of weak Raman scattering cross section by using RR spectroscopy to enhance Raman signal of photosynthetic microorganisms. It also combines SIP with RR spectroscopy to build a fast hyperspectral imaging technique which quantitatively measures the carbon fixation at single-cell level. Chapter 3 was converted into a paper and published:

Li M., Canniffe D. P., Jackson P. J., Davison P. A., FitzGerald S., Dickman M. J., Burgess J. G., Hunter C. N. and Huang W. E. (2012). Rapid

Resonance Raman micro-spectroscopy to probe carbon dioxide fixation by single cells in microbial communities. *ISME Journal* 6: 875-885.

Chapter 4 addresses the problem of weak Raman cross section by attaching synthesised silver/gold nanoparticles to single microbial cells to in an attempt to achieve the SERS effect. Chapter 4 contains the author's M.Phil.-to-Ph.D. transfer report and additional experimental results.

In Chapter 5, the combination of SIP and Raman spectroscopy was applied to a system consists of carbon source, bacteria and predatory nematodes in order to track the carbon flow in this food chain. A novel quantitative Raman spectral marker for ^{13}C incorporation was reported which has a different 'red-shift mode' compared to the previously published spectral marker. The biochemical and biophysical processes that are responsible for this difference were studied. Chapter 5 was converted into a paper and submitted:

Li M., Gibson C. M., Fowler P. W., Huang W. E. and Jousset A. (2012). Monitoring carbon flow in microbial communities and revealing biochemical pathways using stable isotope probing and Raman spectroscopy. Submitted to *Analytical Chemistry*

The study reported in Chapter 6 is the first step towards the proposed RACS system. It proves the concept that using the combination of SIP, RR spectroscopy and microfluidic device can rapidly profile carbon dioxide fixation in photosynthetic communities. Chapter 6 was converted into a paper and published:

Li M., Ashok P.C., Dholakia K. and Huang W.E. (2011). Raman activated cell counting for profiling carbon dioxide fixing microorganisms. *Journal of Physical Chemistry A* in press, DOI: 10.1021/jp212619n.

Chapter 7 reports the quantitative measurement of ^{15}N-incorporation in the single cells of an important marine bacterial strain *Ruegeria pomeroyi* DSS-3 by Raman spectroscopy and multivariate analysis. Chapter 7 was converted into a paper and in preparation for submission:

Li M., Wharfe E.S., Chen Y. and Huang W.E. (2012). Quantitative measurement of nitrogen uptake in single cells by Raman spectroscopy.

Chapter 8 briefly summarises the thesis and recommends potential follow-up studies for the future research.

Appendix: CD-ROM

Chapter 2: Single-cell Raman spectroscopy for cell sorting and imaging

2.1 Introduction

All organisms on the earth, including bacteria, plants and animals, derive from single cells. Genetically identical parent cells can produce cells with different functions due to the intrinsic variation in gene expression and gene regulation amongst the individual offspring cells. Traditional bulk measurements average different cell phenotypes but what occurs at the level of individual cells has profound biological implications in cell development, evolution and adaptation, which include embryonic cell specialisation and development, cell differentiation, cancer cells' resistance to chemotherapy and radiotherapy, bacterial antibiotic resistance, etc. Microbiologists are specifically interested in single-cell techniques because most microorganisms (>99%) have not yet been cultured in the laboratory. Increasing evidence indicates that these uncultured microorganisms play crucial roles in ecosystems and have a profound impact on global warming (through carbon/nitrogen cycles), food security (through maintaining soil health and promoting plant growth), and bioremediation of environmental pollution [55, 56]. The investigation of uncultured bacteria at single-cell level circumvents the cultivation issue and allows experiments to reveal their *in situ* ecological roles, providing important evidence to predict the dynamic change of microbial communities. To date, the major culture-

independent approach used to study microbial communities is metagenomics, which is a top-down method that elucidates the microbial structure and gene pools of unculturable microorganisms [14]. However, for complex microbial communities, metagenomic sequence alone is usually unable to untangle the links between sequences and genomes, genes and functions, and ecological roles and species. These difficulties can be tackled by bottom-up methods that enumerate and characterise the genotypes and phenotypes of individual cells in the community.

Single-cell bio-analysis can be generally classified as indirect or direct measurement (Figure 2.1). A typical indirect measurement is external fluorescent labelling, which is the basis for fluorescent imaging and fluorescence activated cell sorting (FACS). However, it is better to directly measure intrinsic information from single cells in a non-invasive, label-free and *in vivo* manner. Single-cell Raman spectroscopy (SCRS) meets these criteria by providing intrinsic chemical 'fingerprints' of single cells (Figure 2.1). SCRS usually relies on confocal Raman microscopes that acquire Raman spectra from a small volume of sample such as one bacterium [44]. A typical single-cell Raman spectrum contains a rich cellular chemical profile, including hundreds Raman bands which can be assigned to different cellular compounds such as nucleic acids, proteins, carbohydrates and lipids. SCRS enables the characterisation of different cell types and can reveal physiological and phenotypic changes in living single cells [20]. Raman-FISH, combining SCRS and fluorescent *in situ* hybridisation (FISH), is able to visualise, by FISH-probing, cells in a microbial

community and simultaneously acquire single-cell Raman spectra (Figure 2.1) [26, 57]. As Raman-FISH has recently been reviewed [20], this chapter focuses on the application of SCRS in single-cell physiological analysis, Raman activated cell sorting (RACS) and Raman imaging.

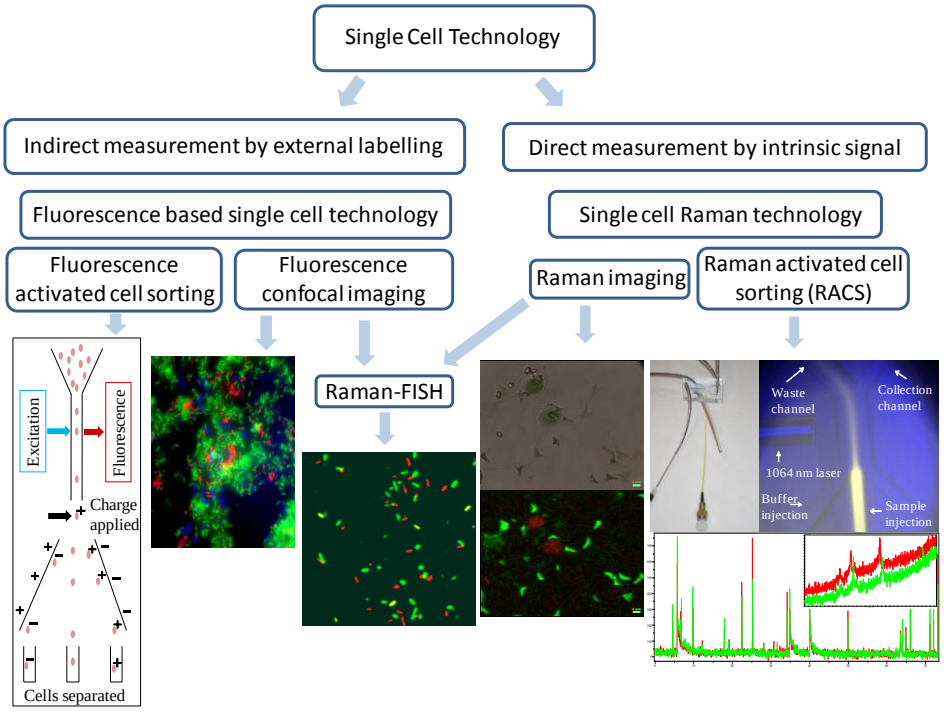

Figure 2.1 Overview of the single-cell bio-analysis.
Single-cell bio-analysis can be generally classified as indirect and direct measurements. A typical indirect measurement is fluorescence imaging which is sensitive but requires external labelling. Single-cell Raman spectroscopy (SCRS) is a non-invasive and label-free technique. Single-cell Raman spectra are cells' 'fingerprints' that reflects their phenotypes and physiological states. Raman-FISH is a combination of fluorescence labelling and Raman spectroscopy [58]. Raman imaging is a functional imaging technique based on Raman spectra of single cells. Raman imaging has been used to distinguish active CO_2-fixers (red) and from inert cells (green) [21]. Raman activated cell sorting (RACS) is able to separate cells according to their Raman spectra.

2.2 Challenges facing single-cell Raman spectroscopy

In order to apply SCRS to biological analysis, two major challenges need to be addressed: weak Raman signal and the interpretation Raman spectral data. A long acquisition time (from about 10 s to minutes) is usually required to obtain a good Raman spectrum from a single cell with high signal-to-noise ratio. Although it has been shown that single-cell Raman spectra of some bacterial species can be acquired within 10 s using relatively powerful laser [20], an even shorter acquisition time at sub-second level is desirable to improve the throughput of Raman spectroscopic analysis [21, 59]. Resonance Raman (RR) spectroscopy, coherent anti-Stokes Raman spectroscopy (CARS), stimulated Raman spectroscopy (SRS) and surface enhanced Raman scattering (SERS) have been applied to biological samples to enhance Raman signals by several orders of magnitude (Figure 2.2). Since Raman spectroscopy measures all the Raman-active molecular vibrations, numerous Raman bands of biological molecules appear in the 'fingerprint region' from about 400 to 1800 cm^{-1}. Translating Raman spectra into meaningful information is often challenging. Raman spectra of many pure chemicals have been analysed and well-documented [60], with commercial availability of Raman databases and free-to-access Raman spectra of chemical products (e.g. Sigma–Aldrich UK). But the identification of biological molecules by Raman spectra is far from being standardised. Several recent reports provided Raman band assignments and a spectrum database for some biological molecules, which help to link single-cell Raman spectra to the biochemical entities [20, 61, 62].

2.3 Resonance Raman spectroscopy

When the frequency of incident laser matches the absorption bands of electronic transitions of RR-active molecules, a resonance Raman (RR) effect may occur. RR may enhance Raman signal by 6 orders of magnitude (Figure 2.2). RR spectroscopy selectively enhances RR-active molecules in cells. Raman bands of those molecules can be very strong and dwarf Raman bands from other biological molecules. Typical RR-active biological compounds include various pigments (e.g. carotenoids, bacteriorhodopsin and proteorhodopsins) and metalloproteins. RR spectroscopy has been used to study red blood cells and viral DNA [63-65]. Surface enhanced resonance Raman scattering (SERRS) combines the strengths of both the SERS and RR. It has been applied to analyse the *in vivo* activity and enantioselectivity of 14 different hydrolases, with a sensitivity of 0.8 pmol enzyme/mL [66]. An important aspect of RR spectroscopy is that it is a suitable technique to study photosynthetic cells because essential photosynthetic pigments such as carotenoids have strong RR bands [21, 31]. Carotenoids are non-fluorescent light-harvesting (LH) antenna and singlet oxygen quenchers, which are essential elements of LH complexes in nearly all photosynthetic microorganisms [67]. Caused by the incorporation of ^{13}C-bicarbonate, the RR bands of single photosynthetic microorganisms displayed distinctive Raman red-shift, the extent of which was shown to be proportional to the ^{13}C content in single cells [21].

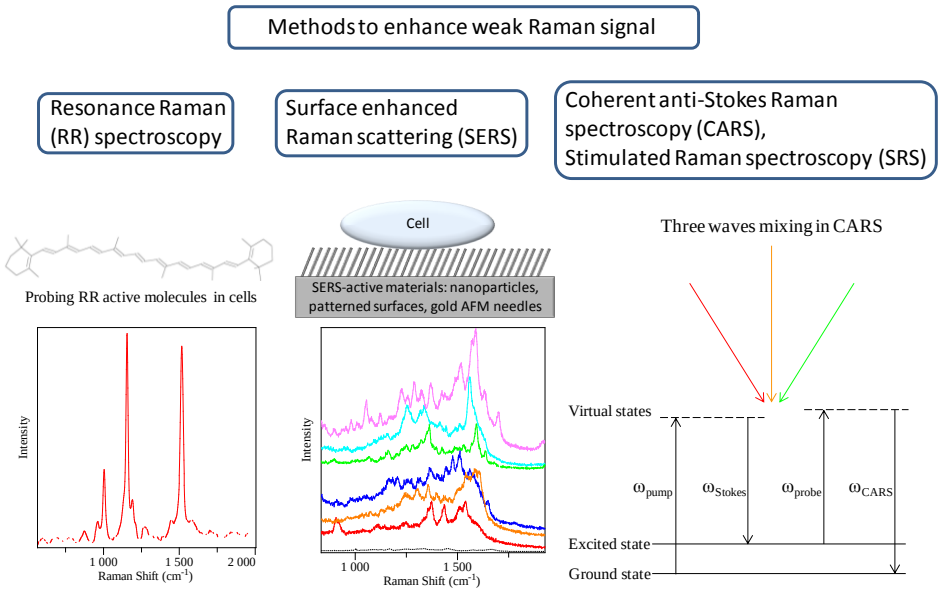

Figure 2.2 Three methods to enhance Raman signal.
In comparison with spontaneous Raman spectroscopy, Resonance Raman (RR) spectroscopy is able to enhance Raman signals by up to 6 orders of magnitude, but it selectively enhances certain RR-active molecules. SERS enhancement can be as high as 14 orders of magnitude, but it requires the introduction of nano-materials to biological samples and also suffers from the non-reproducibility. CARS and SRS employ multiple laser beams to increase Raman signal by about 1000 times, but the range of Raman spectra is defined by the pump and Stokes lasers.

2.4 Coherent anti-Stokes Raman spectroscopy and stimulated Raman spectroscopy

A CARS signal arises when the frequency difference between a pump laser ν_p and a Stokes laser ν_s matches the frequency of a Raman-active molecular vibration, which generates a strong anti-Stokes Raman signal (Figure 2.2) [68]. Owing to its nonlinear and coherent nature, a CARS spectrum is about 1000 times stronger than a spontaneous Raman spectrum [69] and CARS measurement can penetrate as deep as 0.4 mm [68]; thus CARS is useful in generating chemical images of biological samples (mostly targeting lipids)

and allows 3D imaging of tissues and biofilms [68]. SRS is another form of nonlinear Raman spectroscopy [70]. In contrast to CARS, which detects the vibrational coherence, SRS detects the vibrations of the excited population. SRS overcomes some problems associated with CARS microscopy and offers several advantages, including generating identical spectra as the spontaneous Raman spectroscopy, and being free from non-resonant and fluorescent background [70]. Unlike spontaneous Raman spectroscopy and RR spectroscopy, CARS and SRS employ multiple laser beams. The range of CARS and SRS Raman spectra is defined by the pump and Stokes lasers used in the experimental setup.

2.5 Surface enhanced Raman scattering

Surface enhanced Raman scattering (SERS) was first discovered in the 1970s, and it was found that the Raman signal can be up to 14 orders of magnitude higher than that of spontaneous Raman spectroscopy if a molecule is associated to a roughened noble metal (often silver or gold) surface (Figure 2.2) [71]. SERS is so sensitive that the detection of single molecules has been demonstrated [35, 36, 72]. Gold and silver are usually used to prepare SERS-active surfaces and this can be implemented in several ways using either nanoparticles (NPs) [73, 74], the tip of an atomic force microscopy (AFM) needle [75] or patterned surfaces with nanometre level roughness [76]. Although the mechanism of SERS is not completely clear, it has been proposed that SERS enhancement originates mainly from

the excited surface plasmon of the metal surface (the electromagnetic enhancement) [28]. However, the SERS effect is dependent on the distance between the metal surface and the target molecules; experimental evidence has shown that effective SERS enhancement decays considerably within 10 nm from the surface of the metal [37]. To apply SERS to single living cells is not simple as it is difficult to keep cells close enough to the SERS-active surface. Most small molecules serving as linkers between SERS-active surface and cells can easily exceed 10 nm in size. It has been found that the strongest SERS enhancement 'field' is situated in the narrow space between closely placed nanostructures [77]. Therefore, if the analytes (e.g. proteins, DNA, lipids or other biological macromolecules) are entrapped between the nanoparticles during controlled aggregation, SERS signal can be improved. In the three most popular implementations of SERS as shown in Figure 2.2, nanoparticles are the most suitable and easiest method for studying living cells because it does not require drying cells on a surface or vacuum conditions, allowing living single cells to be analysed and sorted in a flow cytometry-like Raman-microfluidic chip system. However, the majority of colloidal nanoparticles need stabilising agents on their surfaces to prevent aggregation, which occupy the most effective range of the SERS effect and can prevent nanoparticles from attaching to cells. As a result, SERS spectra taken with colloidal nanoparticles should be interpreted cautiously because any substance absorbed on the surface of nanoparticles, including the stabilisers, may be responsible for generating strong SERS signal. This becomes more challenging when it is difficult to predict which biological

molecules the nanoparticles bind to. Another problem associated with SERS is its well known non-reproducibility, which produce different spectra with each measurement (as shown in Figure 2.2).

2.6 Single-cell physiology analysis

Spontaneous Raman spectra of cells have been demonstrated to discriminate between bacterial species, different growth phases or physiological states of the same species without *a priori* knowledge [44, 46, 47, 78-80]. Andrews *et al.* used Raman spectroscopy to identify biological molecules such as DNA, lipids and proteins that influence the biofilm formation and bacterial attachment to various surfaces [80]. Interestingly, SCRS spectra indicated that *Rhodococcus* sp. and *Sphingomonas* sp. in planktonic phase synthesised carotenoids whereas the cells in biofilm were free from carotenoids even though they were grown in the same culture [80]. Since Raman spectroscopy is sensitive to subtle changes in the vibrational frequencies of chemical bonds, Raman spectroscopy and stable isotope probing (SIP) can be combined to identify cells that incorporate ^{13}C- or ^{15}N-substrates. Raman-SIP methods reveal metabolic activities and link species with their ecological functions [21, 26, 44, 57, 81]. Raman-SIP methods can be sensitive enough to achieve quantitative or semi-quantitative detection of ^{13}C-incorporation at single-cell level [21, 44]. Raman-SIP has been used to differentiate *Protochlamydia amoebophila* into two distinct physiological states (reticulate and elementary bodies), both of which were, unexpectedly,

found to be active outside the host cells and infective for 3 weeks [81]. Hall *et al.* employed SCRS to study the stoichiometry and found the results comparable to that of traditional bulk measurements [82].

2.7 Raman activated cell sorting

A few cell sorting techniques are listed and compared in Table 2.1. Cell sorting mechanism and decision-making criteria are the two key factors in single-cell sorting techniques. Flow cytometry is a high-throughput cell sorting technique with sorting rates in the range of 10,000 - 20,000 cells / s. Microfluidics-based cell sorting usually has lower sorting rate than flow cytometry. However, a microfluidic chip is flexible to use for different purposes and combine with different detection method, e.g. confocal Raman microscope, allowing the separation of cells based on their intrinsic physical, chemical and biological properties. As the flow in the microfluidic device is usually laminar flow, accurate control of cell separation is possible. A microfluidic device made from polydimethylsiloxane (PDMS) is also inexpensive and disposable. In addition, with the development of single-cell genome amplification, a few cells of interest can provide sufficient genomic DNA for sequencing using multiple displacement amplification, which enables the identification and many other molecular biological assays to be performed on the sorted cells [27].

Of the key importance to cell sorting is the choice of sorting criteria. Cells can be isolated according to fluorescent labelling, size, morphology, optical

property (e.g. reflection index) as well as Raman spectra (Table 2.1). FACS usually relies on various external fluorescent labelling which limits its maximum simultaneous measurements to 12 - 17 parameters [83]. Single-cell mass spectrometry has also been developed to simultaneously examine 31 binding antibodies of human bone marrow at single-cell level; however, it is destructive and relies on external antibody labelling [84]. Cell sorting based on morphology is not widely adopted by researchers, because it is usually unclear how to link cell morphology to their functions. RACS enables the separation of cells according to their intrinsic chemical 'fingerprint' with minimal pre-treatment, thus cells are potentially viable after sorting [27]. In RACS, isolated cells may be used on-chip for cultivation or DNA amplification. RACS based on spontaneous Raman spectroscopy has been reported as a proof of concept in which microfluidic devices and optical tweezers were used to capture, analyse and sort single cells with a relatively low throughput [27, 85]. A couple of papers reported the effort to integrate SERS and CARS with a microfluidic device in order to increase the cell sorting rate by shortening Raman signal acquisition time [86, 87]. Camp and co-workers employed multiplex coherent anti-Stokes Raman scattering to measure lipid-rich cells in a yeast culture at a rate of 100 spectra / s [86]. Taking the advantage of the SERS effect, Walter and co-workers classified nine *Escherichia coli* strains by mixing silver colloid with ultrasound-treated cells and reduced the Raman signal acquisition time to 1 s [87]. In the light of recent advances in RR, SERS and CARS, it is foreseeable that high-throughput RCAS can be achieved in the near future.

Table 2.1 Comparison of different cell sorting techniques.

Cell sorting technique	Type of signal	Sorting mechanism	Invasive/non-invasive labelling	Reference
FACS	Autofluorescence/fluorescent labelling	Selectively applying electrostatic charge to droplets based on their fluorescent signal	Invasive/non-invasive	[88]
Micromanipulation	Fluorescent labelling, size, morphology, optical property (reflection index)	Mechanical (microcapillary), optical force (laser), electrokinetic, magnetic manipulation	Invasive/non-invasive	[89-91]
Microdissection	Fluorescent labelling	Cells on a membrane were cut by a dissecting laser and captured	Invasive/non-invasive	[92]
RACS	Raman spectra	Separating cells in microfluidic channels based on their Raman signal	Non-invasive	[27, 85, 86]

2.8 Raman imaging

Raman imaging is the generation of pseudo-colour images in which each pixel is produced according to the relative intensities of the defined Raman bands (Figure 2.1). It has been used to image viruses [93], spores [46], bacterial species, and phenotypic variations in an isogenic population [53]. Raman-FISH has been applied to investigate environmental samples and identified an uncultured *Acidovorax* sp. strain which played a key role in naphthalene bio-degradation in contaminated groundwater [57]. An on-line florescence suppression module for Raman spectroscopy has been reported and is potentially helpful for Raman imaging [94].

Raman-SIP method has been applied to image a bacterial population; it differentiated ^{13}C-cells from ^{12}C-cells but took several hours [58]. RR, CARS, SRS and SERS are all potential methods to shorten the time required in Raman imaging. CARS and SRS are excellent Raman imaging tools, especially for lipids content, but they are less useful when Raman bands in the 'fingerprint' region are needed [95]. SERS can be highly sensitive, but requires the attachment of nano-materials to cells. RR-active molecules in cells, e.g. carotenoids, can be used as markers for RR imaging [21].

Using Ca-dipicolinic acid (Ca-DPA) as a marker, Li and co-workers combined Raman spectroscopy, phase contrast microscopy and optical tweezers to image the dynamics of germination of single *Bacillus cereus* spores [96]. Raman imaging of single cells in isogenic populations demonstrated its unique advantage in identifying phenotypically different

cells without any labelling. Wide cell-to-cell variations were found in isogenic populations of model strains *Bacillus thuringiensis*, *Legionella bozemanii* and *Bacillus cereus* [53, 97].

Using carotenoids as intrinsic markers, single-cell RR spectroscopy has been used to identify active CO_2-fixers on the ms-per-cell timescale in a quantitative manner [21]. In this study, Li and co-workers showed that RR imaging was sensitive to detect low level of ^{13}C content (10 %) in single cells; strong RR signal also shortened the experimental time so that a 93 μm by 73 μm Raman image with 1 μm spatial resolution took a few minutes to generate [21]. Raman imaging can be followed by a laser micro-dissection step to selectively cut and separate cells of interest for cultivation or genomic amplification and sequencing.

2.9 Conclusion and remarks

SCRS and its derivative techniques such as Raman-FISH, RCAS, Raman imaging are ideal bio-analytical tools for studying single cells. The main problem that hampers a broader application of Raman spectroscopy in cell biology is its naturally weak signal intensity. To overcome this problem, RR, CARS, SRS and SERS have been explored to enhance Raman signal. RR is able to enhance Raman signals by up to 6 orders of magnitude and is particularly suitable for studying photosynthetic microorganisms. SERS enhancement can be as high as 14 orders of magnitude, but it requires the labelling with nano-materials and may suffer from the non-reproducibility

of SERS spectra. Further studies on the SERS enhancement mechanisms and the optimisation of nanoparticle-cell interaction could pave the way for wider application of SERS in single-cell research. CARS spectra are three orders of magnitude stronger than spontaneous Raman spectra and have been used for imaging [98]. Other ways to enhance Raman signals would rely on instrumentation improvement, e.g. increasing incident laser power, improving the sensitivity of the spectrometer, and simultaneous multi-measurement [99]. A typical single-cell Raman spectrum contains a large number of Raman bands representing many biological molecules; thus, data interpretation and analysis are also an area of interest. Advanced multivariate analysis and the establishment of a biological Raman database would help to tackle this challenge [79].

Chapter 3: Rapid Resonance Raman micro-spectroscopy to probe carbon dioxide fixation by single cells in microbial communities

3.1 Introduction

Photosynthetic microorganisms including bacteria and algae are essential to aquatic life and the global carbon budget [100, 101] but the precise ecological roles of many of these species remain ill-defined due to cultivation difficulties which have led to the development of methods for detecting uncultured cells in the environment [56, 102, 103]. Some uncultured photosynthetic bacteria and microalgae have been found to play crucial roles in carbon or nitrogen cycling [104-110]. Recently, culture-independent approaches (e.g. *in situ* hybridisation and 18S-rRNA sequencing) have been employed to reveal two new groups of photosynthetic eukaryotes that play key roles in CO_2 fixation in the subtropical and tropical northeast Atlantic Ocean. These groups, Euk-A and Euk-B, have not yet been cultivated and, in the case of Euk-B, culturing conditions for closely related species have never been found [111]. It is reasonable to hypothesise that large populations of uncultivated photosynthetic bacteria and algae remain to be discovered in the oceans. It is essential to monitor the photosynthetic activity of bacteria and algae including those hitherto-uncultivated microorganisms, and to understand

their dynamic processes in relation to CO_2 fixation and climate change. In addition, uncultured oceanic photosynthetic bacteria and algae represent an untapped biotechnological resource that could lead to the discovery of new biomedical products and biocatalysts [112-114]. Therefore, it would be useful to develop a culture-independent method to unravel the ecological function of photosynthetic bacteria and algae *in situ*, and to reveal their roles in the natural environment in terms of their relative contribution to carbon fixation.

Raman micro-spectroscopy has been shown to be a useful tool to study single microbial cells [20, 26, 27, 44, 57, 58, 78, 81, 82, 115]. In combination with other biological assays such as stable isotope probing (SIP) and fluorescence *in situ* hybridisation (FISH), Raman single-cell techniques can link bacterial species to their ecological roles without cultivation [57]. Raman spectroscopy detects the vibrations of chemical bonds of molecules through the inelastic scattering of incident laser light. Raman micro-spectroscopy provides intrinsic chemical profiles of microorganisms and enables us to study single microorganisms [44]. A typical Raman spectrum contains a rich cellular chemical profile, including information on nucleic acids, proteins, carbohydrates, lipids and pigments (e.g. carotenoids), which allows the characterisation of different cell types, as well as physiological and phenotypic changes [20, 26, 44, 57, 58, 78, 81, 82]. Raman imaging is a hyperspectral technique which acquires a full Raman spectrum at each defined point (pixel). Resultant spectra can be used to generate pseudo-colour images based on specific Raman bands. Since

Raman bands relate to chemical entities within the sample, the Raman images can be used to illustrate the distribution of chemical components. Raman imaging could visualise the chemical composition of individual cells in a microbial community as it provides micrometre-level spatial resolution and a temporal dimension to study microbial identity and ecophysiology in complex microbial communities [57]. However, the physical process of inelastic light scattering that underlies Raman spectroscopy is a rare event, with about one in 10^6 - 10^8 photons interacting with the sample undergoing Raman scattering. Typically, the acquisition of a single-cell Raman spectrum with good signal-to-noise ratio takes at least a few seconds, making Raman imaging time-consuming and hindering it from high-throughput searching for microorganisms which have incorporated a labelled compound or characterised by a specific chemical composition. Resonance Raman (RR) spectroscopy can enhance the Raman signal up to 10^6-fold, which significantly reduces the acquisition time of Raman spectra [31]. RR occurs when the frequency of incident laser matches the absorption bands of electronic transition of RR-active molecules. Many biological molecules are RR-active compounds and carotenoids are typical analytes for RR spectroscopy [31, 116]. More importantly, nearly all photosynthetic microorganisms contain carotenoids which are essential elements of light-harvesting (LH) complexes and singlet oxygen quenchers [117-120].

In this study, we obtained single-cell RR (SCRR) spectra from carotenoid-containing bacteria and microalgae using short acquisition times on

millisecond level. SIP using ^{13}C-bicarbonate was employed to link bacterial species with their CO_2-fixation activities.

3.2 Materials and methods

3.2.1 Chemicals, media, strains, and growth conditions

All chemicals used in this study were purchased from Sigma-Aldrich UK unless otherwise stated. The ^{13}C-sodium bicarbonate contains 98 % ^{13}C (Catalog number 372382). The microalgae strain AMA was isolated from Arctic supraglacial sites. *Synechocystis* sp. PCC 6803 and *Synechococcus elongatus* PCC 7942 were from our laboratory collection. Non-photosynthetic bacteria strains GWO, GWY and GWR with orange, yellow and red pigments, respectively, were isolated from contaminated groundwater in southwest UK [57]. AMA, *Synechocystis* sp. PCC 6803 and *Synechococcus elongatus* PCC 7942 strains were grown in BG-11 media with sodium bicarbonate as the sole carbon source. To examine the integration of ^{13}C in photosynthetic microorganisms, *Synechocystis* sp. PCC 6803 and *Synechococcus elongatus* PCC 7942 strains were grown in liquid BG-11 medium supplemented with various proportions of ^{12}C- and ^{13}C-bicarbonate. The final concentration of the total carbon source (^{12}C- and ^{13}C-bicarbonate combined) was 5 mM. Carbon-13 content of 1.1 (^{13}C natural abundance), 10.8, 25.3, 49.6, 73.8 and 98 % were achieved by mixing 1 M filter-sterilised ^{12}C- and ^{13}C-sodium bicarbonate solutions in appropriate ratios before adding to the BG-11 media. The ^{13}C levels were

chosen to cover the entire range from the natural background level to the highest available enriched ^{13}C source. Carbon-12 and carbon-13 were mixed in integer ratios, e.g. 1:9 or 1:1, to ensure the reproducibility and simplicity of experimental procedures. The ^{12}C-sodium bicarbonate contains 1.1 % ^{13}C because this is the natural abundance of ^{13}C, and the ^{13}C-sodium bicarbonate used in this study contains 98 % ^{13}C. The ^{13}C content of each culture vessel was then calculated using these values. Bacterial strains GWO, GWY and GWR were grown and maintained on R2A agar plates (Oxoid, UK).

Seawater was sampled from the coast near the Dove Marine Laboratory of Newcastle University in northeast England. Photosynthetic microorganisms in the seawater samples were enriched by incubation under open-air conditions about 50 m from shore for several months. Original seawater was used to maintain the natural photosynthetic microorganism assemblages.

3.2.2 Microcosm setup for cyanobacterial cultures

A degasification step was done prior to the incubation in order to remove dissolved CO_2 in the BG-11 medium. This was achieved by boiling the BG-11 medium in a microwave oven for 1 minute. Deionised water (10 mL per 50 mL BG-11) was added to the BG-11 medium to compensate for the loss of water during the degasification. A 0.45-μm filter attached to a syringe filled with sodium hydroxide pellets was linked to the bottle cap immediately after the degasification and the bottle cap was fastened (Figure S3.1), and the medium was allowed to cool to room temperature. Pre-mixed ^{12}C- and ^{13}C-sodium bicarbonate solution and 50 μl of cyanobacterial cell

suspension (about 10^8 cells / mL) were then added to the BG-11 medium by quickly opening the cap and re-sealing the bottle with a closed cap. *Synechocystis* sp. PCC 6803 was grown in media with ^{13}C content of 1.1 (^{13}C natural abundance), 10.8, 25.3, 49.6, 73.8 and 98 %. *Synechococcus elongatus* PCC 7942 was grown in media supplemented with ^{13}C content of 1.1 (natural abundance), 49.6 and 98 %. The ^{13}C-content was corrected by taking account of ^{13}C natural abundance and the 98 % ^{13}C-bicarbonate used in the study. The culture vessel was incubated at 30 °C and 50 µmol photons m^{-2} s^{-1} in an orbital shaker, agitated at 150 RPM for 4 days (Innova 44 illuminated rotary incubator, New Brunswick Scientific, UK).

3.2.3 Incubation of seawater samples

Thirty millilitres of the seawater was sampled and ^{13}C-$NaHCO_3$ was added to a final concentration of 2 mM. The seawater samples were incubated in closed bottles at room temperature for 8 days in natural light. The seawater was also incubated with 2 mM ^{12}C-$NaHCO_3$ under the same conditions as a control sample to provide a reference for the observation of Raman red-shift.

3.2.4 Raman micro-spectroscopy analysis

Cells were sampled from microcosms and washed with deionised water before Raman micro-spectroscopic analysis. Each cellular suspension (5 - 10 µl) was spread on a calcium fluoride (CaF_2) slide and allowed to air-dry. Single-cell resonance Raman (SCRR) spectra were acquired using a confocal Raman microscope (LabRAM HR, HORIBA Scientific, UK)

equipped with an integrated Olympus microscope (model BX41). A 100× magnifying dry objective (NA = 0.90, Olympus, UK) was used to observe and acquire Raman signals from single cells. The laser beam was targeted on the cell visually using an integrated camera and a motorised XYZ stage (0.1 µm step). The Raman scattering was excited with a 532-nm Nd:YAG laser (Torus Laser, Laser Quantum, UK). The laser power on a single cell was about 3.5 mW. The detector was a CCD detector kept at -70 ^{o}C (Andor, UK). The system was run with a confocal pinhole diameter of 100 µm, enabling a spatial resolution of approximately 1 µm. Each Raman spectrum was acquired between the range 2172 cm^{-1} and 557 cm^{-1}, with 1021 data points and a spectral resolution of about 1.5 cm^{-1}. LabSpec software (HORIBA Scientific, UK) was used to control the Raman system and acquire Raman spectra. Acquisition times for SCRR spectra were 100 ms for single cell measurements and 1 - 30 ms for Raman imaging. For each pure or mixed culture samples, 20 single cells were randomly chosen and measured. Beta-carotene was used as a carotenoid control and was measured under the same condition as SCRR.

3.2.5 Raman imaging

SWIFT (HORIBA Scientific, UK) imaging function was coupled into the Raman systems, which allows significant reduction in the time needed for generating Raman images when very short spectrum acquisition time is used (milliseconds in this study). In contrast to traditional start-stop mapping methods, samples are continuously scanned beneath the laser beam, and spectra are acquired ‘on the fly’ as the sample is scanned in the SWIFT

mode. SWIFT was employed to generate Raman images of photosynthetic bacterial populations in which the cells had different ^{13}C-content. Three 1:1 mixed cyanobacterial cultures were imaged by SWIFT: 1) *Synechocystis* sp. PCC 6803 cells grown in 73.8 % ^{13}C-bicarbonate BG-11 medium mixed with cells grown in ^{12}C-bicarbonate BG-11 medium; 2) *Synechocystis* sp. PCC 6803 cells grown in 10.8 % ^{13}C-bicarbonate BG-11 medium mixed with cells grown in ^{12}C-bicarbonate BG-11 medium; 3) *Synechocystis* sp. PCC 6803 cells grown in 10.8 % ^{13}C-bicarbonate BG-11 medium mixed with *Synechococcus elongatus* PCC 7942 grown in ^{12}C-bicarbonate BG-11 medium. SWIFT was also used to image the seawater samples incubated with ^{13}C-$NaHCO_3$ and ^{12}C-$NaHCO_3$ to visualise the ^{13}C-incorporated photosynthetic cells. Each Raman images was acquired within minutes and the acquisition time of each pixel was 1 ms for mixed cultures, and 10 - 30 ms for the seawater samples. A step size of 0.5 μm (4 million pixels mm^{-2}) was used to generate the Raman images for cyanobacteria culture mixtures; a step size of 1 μm was used for the seawater samples. Raman images were analysed with LabSpec (HORIBA Scientific, UK), and were generated by classical least squares (CLS) modelling of hyperspectral data sets. At each image pixel, a linear combination of factors was calculated to estimate the measured spectrum, such that

$$I_i = \sum_{k=1}^{l} a_{ik} A_k + \varepsilon_i$$

where I_i is the i^{th} measured spectrum of the data set, A_k is the k^{th} loading input to the calculation, a_{ij} is the score of the spectrum I_i with respect to the

loading A_k, $a_{ij}A_k$ is a factor, and ε_i is the error between the spectrum (measurement) I_i and the estimation $\sum_{k=1}^{l} a_{ik}A_k$.

Loading spectra (A_k) were selected by averaging spectra from manually selected regions of interest (ROI) within the data set. The images display scores (a_{ik}) as a function of X and Y axis positions. The green or yellow colour in the Raman images indicated the ^{12}C-carotenoids in cells, while the red colour indicated the ^{13}C-carotenoids in cells (characterised by the red shifted resonance Raman peaks). In the Raman images of seawater samples, the purple colour was defined as the fluorescence because some organisms with autofluorescence were observed, which appeared as a broad, featureless spectrum without the expected sharper RR peaks.

3.2.6 Raman spectra analysis

All Raman spectra were recorded, smoothed and baseline-corrected using LabSpec. Spectra smoothing was performed by the Savitsky-Golay smoothing method. Positions of the SCRR bands were determined using LabSpec and were subsequently imported to SPSS 15 (IBM Corporation, NY, USA) for further analysis. The positions of SCRR Raman bands of *Synechocystis* sp. PCC 6803 and *Synechococcus elongatus* PCC 7942 were analysed statistically to establish a relationship between the extent of red-shift and ^{13}C-content in cells. The wavenumbers of the Raman bands were plotted against the ^{13}C content, with the error bars and linear regression lines (SPSS 15). Two-sample t-tests were performed in SPSS between the ^{12}C

and 10.8 % ^{13}C PCC6803 samples on three major bands of SCRR. MVSP 3.13g (Kovach Computing Services, UK) was used to perform principal component analysis (PCA) for SCRR spectra.

3.2.7 Absorbance analysis of Synechocystis sp. PCC 6803

Five millilitres of *Synechocystis* sp. PCC 6803 were harvested by centrifugation at 3000 RCF for 5 min. The cells were then re-suspended in the same volume of phosphate buffer solution. To obtain a light absorbance spectrum of *Synechocystis* sp. PCC 6803, 200 µl of cells was scanned in the visible range using a microplate reader (Synergy 2, BioTek, VT, USA). The absorbance spectrum was recorded in triplicate with a spectral resolution of 5 nm in the range of 400 - 750 nm.

3.2.8 Mass Spectrometry analysis of ^{13}C-content of Synechocystis sp. PCC 6803 proteins

Batches of *Synechocystis* sp. PCC 6803 cells were grown in BG-11 media with different percentages of ^{13}C-bicarbonate (1.1, 10.8, 49.6, and 98 %) as the sole carbon source. The growth conditions were the same as described above. After 4 days' growth, 5 ml of each culture were sampled for single-cell Raman spectroscopy analysis. Meanwhile, 10 ml of each culture were taken and the cells were harvested by centrifugation at 4,000 RCF for 10 min. Cells from each *Synechocystis* sp. PCC 6803 sample were re-suspended in 0.2 ml of SDS sample buffer containing tracker dye and 0.05 % (v/v) mercaptoethanol. After incubation at 90°C for 10 min, 15 µl was applied to a NuPAGE Bis-Tris gel (1.0 mm, 12 %; Invitrogen, Paisley, UK)

according to the manufacturer's protocol. The gel was stained with colloidal Coomassie Blue (BioRad Laboratories, Hemel Hempstead, UK) and the same prominent protein band (at 50 - 75 kDa) excised from the four lanes (Figure S3.2). The bands were subjected to in-gel tryptic digestion according to a published protocol [121].

The extracted peptides were separated on an UltiMate 3000 nanoflow liquid chromatography system (Dionex, Camberley, UK), using 5 mm × 300 µm (trapping) and 150 mm × 75 µm (analytical) PepMap C_{18} reverse-phase columns (Dionex). Linear gradient elution was from 97 % solvent A (0.1 % formic acid in 3 % acetonitrile) to 35 % solvent B (0.1 % formic acid in 97 % acetonitrile) at a flow rate of 300 nL/min for 40 mins. On-line mass spectrometry was done on a Maxis UHR-TOF (Bruker Daltonics, Coventry, UK) using profile MS with automatic dependent MS/MS data acquisition.

The nano LC-MS/MS data file corresponding to the incorporation experiment at natural isotopic abundance was used as input for database searching (Mascot software supplied by Matrix Science, London, UK) to identify the protein band and its component tryptic peptides. The ^{13}C-incorporation ratios in the samples were determined by comparison of the observed isotope distribution pattern of the representative peptide with the theoretical isotope distribution pattern generated using IsoPro v3.1 (http://sites.google.com/site/isoproms).

3.3 Results

3.3.1 Cells containing carotenoids display strong resonance Raman effect

The absorption spectrum of *Synechocystis* sp. PCC 6803 in the visible range showed peaks at 440, 620 and 670 nm (Figure S3.3). Carotenoids absorb light in the 400 - 550 nm range [122], and the 532 nm laser for Raman excitation used in this study preferentially excites the carotenoids rather than the chlorophyll pigments.

RR spectra of carotenoid molecules display characteristic Raman bands: *v*1, *v*2 and *v*3 (Figure 3.1). The sharp and strong *v*1 (stretching mode of the C=C bonds at about 1515 cm^{-1}), *v*2 (stretching mode of the C-C bonds at about 1155 cm^{-1}) and *v*3 (deformation of the methyl groups at about 1003 cm^{-1}) peaks can be unambiguously assigned to carotenoids [31, 119, 123]. The position of the *v*1 band varies according to the length of the conjugated carbon chain of carotenoids [31, 54, 119, 123]. The *v*2 band varies depending on the molecular conformation, and the *v*3 band is related to the carotenoid methyl groups [31, 54, 119, 123]. With the 532 nm laser excitation, the RR bands of carotenoids were so strong that the SCRR spectra of carotenoid-containing microorganisms predominantly displayed the *v*1, *v*2 and *v*3 Raman bands. The positions of the *v*1 band, in particular, varied significantly amongst different microorganisms, with the *v*2 and *v*3 bands also affected to a lesser extent (Figure 3.1). We noted a variation of 17.2, 1.7, and 4.9 cm^{-1} for *v*1, *v*2 and *v*3 band, respectively.

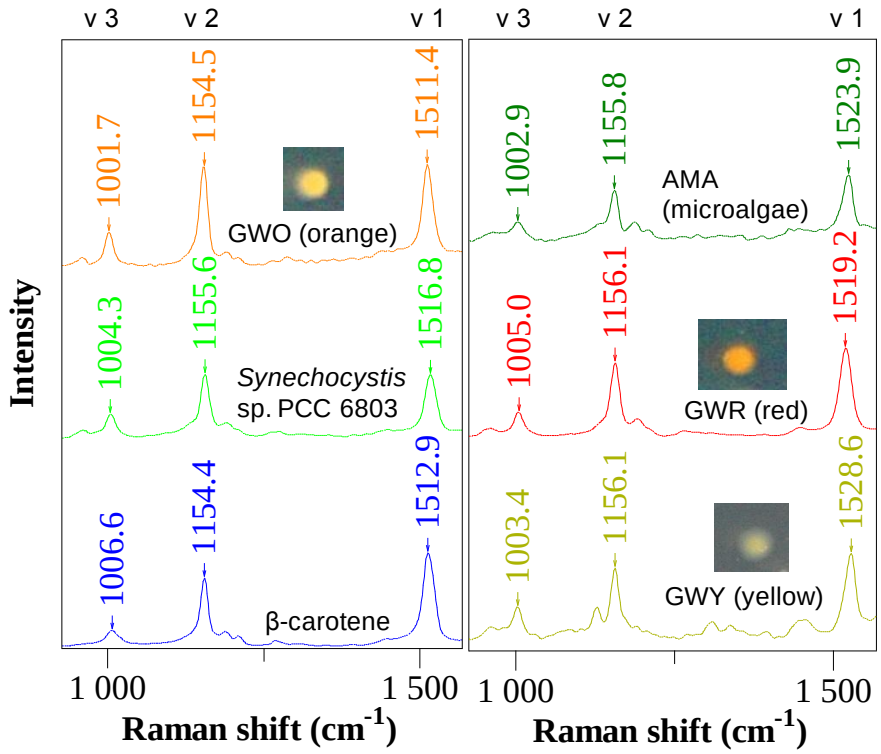

Figure 3.1 SCRR spectra of *Synechocystis* sp. PCC 6803, microalgae and bacteria with carotenoid pigments.
The dominant Raman bands of SCRR spectra were from carotenoids, as shown by comparison with the spectrum of pure β-carotene.

3.3.2 The red-shift of SCRR spectra due to ^{13}C- incorporation

Figure 3.2 shows the SCRR spectra of *Synechococcus elongatus* PCC 7942 and *Synechocystis* sp. PCC 6803 grown in media supplemented with different proportions of ^{13}C-bicarbonate. The RR bands of both species displayed Raman red-shift, the extent of which was dependent on the level of ^{13}C-bicarbonate in the growth media. For *Synechococcus elongatus* PCC 7942, the ν1, ν2 and ν3 bands shifted from 1522.0, 1157.7 and 1006.0 cm^{-1} to 1484.9, 1128.2 and 989.5 cm^{-1}, respectively (Figure 3.2). For *Synechocystis* sp. PCC 6803, the *ν*1, *ν*2 and *ν*3 bands shifted from 1516.8,

1155.6 and 1004.3 cm^{-1} to 1480.9, 1125.3 and 988.6 cm^{-1}, respectively (Figure 3.2). In the range of 1.1 - 98 % ^{13}C, the *v*1 band had the greatest (about 36 cm^{-1}) and the *v*3 band had the smallest (about 16 cm^{-1}) red-shift; the *v*2 band had an intermediate red-shift measured about 30 cm^{-1} (Table 3.1). This experiment encompasses the full range of labelling considering that the natural abundance of ^{13}C is 1.1 % and the ^{13}C content in ^{13}C-sodium bicarbonate supplied by Sigma-Aldrich UK is 98 %.

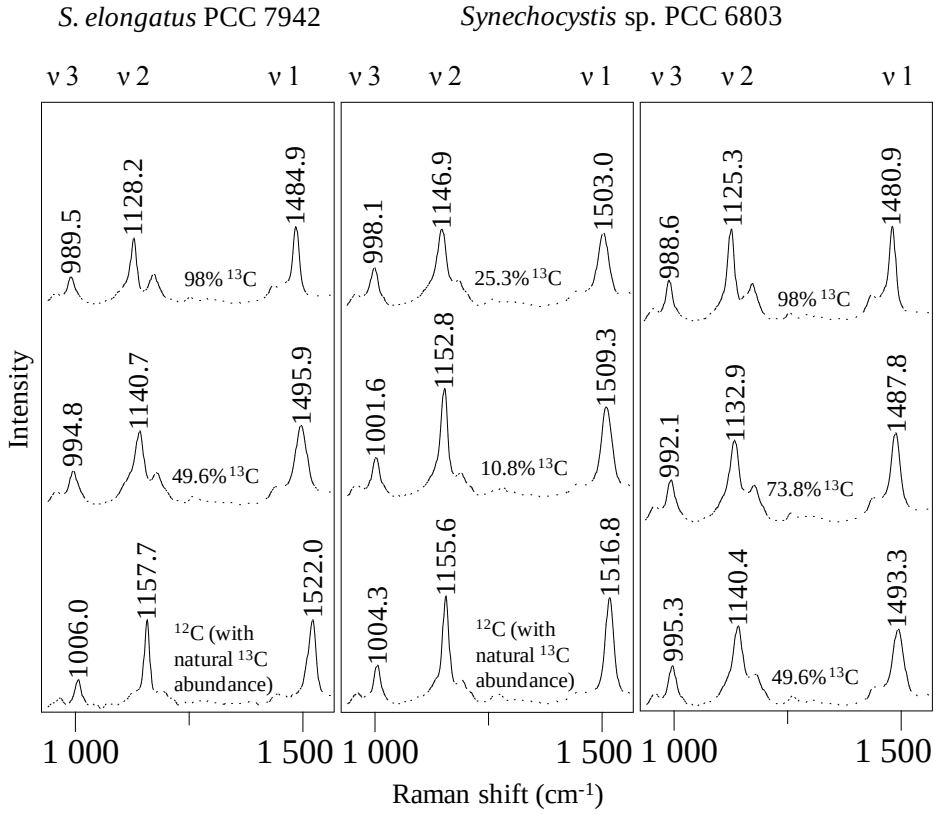

Figure 3.2 RR spectra of *S. elongatus* PCC 7942 and *Synechocystis sp.* PCC 6803 grown in media containing different percentages of ^{13}C-bicarbonate.

Table 3.1 Raman red-shift due to ^{13}C-incoporation (cm^{-1})

Carotenoid bands	*Synechococcus elongatus* PCC 7942	*Synechocystis* sp. PCC 6803
*v*1	37.1	35.9
*v*2	29.5	30.3
*v*3	16.5	15.7

Figure 3.3 shows that the extent of the red-shift of the ν1, ν2 and ν3 Raman bands was proportional to the ^{13}C content of cells, suggesting that the spectral red-shift can be used as a quantitative marker for ^{13}C-incorporation. Linear regression of data obtained from twenty randomly chosen single cells from three biological replicates (Figure 3.3) demonstrated that the three Raman bands shifted in a linear manner (linear regression $R^2 > 0.9$). It is notable that the red-shifts of the *Synechocystis* sp. PCC 6803 bands show distinguishable differences between the ^{12}C (containing natural abundance of 1.1 % ^{13}C) and 10.8 % ^{13}C-cells (Figure 3.3). The t-tests of the ν1, ν2 and ν3 bands between the ^{12}C and 10.8 % ^{13}C samples indicate that these differences were significant (P-values < 0.001). The slopes of the ν1, ν2 and ν3 regression lines of *Synechococcus elongatus* PCC 7942 and *Synechocystis* sp. PCC 6803 were slightly different (Figure 3.3). However, for each cell type the ν1, ν2 and ν3 bands show a stepwise shift to lower energy wavenumbers with increasing ^{13}C content in cells (Figure 3.2 and Figure S3.4), which makes it possible to establish a calibration to estimate the ^{13}C content of a single cell based on its RR spectrum (Figure 3.3). PCA was carried out using the whole SCRR spectra and the results showed

distinct separations amongst samples with different ^{13}C content (Figure S3.5). The largest PCA loadings at axis 1 and 2 were associated with the ν1 and ν2 bands, indicating that these spectral features are the most important factors for the classification of the SCRR spectra based on their ^{13}C content.

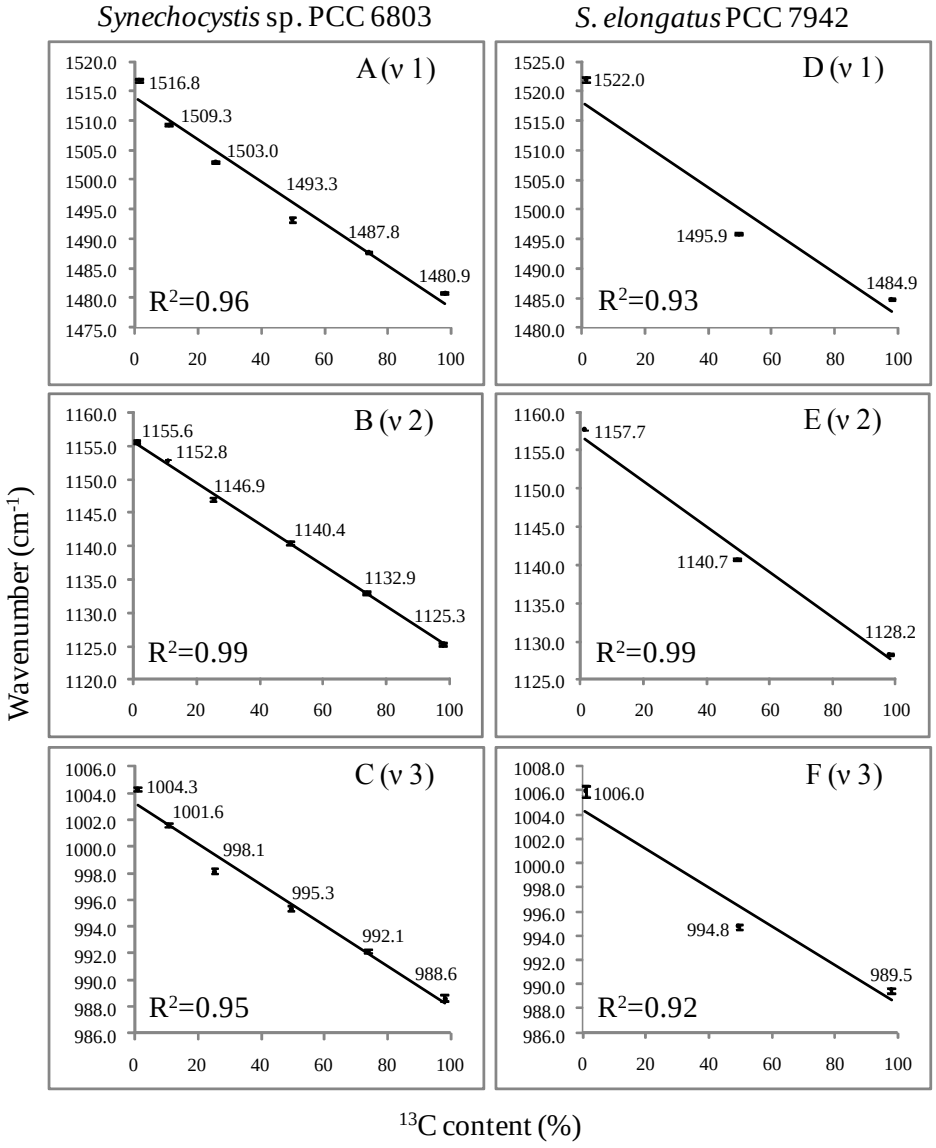

Figure 3.3 Liner relationship between Raman red-shift and ^{13}C content. Linear regression of the red shift of the ν1 (A), ν2 (B) and ν3 (C) bands of the ^{13}C-incorporated *Synechocystis* sp. PCC 6803 single cells and the ν1 (D), ν2 (E) and ν3 (F) bands of the ^{13}C-incorporated *S. elongatus* PCC 7942 single cells. Error bars show the standard error of 20 replicates.

3.3.3 Mass spectrometry results of the ^{13}C-incorporation in cells matched SCRR analysis

Mass spectrometry (MS) was applied to analyse ^{13}C-incorporation in *Synechocystis* sp. PCC 6803. MS analysis of extracted proteins was used to determine the levels of ^{13}C-incorporation in cells. The MS spectra of a representative peptide GGTQGIVGTTAANLNR $[M+2H]^{++}$ identified in the protein Slr1841 of *Synechocystis sp.* PCC 6803 grown in 1.1, 10.8, 49.6 and 98 % ^{13}C is shown in Figure 3.4. The mass shift observed in the MS spectra is due to ^{13}C-incorporation in the peptide (Figure 3.4). The percentage of ^{13}C-incorporation was determined by comparing the observed and theoretical isotopic distribution patterns. The results showed that ^{13}C content in the peptide were 1.1, 13, 54 and 96 %, respectively (Figure 3.4 and Figure S3.6). The SCRR spectral analysis of 20 randomly chosen single cells from each sample indicated that the corresponding samples contained respectively 1.1±0.4, 9.4±0.5, 51±0.7 and 95±0.6 % of ^{13}C incorporated in the cells according to the calibration lines established in Figure 3.3. The results verified that the ^{13}C content of single cells measured by SCRR spectroscopy indeed reflect the ^{13}C-incorporation percentages in the whole cells.

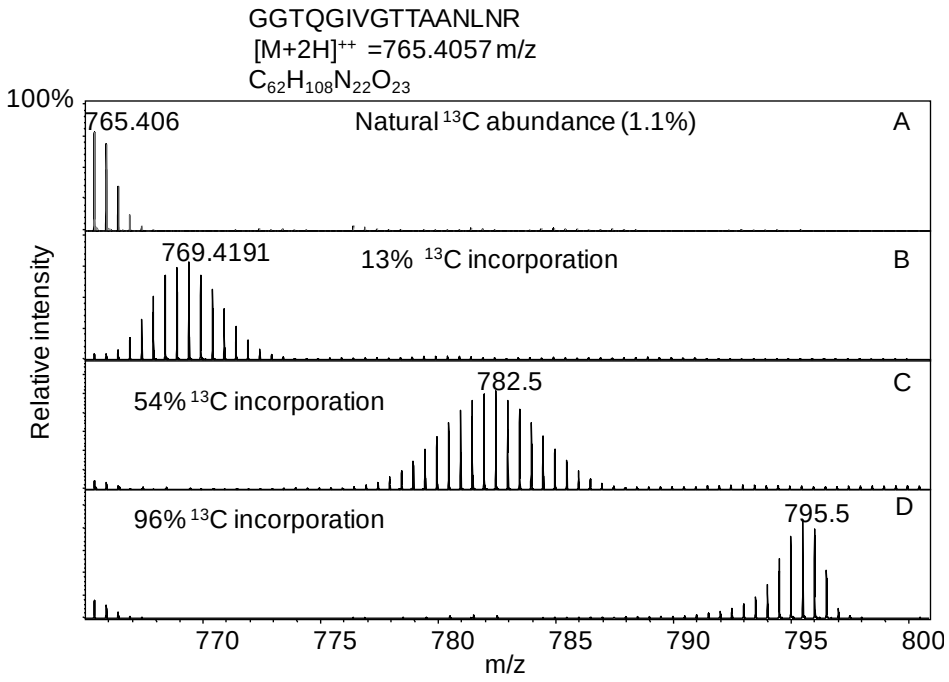

Figure 3.4 Mass spectra of a representative peptide.
Mass spectra of peptide GGTQGIVGTTAANLNLR in protein Slr1841 of *Synechocystis* sp. PCC 6803 with different ^{13}C-incorporation ratios. The mass-charge ratios of the modal ions are labelled.

3.3.4 Raman images differentiate cells with different levels of ^{13}C-incorporation

To demonstrate the potential of RR spectroscopy as an *in situ* functional imaging technique for photosynthetic microorganisms, two-dimensional Raman imaging was carried out on the three different cyanobacterial cell mixtures described in the Materials and Methods section (Figure 3.5). The spectra shown in Figure 3.5 are SCRR spectra taken at the centre of the circled cells with a 1 ms acquisition time. The optical images matched with the pseudo-colour Raman images as the green colour and the red/yellow colour indicate the locations of ^{12}C- and ^{13}C-incorporated single cells, respectively (Figure 3.5). Figure 3.5A shows a clear difference between ^{12}C-

and 73.8 % ^{13}C-incorporated cells. The SCRR-based Raman imaging was sensitive enough to distinguish a subtle difference between cells with 1.1 % and 10.8 % ^{13}C content (Figure 3.5B and Figure 3.5C). As shown in Figure 3.5C, the Raman images based on RR spectra were consistent with the known morphology of rod-like *Synechococcus elongatus* PCC 7942 cells and spherical *Synechocystis* sp. PCC 6803 cells.

A

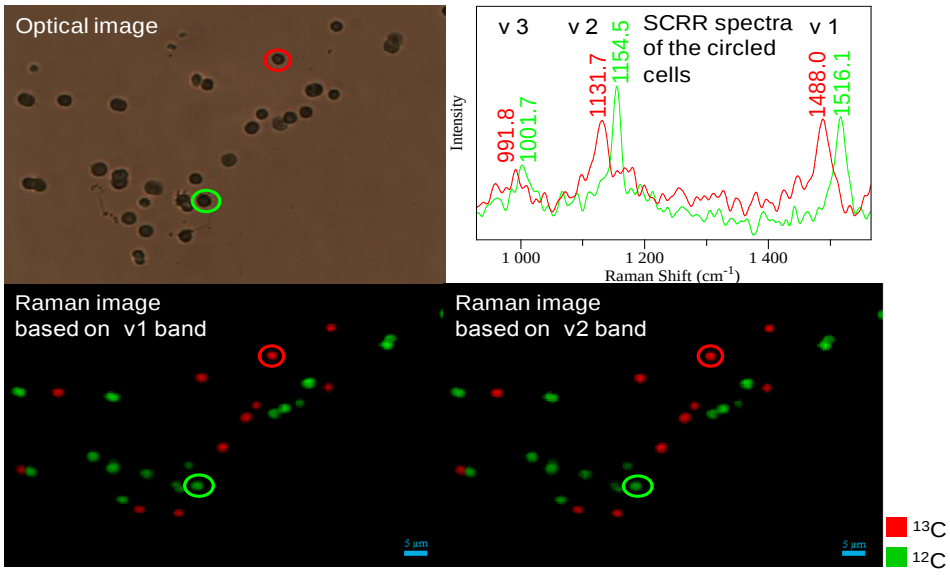
Optical image
v 3
v 2
SCRR spectra of the circled cells
v 1
991.8
1001.7
1131.7
1154.5
1488.0
1516.1
Intensity
1 000
1 200
1 400
Raman Shift (cm-1)
Raman image based on v1 band
Raman image based on v2 band
5 µm
13C
12C

B

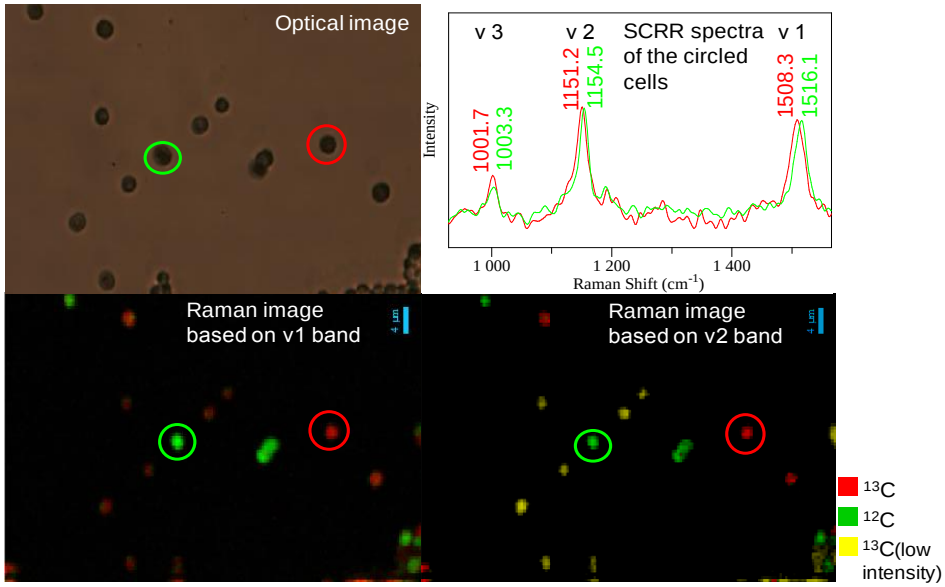
Optical image
v 3
v 2
SCRR spectra of the circled cells
v 1
1001.7
1003.3
1151.2
1154.5
1508.3
1516.1
Intensity
1 000
1 200
1 400
Raman Shift (cm-1)
Raman image based on v1 band
Raman image based on v2 band
4 µm
13C
12C
13C(low intensity)

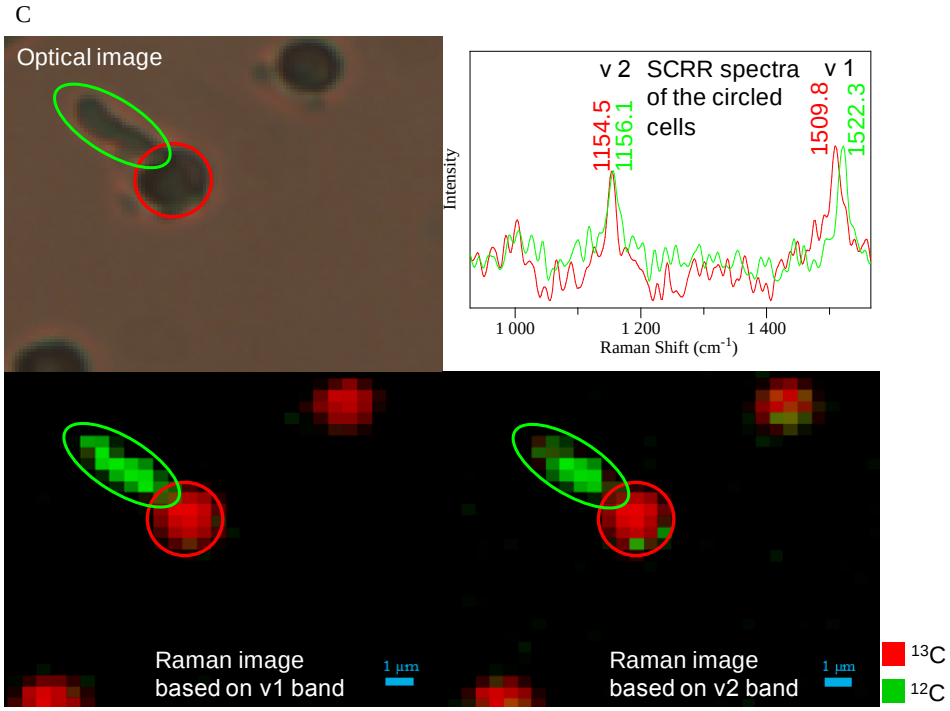

Figure 3.5 Raman images of mixed cell cultures with different ^{13}C content. *Synechocystis* sp. PCC 6803 grown in BG-11 medium supplemented with 73.8 % ^{13}C mixed with the same species grown in BG-11 medium supplemented with ^{12}C (A); *Synechocystis* sp. PCC 6803 grown in BG-11 medium supplemented with 10.8 % ^{13}C mixed with the same species grown in BG-11 medium supplemented with ^{12}C (B); *Synechocystis* sp. PCC 6803 grown in BG11 medium supplemented with 10.8 % ^{13}C mixed with *S. elongatus* PCC 7942 grown in BG-11 medium supplemented with ^{12}C (C). Two Raman images were generated for each mixture based on the ν1 and ν2 bands, respectively. ^{13}C-cells are displayed in red and ^{12}C-cells in green. Some ^{13}C-cells had lower signal strength and are displayed in yellow. SCRR spectra are coloured to correspond to the ^{13}C-cells and ^{12}C-cells indicated by red and green circles, respectively.

Figure 3.6 shows that Raman images can be used to distinguish ^{13}C-labelled microorganisms at single-cell level within a complex microbial community in real seawater samples. The sample incubated with ^{12}C-bicarbonate provided a reference to estimate ^{13}C content of diverse photosynthetic microorganisms (Figure 3.6A). The Raman images in Figure 3.6B and Figure 3.6C suggest that after 8 days' incubation with ^{13}C-bicarbonate,

some species have started to incorporate ^{13}C into their cell components. The Raman imaging results showed that the cells, tentatively identified as a microalga *Tetraselmis* sp. (cell 1b, 2b in Figure 3.6B and cell 2c in Figure 3.6C) and diatom *Phaeodactylum tricornutum* (cell 4c, a tip of this triradiate shaped microorganism in Figure 3.6C) were actively fixing inorganic carbon source. Some cells were potentially photosynthetic species (e.g. cell 3b in Figure 3.6B) but incorporated little ^{13}C into the cells. *Tetraselmis* sp. and *Phaeodactylum tricornutum* were identified and designated by Zhang [124]. Figure 3.6C shows that at least four different species had incorporated ^{13}C: *Tetraselmis* sp. strain, *Phaeodactylum tricornutum* and unidentified rod-shaped cells 1c and 3c, which show a red-shift of RR bands comparing with control cells grown in seawater with ^{12}C-bicarbonate. Based on the red-shift of the RR bands as shown in Figure 3.6B (cell 1b and 2b) and Figure 3.6C (cell 2c), *Tetraselmis* sp. strain was estimated to had incorporated approximately 20 % ^{13}C into cellular compounds after 8 days' incubation using the calibration lines in Figure 3.3. This estimation is based on the observation that the positions of the ν2 Raman bands in different species do not vary significantly as previously described.

A

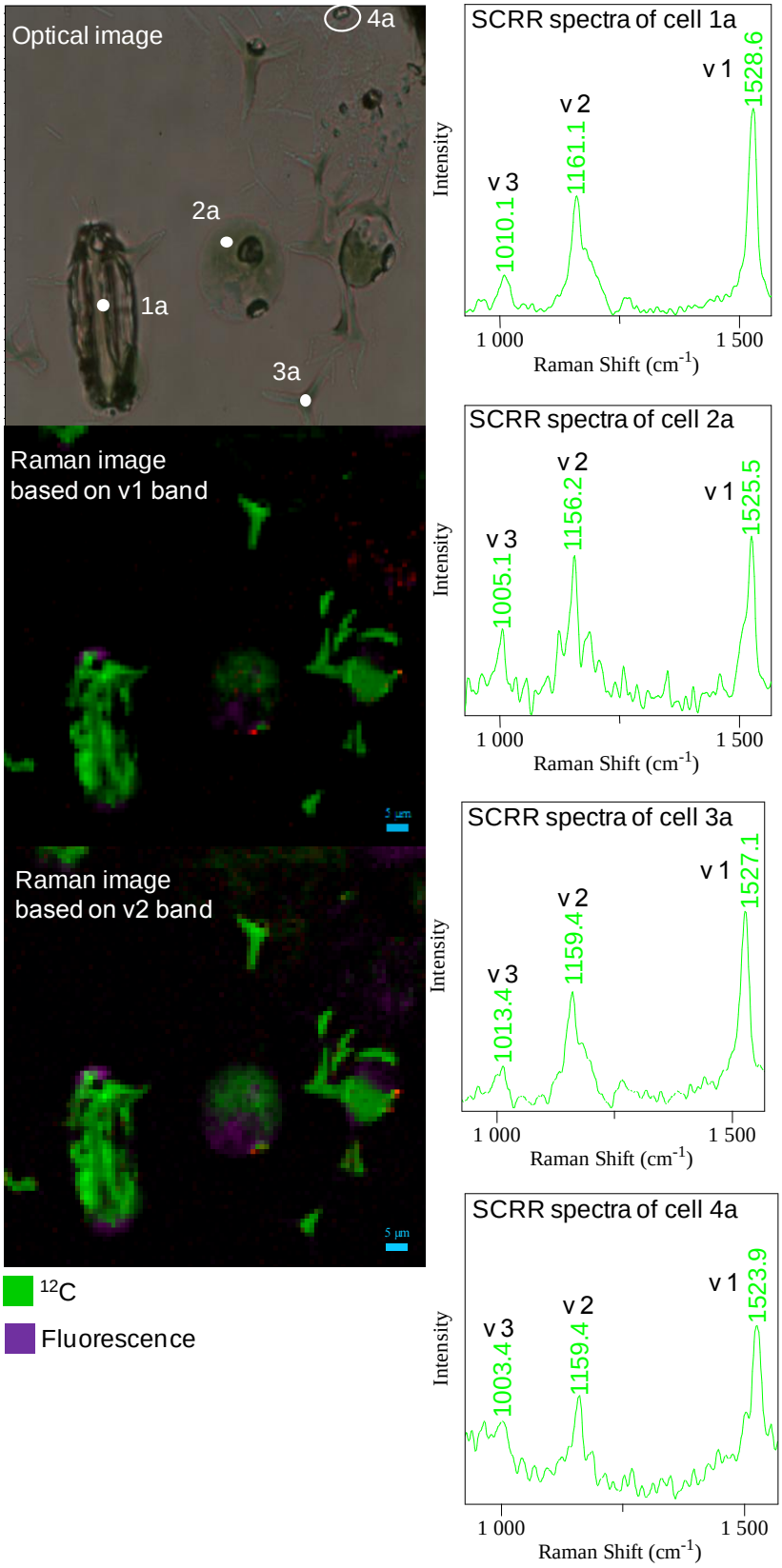
Optical image
4a
2a
1a
3a
Raman image
based on v1 band
5 µm
Raman image
based on v2 band
5 µm
12C
Fluorescence
SCRR spectra of cell 1a
v 1
1528.6
v 2
1161.1
v 3
1010.1
Intensity
1 000
1 500
Raman Shift (cm-1)
SCRR spectra of cell 2a
v 2
1156.2
v 1
1525.5
v 3
1005.1
Intensity
1 000
1 500
Raman Shift (cm-1)
SCRR spectra of cell 3a
v 1
1527.1
v 2
1159.4
v 3
1013.4
Intensity
1 000
1 500
Raman Shift (cm-1)
SCRR spectra of cell 4a
v 1
1523.9
v 2
1159.4
v 3
1003.4
Intensity
1 000
1 500
Raman Shift (cm-1)

B

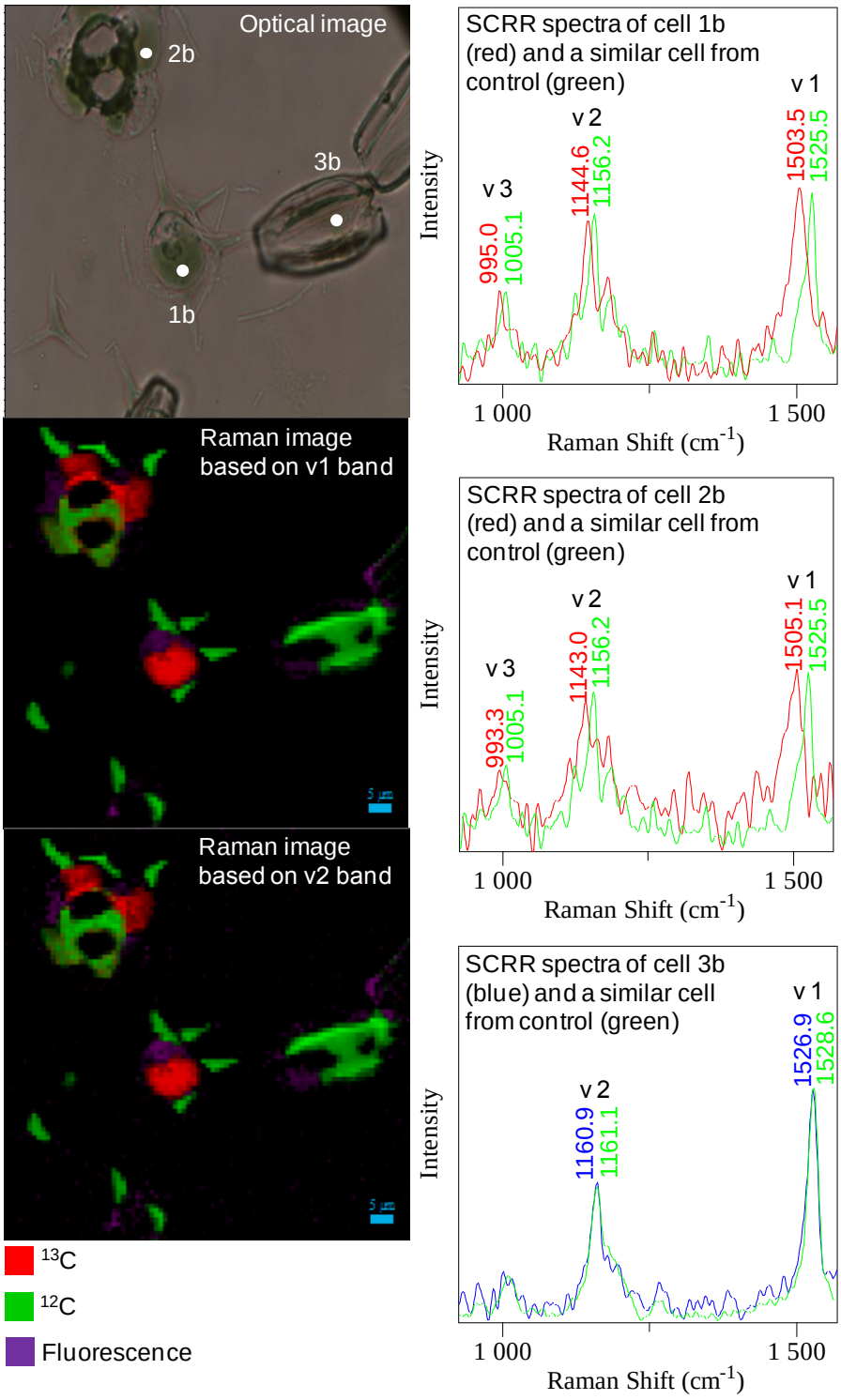
Optical image
2b
3b
1b
Raman image based on v1 band
Raman image based on v2 band
^{13}C
^{12}C
Fluorescence
SCRR spectra of cell 1b (red) and a similar cell from control (green)
v 1
v 2
v 3
1503.5
1525.5
1144.6
1156.2
995.0
1005.1
Intensity
1 000
1 500
Raman Shift (cm^{-1})
SCRR spectra of cell 2b (red) and a similar cell from control (green)
v 1
v 2
v 3
1505.1
1525.5
1143.0
1156.2
993.3
1005.1
Intensity
1 000
1 500
Raman Shift (cm^{-1})
SCRR spectra of cell 3b (blue) and a similar cell from control (green)
v 1
v 2
1526.9
1528.6
1160.9
1161.1
Intensity
1 000
1 500
Raman Shift (cm^{-1})

C

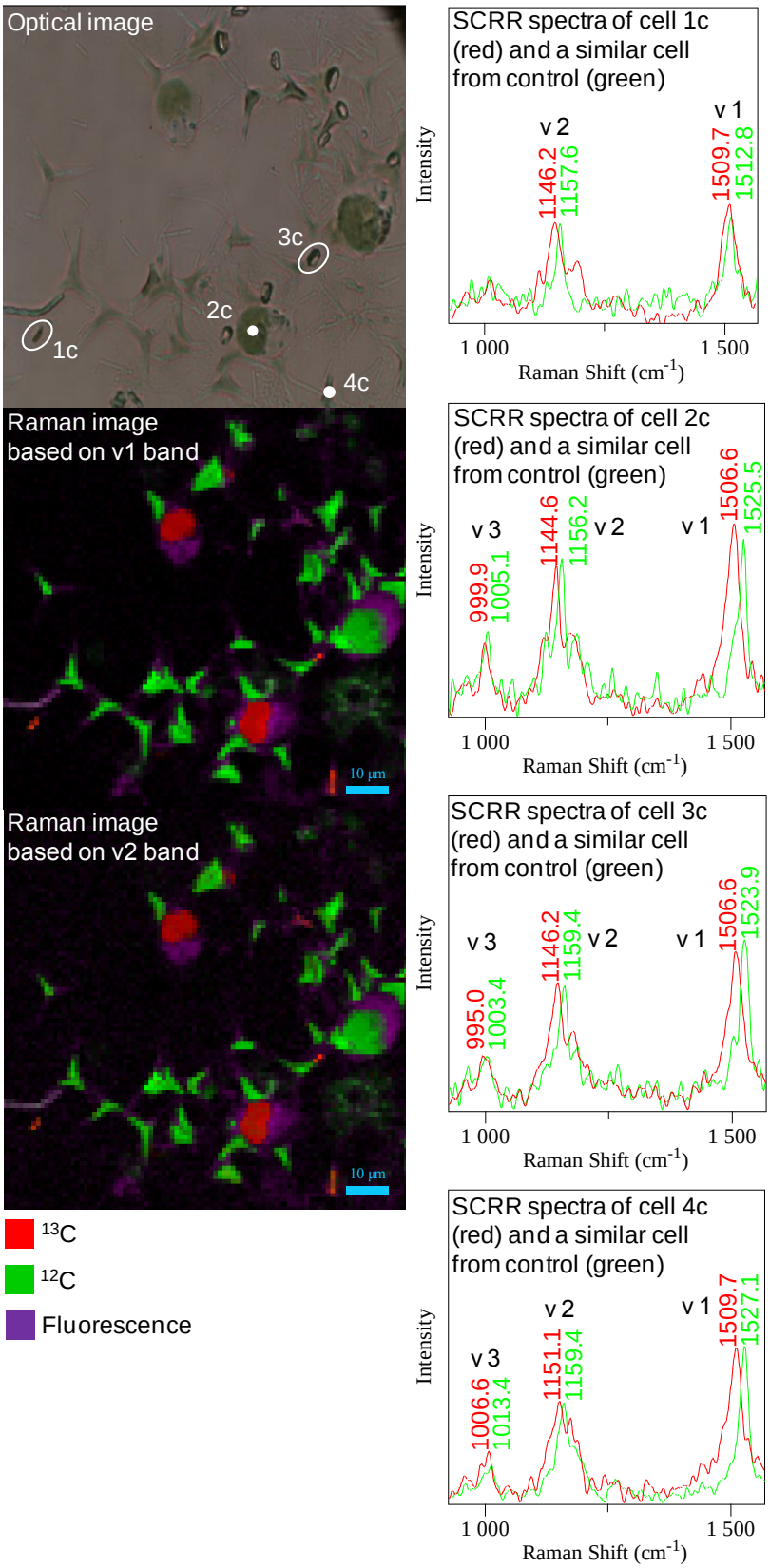
Optical image
3c
2c
1c
4c
Raman image
based on v1 band
10 µm
Raman image
based on v2 band
10 µm
13C
12C
Fluorescence
SCRR spectra of cell 1c
(red) and a similar cell
from control (green)
Intensity
v 2
1146.2
1157.6
v 1
1509.7
1512.8
1 000
1 500
Raman Shift (cm-1)
SCRR spectra of cell 2c
(red) and a similar cell
from control (green)
Intensity
v 3
999.9
1005.1
1144.6
1156.2
v 2
v 1
1506.6
1525.5
1 000
1 500
Raman Shift (cm-1)
SCRR spectra of cell 3c
(red) and a similar cell
from control (green)
Intensity
v 3
995.0
1003.4
1146.2
1159.4
v 2
v 1
1506.6
1523.9
1 000
1 500
Raman Shift (cm-1)
SCRR spectra of cell 4c
(red) and a similar cell
from control (green)
Intensity
v 3
1006.6
1013.4
v 2
1151.1
1159.4
v 1
1509.7
1527.1
1 000
1 500
Raman Shift (cm-1)

Figure 3.6 Raman images of a seawater sample.
Raman images of the seawater sample that was grown in original sea water supplemented with 2 mM ^{12}C-bicarbonate (A) and 2 mM ^{13}C-bincarbonate (B, C). Two Raman images were generated based for each sample on the ν1 and ν2 bands, respectively. ^{13}C-cells are displayed in red. Purple colour indicates the fluorescent region of the cells. SCRR spectra corresponding to the marked cells are shown.

3.4 Discussion

Raman spectra from single cells can be used as an intrinsic chemical 'fingerprint' without external labelling [20, 26, 44, 57, 58, 78, 81, 82]. However, broad application of Raman spectroscopy in environmental microbiology is hindered by the naturally weak Raman signal. This study has demonstrated that by using carotenoids as internal markers, SCRR combined with SIP can distinguish and image CO_2 fixing cells on a millisecond timescale. This method is also suitable for the *in situ* identification and imaging of CO_2 fixing photosynthetic microorganisms in a quantitative manner and will therefore pave the way for the development of a Raman cell sorting device for metabolic analysis of large numbers of environmentally derived uncultured cells.

Cyanobacteria are the largest, most diverse and widely distributed group of photosynthetic prokaryotes [125]. In this study, *Synechococcus elongatus* PCC 7942 and *Synechocystis* sp. PCC 6803 were used as model photosynthetic microorganisms to test the SCRR-SIP methodology. SCRR-SIP was then applied to identify microorganisms that were actively fixing CO_2 in real seawater samples (Figure 3.6), confirming that this technique

could be used to identify and isolate key photosynthetic microorganisms that carry out CO_2 fixation in aquatic environments.

In order to establish a reliable quantitative measurement of the ^{13}C content of photosynthetic microorganisms based on the red-shift of SCRR, it was essential to grow cyanobacterial strains under conditions that minimise the effect of atmospheric CO_2. Preliminary data showed that *Synechocystis* sp. PCC 6803 appears to utilise CO_2 dissolved from the air rather than ^{13}C-bicarbonate in the growth medium. To eliminate any potential influence of CO_2 from the atmosphere, the procedure described in this study was used.

SIP is a method widely used to study carbon and nitrogen flow in ecosystems. Introducing stable isotope compounds into an environmental sample allows researchers to determine which organisms incorporate the substrates of interest. Both mass spectra and vibrational spectra can be used in combination with SIP for single cells. In terms of sensitivity, spatial resolution and quantitative detection, mass spectra-based methods such as secondary ion mass spectrometry (SIMS) are superior over those based on vibrational spectra such as Raman spectroscopy. However, SCRR is a non-invasive method and provides chemical profiles of cells, whilst SIMS is a destructive technique and detects atoms and small ions but not molecules [58]. Nucleic acid-SIP is an effective method for revealing microbial ecological functions in native environments [57, 126-129]. It usually employs equilibrium density gradient centrifugation to separate and analyse ^{13}C-containing nucleic acids [57, 126-129]. Due to the subtle differences in the physical properties between stable isotopes, it will be a challenge to use

the centrifugation-based SIP method for the isolation of ^{13}C-incoporated DNA or RNA if the ^{13}C content in nucleic acids is less than about 50 %. However, in this study, we have demonstrated that SCRR-SIP was sufficiently sensitive to distinguish between cells with 10 % and 1.1 % ^{13}C content (Figure 3.3, Figure 3.4 and Figure S3.4). Applying the SCRR-SIP technique to real environmental samples also demonstrated that it was able to distinguish photosynthetic cells with only about 20 % ^{13}C content (Figure 3.6). Such a high sensitivity suggests that this technique may be useful in the following applications: 1) detection of ^{13}C-incorporated single microbial cells at early stage of incubation, avoiding the cross-feeding problem in SIP and aiding the identification of the species that fix CO_2; 2) observation of the dynamics of ^{13}C-incorporation in different species by taking SCRR spectra or Raman images at different time points during the incubation. In *Synechocystis*, the measured red-shifts of the *v*1 and *v*2 bands at 10 % ^{13}C-incorporation were 7.5 and 2.8 cm^{-1} respectively, indicating that SCRR-SIP may be able to detect ^{13}C-incorporation at levels even lower than 10 %. SCRR-SIP is a non-invasive technique that enables the recovery of cells after measurement. This is especially useful for the study of unculturable microorganisms. For example, the two unknown rod-shaped bacteria identified in Figure 3.6C appeared to fix CO_2 but so far they have not been cultured, and further work is needed to confirm their photosynthetic ability. In certain habitats, a few species of non-photosynthetic chemolithotrophic bacteria which also contain carotenoids have been reported, though these types of bacteria appear to be rare [130]. In marine ecosystems, it is also

increasingly clear that non-photosynthetic autotrophic bacteria are widespread in, for example, oxygen minimum zones [131]. Thus it is also possible that autotrophic non-photosynthetic bacteria exist, and, interestingly, could be detected by this approach if used in future studies. The ν2 Raman bands appeared to vary in a narrower range (usually a few wavenumbers) in different species, making it a potential marker for ^{13}C-incoporation in unidentified photosynthetic microorganisms. However, for samples that consist of unknown species, the error of detection of ^{13}C-incorporation can be raised due to the uncertainty in the position of the RR bands, affecting the estimation of ^{13}C-incorporation ratios. This indicates that a further investigation on the variation of the ν2 RR bands in different carotenoid-containing cells is required.

To search and screen large numbers of single cells from environmental samples, a rapid Raman imaging technique has great potential. Taking Figure 3.5A as an example, a 90.5 × 74.7 μm Raman image that consists of 27,000 Raman spectra/pixels was generated in about 5 minutes with 1 ms acquisition time per pixel. If we assume a grid of 2 μm × 2 μm contains a single cell, up to 10,000 single cells can be imaged in about 30 min. The Raman imaging time can be further reduced by using a more powerful computer, an optimised CCD detector and a refined spectrum readout strategy. It may also be possible to combine a laser micro-dissection system with this technique to selectively dissect and collect single microorganisms of interest for cultivation, genomic amplification and sequencing. In such a way Raman imaging may provide a direct metabolic profiling method for

environmental samples without cultivation, and could help to reveal the precise ecological role of large numbers of unstudied and uncultured microorganisms.

3.5 Supplementary figures

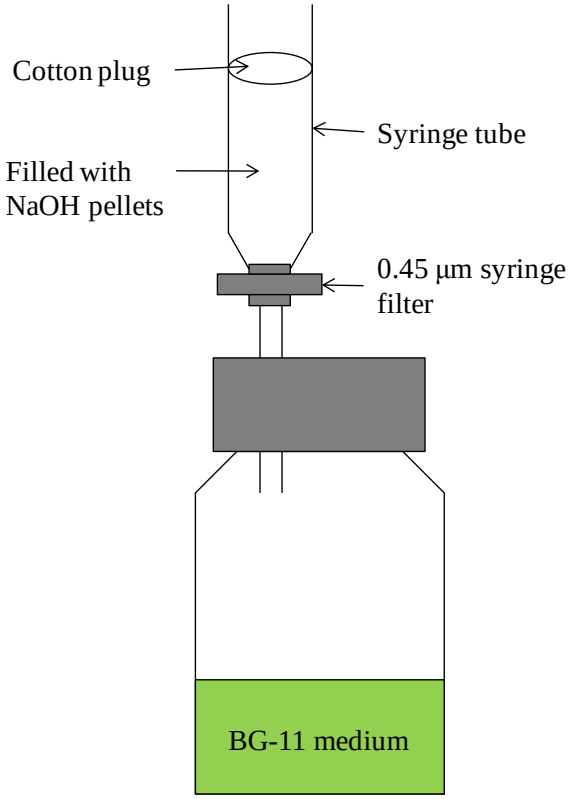

Figure S3.1 Degasification device for BG-11 medium.

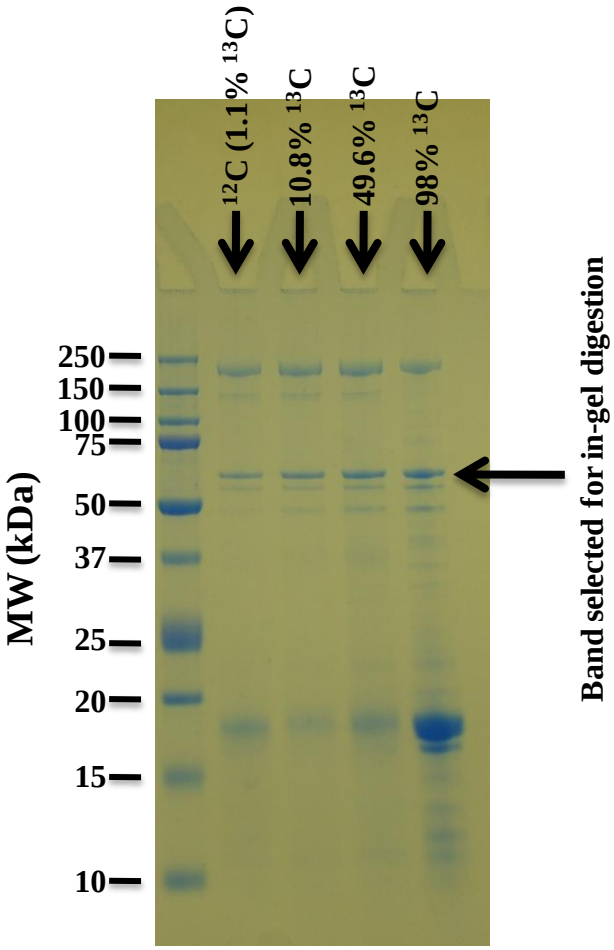

Figure S3.2 NuPAGE Bis-Tris gel of protein extracted from *Synechocystis* sp. PCC 6803 cells.

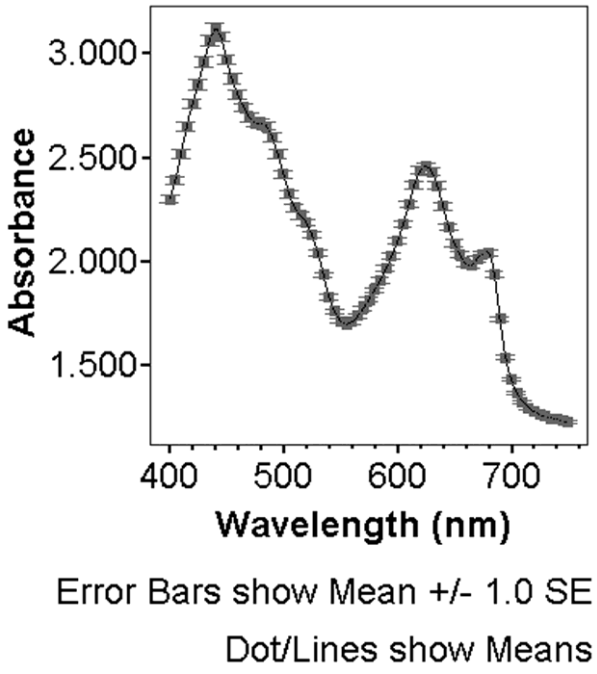

Figure S3.3 Light absorption spectrum of *Synechocystis* sp. PCC 6803 cells.

Synechocystis sp. PCC 6803

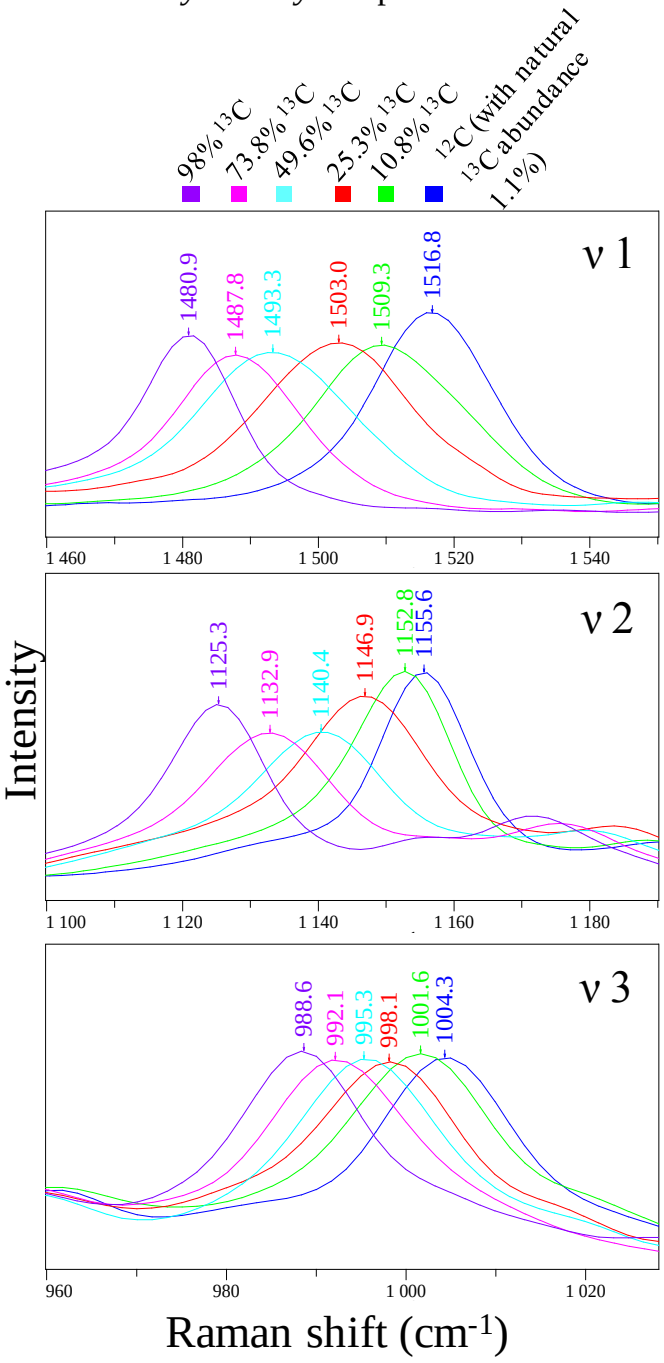

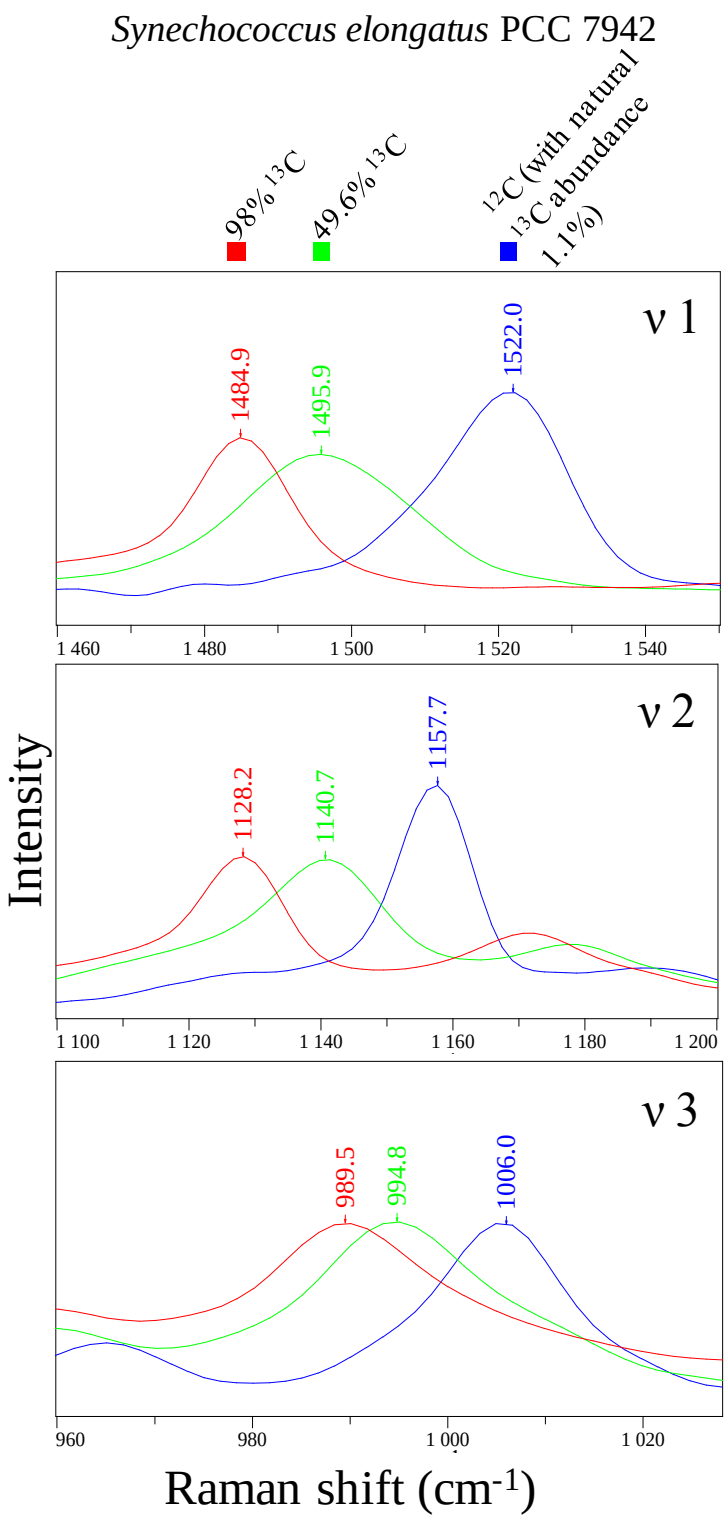

Figure S3.4 Raman red-shift of the three RR bands.

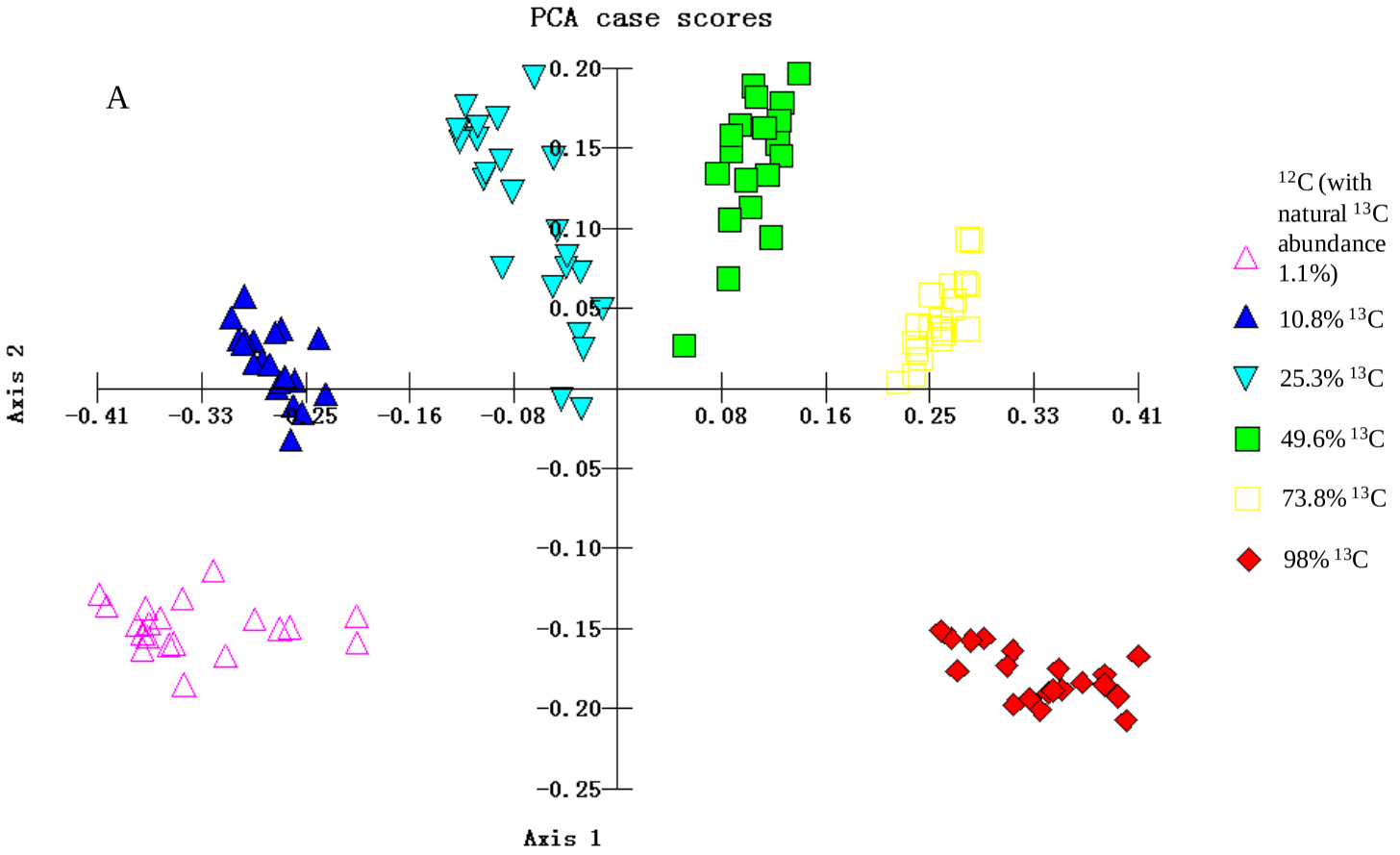
A
PCA case scores
Axis 2
Axis 1
0.20
0.15
0.10
0.05
-0.05
-0.10
-0.15
-0.20
-0.25
-0.41
-0.33
-0.25
-0.16
-0.08
0.08
0.16
0.25
0.33
0.41
12C (with natural 13C abundance 1.1%)
10.8% 13C
25.3% 13C
49.6% 13C
73.8% 13C
98% 13C

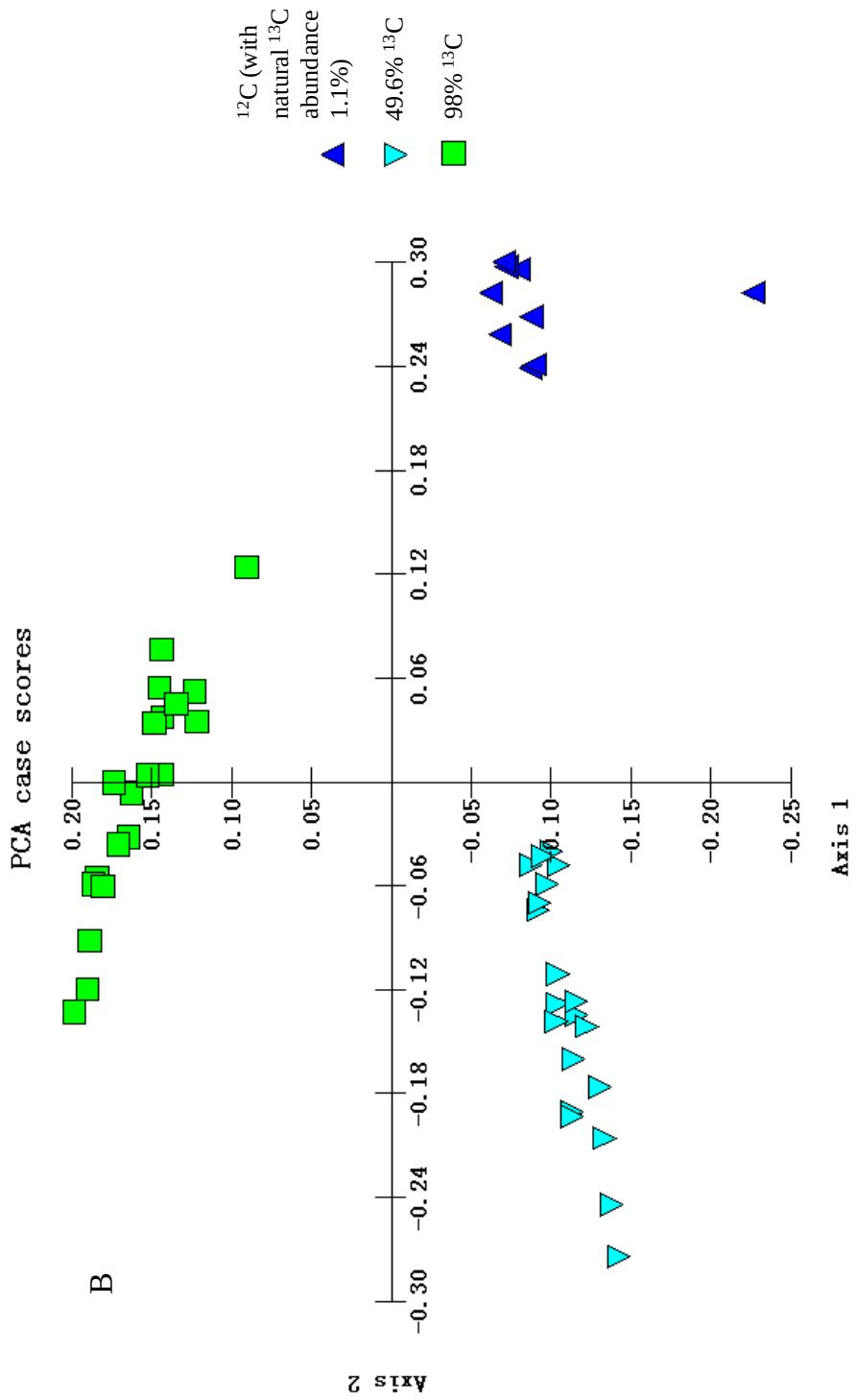

Figure S3.5 PCA results of SCRR spectra of *Synechocystis* sp. PCC 6803 (A) and *Synechococcus elongatus* PCC 7942 (B).

Observed isotopic cluster distributions of the peptide

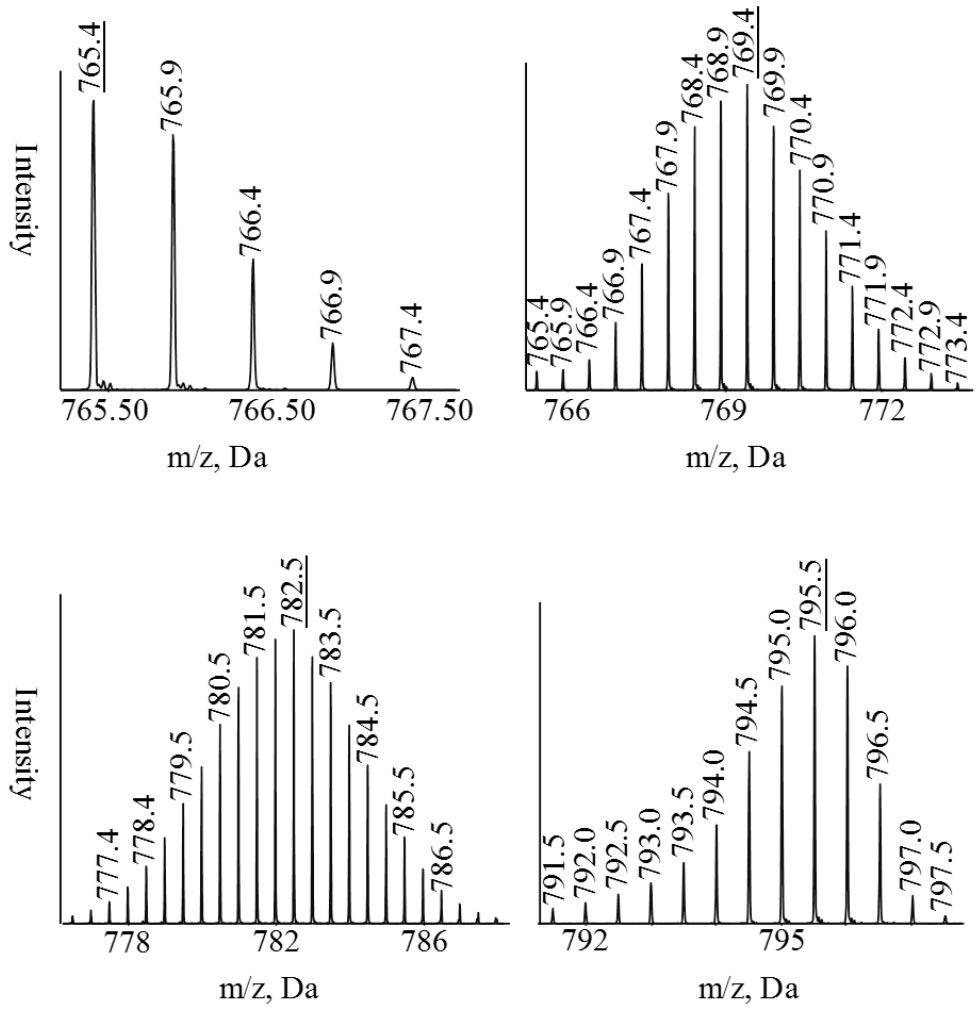

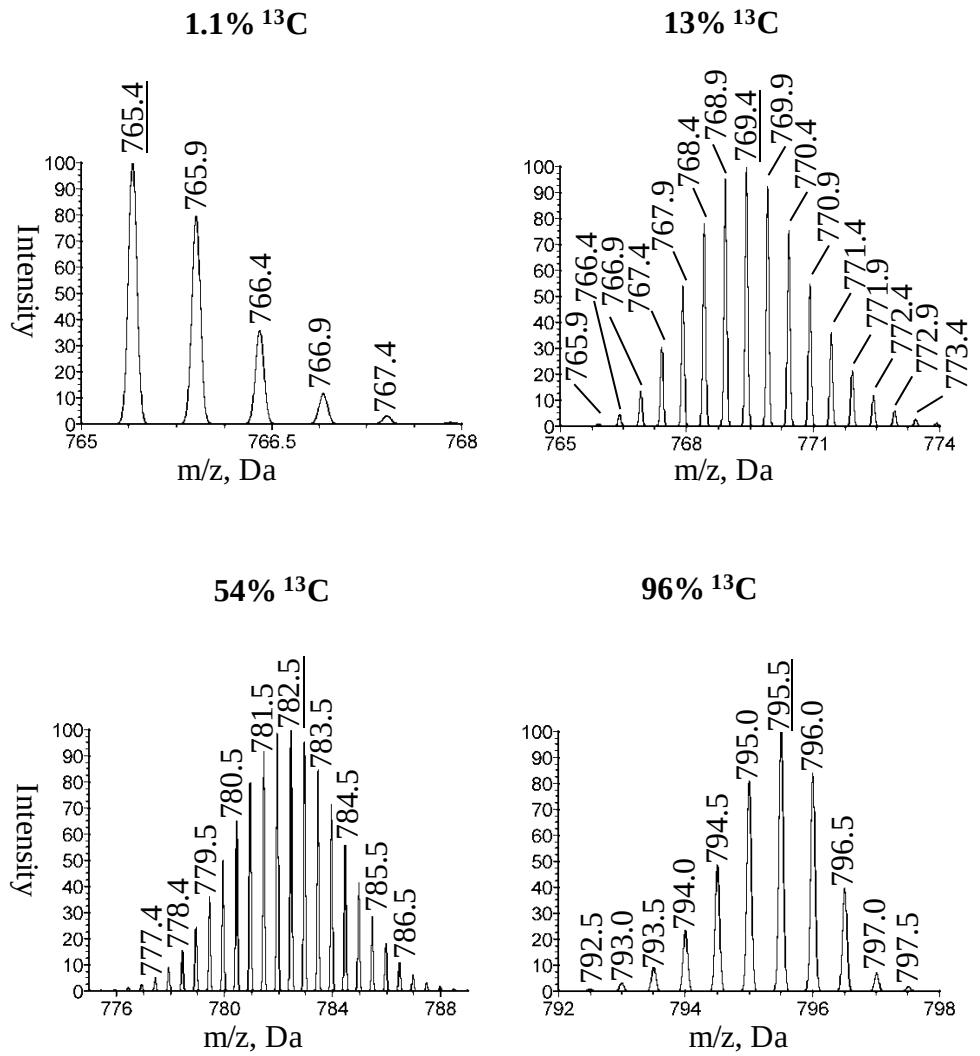

Figure S3.6 Comparison between observed and theoretic isotopic distributions of the representative peptide extracted from *Synechocystis* sp. PCC 6803.

Chapter 4: Synthesis of silver and gold nanoparticles for the application of surface enhanced Raman scattering in environmental microbiology research

4.1 Introduction

Surface enhanced Raman scattering (SERS) was discovered in the 1970s [132-134]. In these pioneering SERS experiments, enhancement factors of 10^5 - 10^6 were achieved from pyridine on the surface of a silver electrode. The general method to achieve a good SERS response is making a 'direct' or very close contact (less than 10 nm) between sample and SERS-active surfaces [37]. There are a variety of methods to prepare SERS-active surfaces and deposit samples on them [135-137].

Like normal, or spontaneous, Raman spectroscopy, SERS has been used to generate unique chemical fingerprints of microorganisms [40, 138-145], and an excellent review article on this subject has been written [146]. The SERS effect takes place on roughened metal substrates and silver or gold are the most commonly used materials; patterned gold or silver surface and colloidal nanoparticles are often used as the SERS-active surfaces [147]. It has been generally agreed that there are two mechanisms that can contribute to SERS. Major enhancement comes from an electromagnetic mechanism based on the resonance of metal surface plasmon and the incident radiation; the charge transfer between the sample molecules and the metal substrate

may also enhance Raman signal [135, 136, 148]. In some SERS experiments, an enhancement factor up to 10^{14} was achieved, therefore single molecules could be detected by Raman spectroscopy [35, 72, 149]. A recent article provided more details about single molecule detection by SERS [150].

In practice, SERS can be implemented together with other types of Raman spectroscopy to suit specific purposes, for example, surface enhanced resonance Raman scattering (SERRS) [151-154], surface enhanced hyper Raman scattering (SEHRS) [155, 156], and tip enhanced Raman scattering (TERS, a combination of SERS and atomic force microscopy) [157-160]. Thanks to its high sensitivity, SERS can be used as a rapid detection of the intrinsic chemical signatures of microorganisms. Comparing with fluorescence, which also gives strong signal, SERS provides molecular structural information as well as high signal to noise ratio.

Zeiri and co-workers reported that by using aqueous redox reactions of $AgNO_3$ and $NaBH_4$, silver particles can be deposited on bacteria or synthesised inside bacteria; the consequent SERS spectra show high similarity between different bacteria species; these spectra are mainly from cell surface and dominated by riboflavin's SERS signature [73, 142, 146]. Jarvis and Goodacre, for the first time, generated robust SERS signals from bacteria to allow the differentiation of microorganisms at species and strain levels [40]. Jarvis and co-workers recently reported that by using the ability of the bacterium *Geobacter sulfurreducens* to provide electron chain to extracellular metal ions reduction, silver particles can be deposited on cell

surface, and by an unclear mechanism gold particles can be generated inside cells, SERS spectra were recorded from both silver and gold labelled cells [138]. Premasiri and co-workers recorded SERS spectra of bacteria of different species by depositing cells on a gold nanoparticle-coated SiO_2 surface [161]; Patel and co-workers followed the same method to obtain SERS spectra of bacteria and demonstrated its potential capability to rapidly identify pathogens [162]. Kao and co-workers obtained reproducible SERS spectra from two bacterial strains on a gold/silver roughened surface and demonstrated that differences in SERS spectra can be observed between Gram-positive and Gram-negative bacteria [163]. Sujith and co-workers observed SERS spectra from silver nanoparticles-labelled living yeast cells and reported both spatial and temporal fluctuations in SERS spectra [164]. Shanmukh and co-workers obtained SERS spectra from different viruses deposited on a rough silver surface and achieved differentiation amongst different species [165].

Other than using SERS to obtain whole-microorganism spectra, its ultrahigh sensitivity can be used to probe specific biological molecules in novel molecular biological techniques, DNA/protein microarray and DNA sequencing, for example. SERS also makes microarrays more ‘colourful’: unlike fluorescent probes which often emit broad and overlapping bands, one can build more powerful multiplex assays with SERS probes because vibrational spectra contain much more information than fluorescence spectra. Sheng and co-workers developed and Reversed-Phase High Performance Liquid Chromatography (HPLC) coupled with Raman

spectrometer and used SERS to detect purine bases at nmol / mmol level [166]. Vo-Dinh and co-workers synthesised a new SERS gene probe by attaching a Raman chromophore to DNA fragments and DNA hybridised with this probe was detected on a SERS-active substrate [167]; Isola and co-workers used similar SERS gene probe as primer in polymerase chain reaction (PCR) and gene sequences of Human immunodeficiency virus (HIV) were detected by a similar method [168]. Kneipp and co-workers demonstrated that without introducing any external labelling, a single adenine molecule was detected by SERS spectra [33]. Cao and co-workers developed a SERS-based DNA microarray by hybridising SERS-active particles with immobilised DNA on a chip; these particles were gold nanoparticles functionalised with oligonucleotides and Raman chromophores [169]. Chen and co-workers developed a protein microarray based on SERS spectra of functionalised ^{12}C and ^{13}C carbon nanotubes [170]. SERS, as a vibrational spectroscopic method, may also be used to investigate distortion in enzyme complexes because the slight changes in chemical bonds are hardly detectable by other method, for instance, X-ray crystallography and nuclear magnetic resonance (NMR) [171].

SERS has brought many new techniques and insights into microbiology and it is under a rapid development [143]. At whole-microorganism level, greatly enhanced Raman signals can provide a better basis for characterisation of microorganisms than spontaneous Raman spectra. SERS can be also used to dramatically enhance signal from certain molecules in microorganisms and exclude interferences of other molecules, for example,

one can design a selective bonding between metal nanoparticles or external Raman chromophores and the biological molecules of interest; in another word, SERS provides an alternative labelling method to conventional procedures such as fluorescent labelling, isotope labelling etc. SERS has also shown its potential as an imaging technique [172-174].

The main drawback of techniques based on SERS spectra is the difficulty in obtaining consistently reproducible spectra from samples, particularly those with great biochemical complexity such as microorganisms. It is well understood that SERS spectral profiles are greatly influenced by the absorbance geometry of analytes, and since this leads to both qualitative and quantitative variance in measurements (even from the same sample), there are still challenges to overcome in the analysis of these data.

The main purpose of adopting SERS in this thesis is to enhance Raman signal of single microorganisms so that a high-throughput Raman activated sorting system (RACS) can be built. RACS will be built by combining a confocal Raman microscope and a microfluidic chip; therefore colloidal nanoparticles can provide suitable SERS-active surfaces. Silver and gold nanoparticles in different sizes can be purchased easily. However, many commercially available nanoparticles had insufficient effect during our preliminary experiments with *Escherichia coli* DH5α and *Acinetobacter* sp. ADP1, possibly caused by the fact that they are usually stabilised by negatively charged citric acid ions and bacteria often have negative surface charge as well. In order to bring SERS-active nanoparticles to the vicinity of

bacteria surface molecules, this chapter reports two methods to synthesise and label bacteria with silver and gold nanoparticles.

Method 1 was similar to the method used in two published papers [73, 142]. But significantly lower concentration of the strong reductant (10 µM instead of 0.1 M) was used to avoid the damage of cellular structure. Some other changes were made to avoid nanoparticles being formed in solution rather than on the surface of bacteria. The nanoparticles synthesised in Method 1 should be almost free from surface coating and attached to bacteria surface.

Method 2 was designed so that silver nanoparticles with positive surface charge can be synthesised. Cysteamine was chosen to coat and stabilised silver nanoparticles in Method 2. Cysteamine is a small molecule with a thiol group on one end of its short C-C chain and an amine group on the other end. Thiol group can form stable bond with gold and silver surface very rapidly at room temperature which has been used widely in recent years in nanotechnology [175-178]. We hypothesise that silver nanoparticles will form permanent bonds with the thiol groups of cysteamine leaving their amine tails interacting with water, which makes the whole nanoparticle positively charged and stable in aqueous solution. Some studies suggested that sulphur's electron orbits exhibit a sp^3-hybridisation when bound with gold but a sp-hybridisation with silver [179]. Therefore the bond angle C-S-Ag should be near 180° on the surface of silver nanoparticles.

4.2 Materials and Methods

All chemicals were purchased from Sigma-Aldrich UK unless otherwise stated.

4.2.1 Bacterial Strains and Growth Conditions

Two Gram-positive bacteria species (*Bacillus* sp. Strain2 and *Rhodococcus* sp. RC92), and three Gram-negative bacteria species (*Acinetobacter* sp. ADP1, *Escherichia coli* DH5α and *Pseudomonas putida* UWC1) were incubated in lysogeny broth (LB, for 24 h) or 30 mM glucose-minimal medium (MM, [180], for 72 h), respectively (Table 4.1).

Table 4.1 Bacterial species and growth conditions

Strain	Growth Medium	Incubation Temperature	Source
ADP1	LB/^{12}C-glucose in MM/^{13}C-glucose in MM/^{12}C-glucose in ^{15}N-MM	30 °C	*
Strain 2	LB/^{12}C-glucose in MM/^{13}C-glucose in MM/^{12}C-glucose in ^{15}N-MM	25 °C	#
DH5α	LB	37 °C	*
UWC1	LB	25 °C	*
RC92	LB	30 °C	*

Note: (1)*: Dr. Wei Huang's (The University of Sheffield) collection. (2)#: Provided by Dr. Owen L Petchey (The University of Sheffield).

4.2.2 Labelling bacteria with silver and gold nanoparticles: Method 1

After cultivation, bacteria were collected by centrifugation (3000 RCF, 10min) and re-suspended in ultrahigh quality (UHQ) water (PURELAB Ultra water purification system, ELGA, UK). This procedure was repeated three times to remove growth media. Washed cells were then re-suspended in 10 µM sodium borohydride solution. Sodium borohydride solution (10 µM) was prepared by diluting ice-cooled 0.1 M sodium borohydride solution in ice-cooled UHQ water. The bacteria in 10 µM sodium borohydride were kept in a 25 °C incubator for 30 min. Extracellular sodium borohydride was removed by vacuum filtration using 0.2 µm membrane filters (Millipore, USA) and residual sodium borohydride was leached by adding UHQ water during filtration (5ml, repeated three times). Membrane filter with bacteria was then transferred into 1 mL UHQ water in an Erlenmeyer flask. Simple shaking or 10 s of sonication was applied to remove cells from the membrane filter into water. Sonication method was described previously [181]. 'Washed' membrane filter was then removed from Erlenmeyer flask and 500 µl of 0.1 M $AgNO_3$ solution or 0.01 M $KAuCl_4$ solution was added. The Erlenmeyer flask was then kept in dark under room temperature and for 30 min. The final procedure was washing silver/gold nanoparticles labelled cells by UHQ water three times using centrifugation as described above.

4.2.3 Labelling bacteria with silver nanoparticles: Method 2

Silver nanoparticles were synthesised first and mixed with cells for labelling in Method 2. Sodium borohydride solution (10 mM) was prepared by diluting ice-cooled 0.1 M sodium borohydride solution in ice-cooled UHQ water. Cysteamine solution was prepared fresh before synthesis. Silver nanoparticles were synthesised in two steps: 1) pre-mixing sodium borohydride solution (10 mM, 0.6 mL), cysteamine solutions (10 mM, 0.3 mL) and UHQ water (28.5 mL) at room temperature; 2) adding silver nitrate solution (10 mM, 0.6 mL) to the mixture while stirring, and continuing stirring for another 10 min. Concentration of $AgNO_3$ in the final reaction mixture was 0.2 mM. In order to separate bigger particles (aggregated particles) from the colloidal solution, it was centrifuged at 16,000 RCF for 5 min, and the supernatant was used to label bacteria. Only *E. coli* DH5α was labelled in Method 2. *E. coli* cells were grown in LB broth and washed three times as described before. In the final washing step, silver nanoparticle colloidal solution, instead of UHQ water, was used to re-suspend pelleted cells, therefore the concentrations of nanoparticles and cells were nearly unchanged from the colloidal solution and growth medium, respectively. The mixture of nanoparticles and cells were kept at room temperature for 5 min with occasional shaking. The final step was washing labelled cells by UHQ water three times using centrifugation as described above.

4.2.4 Measurement of zeta potential of silver nanoparticles

Zeta potential measurement was performed with a Malvern Zetasizer Nano series zeta sizer (Malvern Instruments Ltd., UK). Standard sample cells and protocol for nanoparticles were used. Measurement was done in triplicates. Zeta potential measurement was only performed on nanoparticles synthesised in Method 2.

4.2.5 Raman Spectroscopy

Raman spectra were acquired using a LabRAM HR 800 confocal Raman microscope (Horiba Jobin Yvon Ltd., UK). Its spectral resolution is about 1.5 cm^{-1} using the 600 VIS grating. Cells were air-dried on quartz microscope slides before spectrum acquisition. A 100x dry objective (NA = 0.90, Olympus) was used to focus laser on well separated single cells and collect Raman signal. A 50x dry objective (NA = 0.55, Leica) was used for thick specimen, e.g. riboflavin powder. Raman spectra of single cells were taken using a 633 nm He-Ne laser with a laser power of approximately 7 mW on single cells and an acquisition time of 10 - 30 s.

4.2.6 Transmission Electron Microscopy (TEM)

A Phillips Technai 80 kV transmission electron microscope was used to acquire electron microscopic images of bacteria samples. Samples from Method 1 were prepared following standard procedures for fixing, embedding and sectioning of biological samples [182]. Samples from Method 2 were not embedded or sectioned to retain the visibility of small nanoparticles.

4.2.7 Energy-dispersive X-ray spectroscopy (EDX)

A JEOL 6480 LV scanning electron microscope (SEM) equipped with an Oxford Instruments INCA X-ray analysis system was used for the EDX analysis. The operation voltage was 15 kV. The EDX spectroscopy analyses the characteristic X-rays produced by the interaction between the primary electron beam and the sample. The EDX analysis identifies all elements present with atomic numbers of 5 (boron) and greater with a detection limit of approximately 0.3 % weight. All samples for the EDX analysis were prepared following standard procedures for fixing and embedding of biological samples [182]. EDX analysis was only performed on samples from Method 1.

4.2.8 Spectral Data Analysis

Raman spectra were recorded and displayed using Labspec software (Horiba Jobin Yvon Ltd., UK). Principle component analysis (PCA) was done using MVSP software (version 3.13g, Kovach Computing Services, UK). Whole-spectrum normalisation was performed before PCA to normalise the total integral peak area of each spectrum to a fixed value.

4.3 Results and Discussion

4.3.1 Bacteria labelled in Method 1

As shown in Figure 4.1, SERS labelling dramatically enhanced the Raman signal from a single bacterium. Comparing with the control sample without

SERS labelling, the Raman spectrum was enhanced from ‘no signal’ to a SERS spectrum with strong Raman bands and high signal-to-noise ratio. The enhancement factor is difficult to estimate in this study, because without SERS labelling, increasing acquisition time to even 1000s did not yield any band at the position of strong SERS bands. In labelling Method 1, SERS spectra were found to be temporally reproducible (no significant change was observed when acquiring spectra from a cell consecutively) and relatively consistent between individual cells. SERS spectra were compared to all the reagents used in Method 1 and they were not similar to any of the spectra of reagents. It indicates that observed SERS bands may be of bacteria surface molecules. The TEM images (Figure 4.2) of ADP1 cells labelled with silver nanoparticles show that the silver particles were 5 - 20 nm in size and associated with the surface structure of bacteria. No nanoparticles were observed on unlabelled cells (Figure 4.3). The type and strength of interaction between nanoparticles and bacteria surface are still unknown. However, the nanoparticles were not removed by washing steps or during TEM sample preparation.

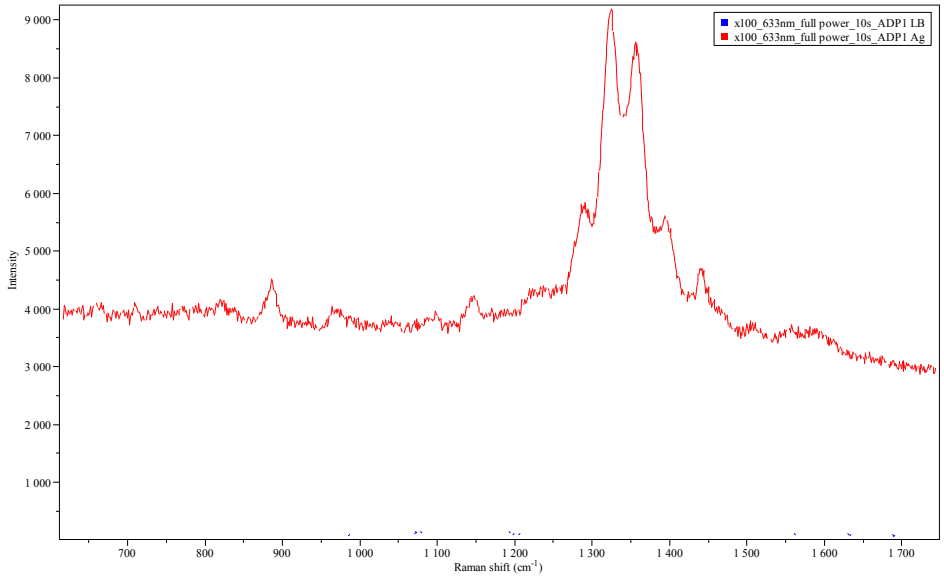

Figure 4.1 Comparison of SERS and normal Raman spectra.
Comparison of single cell Raman spectra (raw data) between a normal ADP1 cell (blue) and an ADP1 cell labelled with silver nanoparticles (red). Both cells were from the same liquid LB culture.

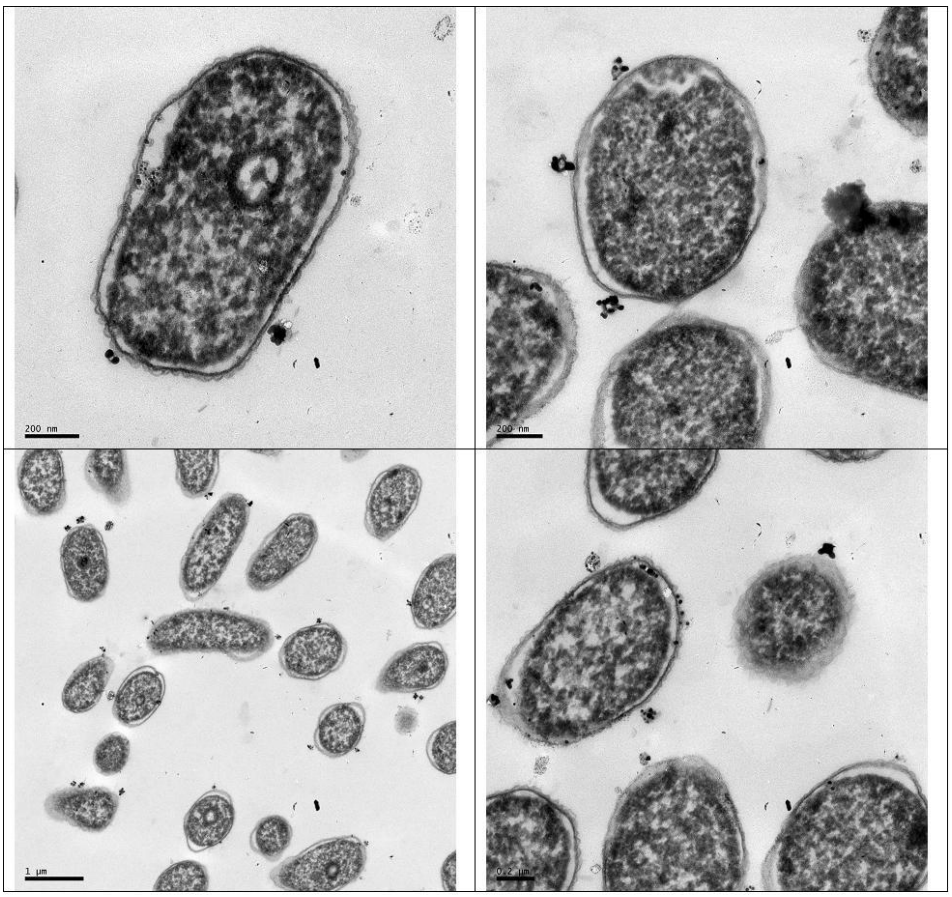

Figure 4.2 TEM images of ADP1 cells labelled with silver nanoparticles.

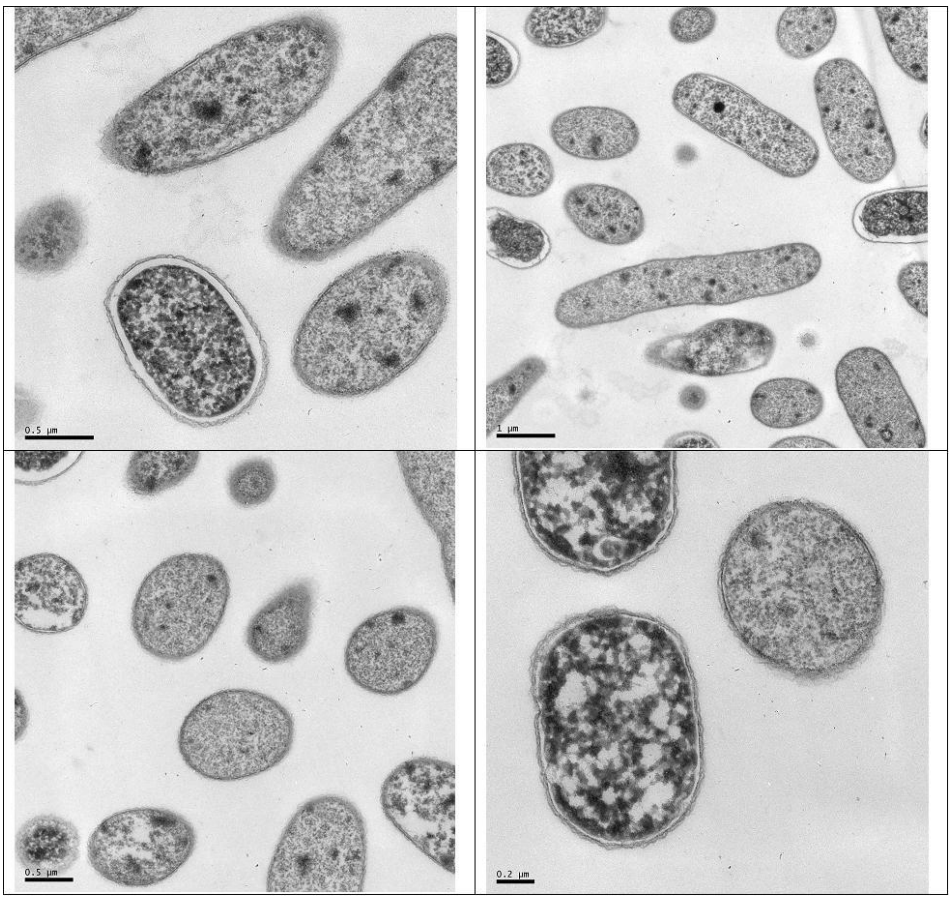

Figure 4.3 TEM images of ADP1 cells without SERS labelling (control).

As shown in Figure 4.4 and Figure 4.5, EDX spectrum of ADP1 cells labelled with silver particles shows strong silver bands whilst no silver signal was detected in the EDX spectrum of ADP1 cells without SERS labelling.

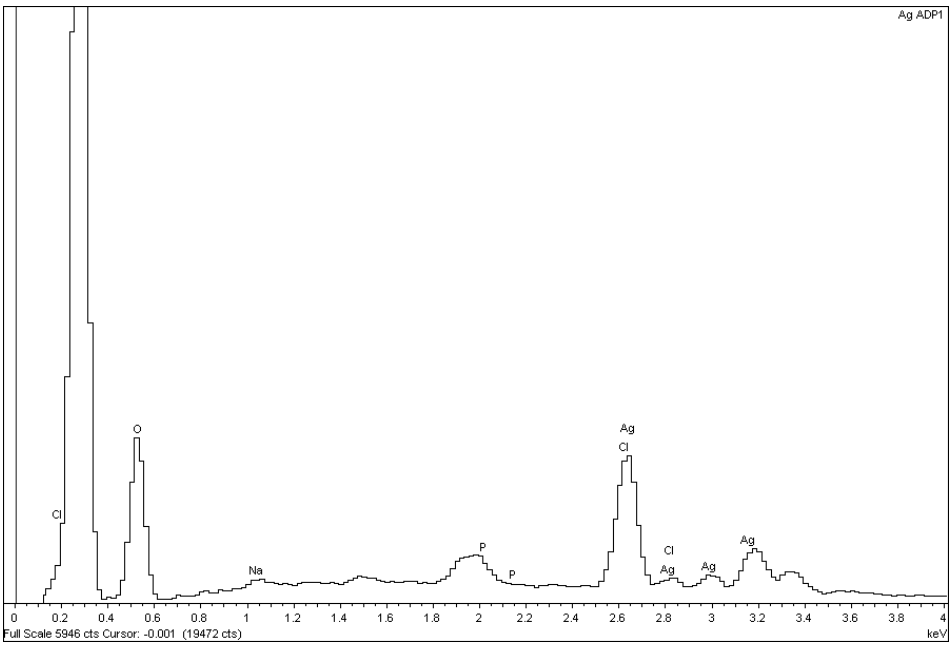

Figure 4.4 EDX spectrum of ADP1 cells labelled with silver nanoparticles.

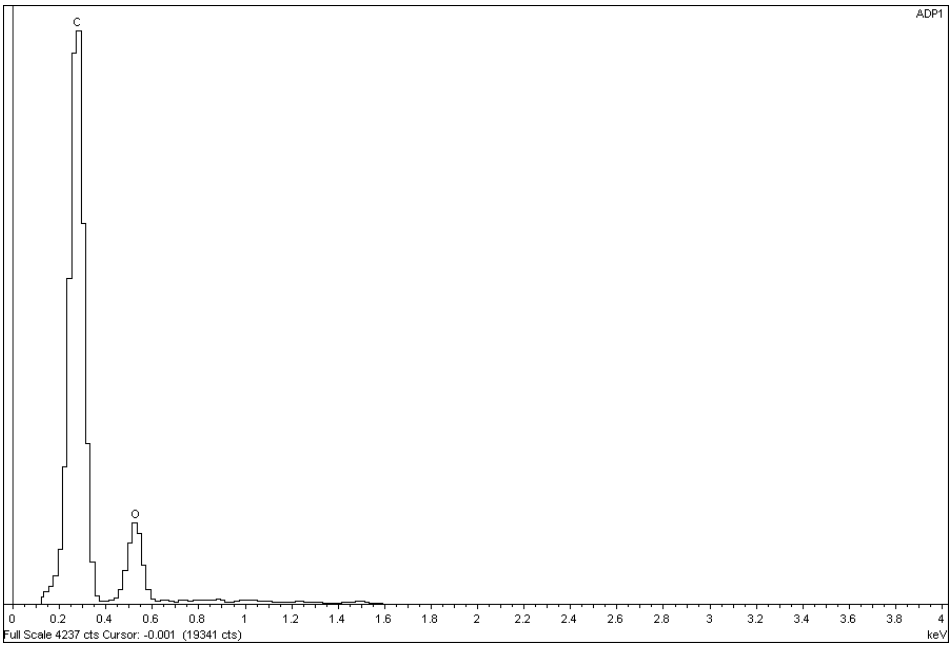

Figure 4.5 EDX spectrum of ADP1 cells without SERS labelling (control).

Figure 4.6 compares SERS spectra of different bacterial species. For each species, 20 randomly chosen single cells were measured and an averaged

spectrum was derived from their spectra. No significant difference was shown in the spectra and no visible clustering is observed in the plot of the first two principle components of PCA. The two strongest peaks in all SERS spectra were at 1325 cm^{-1} and 1359 cm^{-1}. Other peaks were observed at: 887 cm^{-1}, 970 cm^{-1}, 1146 cm^{-1}, 1224 cm^{-1}, 1239 cm^{-1}, 1292 cm^{-1}, 1399 cm^{-1}, 1443 cm^{-1}, 1508 cm^{-1}. Unfortunately, these peaks and other broader bands have not been assigned due to the lack of complete understanding of this heterogeneous reaction which formed the silver nanoparticles. The similarity between SERS spectra of different species indicates that nanoparticles might have labelled similar molecules in all the samples. Because the SERS effect is known to be only effective in short distance, the origin of SERS signal in this study is likely to be the surface structures of bacteria.

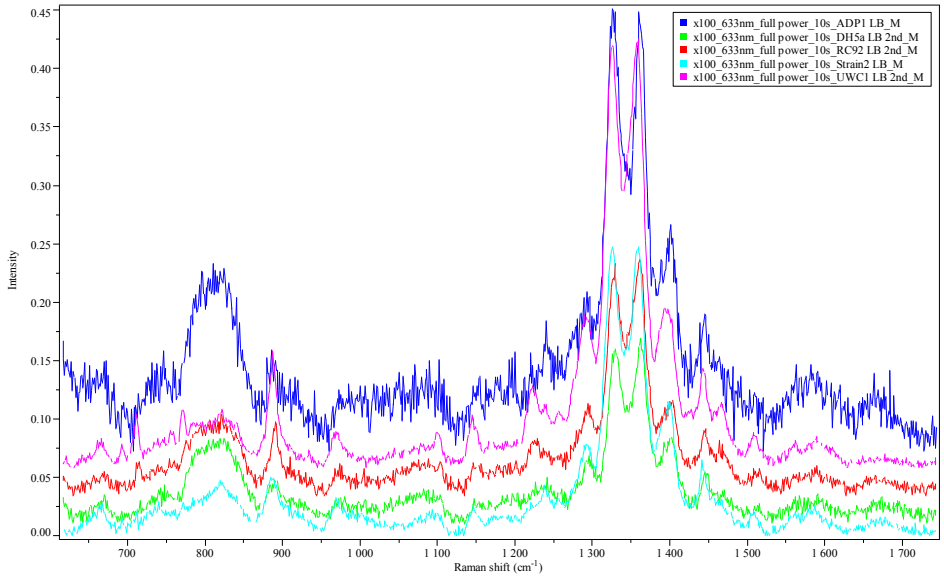

Figure 4.6 Comparison of single cell SERS spectra.
Comparison of single cell SERS spectra (averaged and normalised spectra from raw data) of different bacterial species. All bacteria were from liquid LB culture and labelled with silver nanoparticles. DH5α, UWC1 and RC92 cells were labelled twice by the same method, since the first labelling resulted in spectra of relatively low signal-to-noise ratio.

However, the similarity of SERS spectra may also result from contamination introduced by the labelling process. Contamination is a very important issue in any SERS studies, because very low level of contamination, if absorbed on the SERS-active surface, may generate strong SERS signal.

The effect of culture media was tested on ADP1 cells. No significant effect was found (Figure 4.7), although the SERS spectra of ADP1 grown in glucose-MM were better in terms of signal-to-noise ratio. The effect of the type of metal nanoparticles was also tested (Figure 4.8): by changing silver nanoparticles to gold nanoparticles, no significant difference was observed for ADP1 cells grown either in glucose-MM or LB. SERS spectra of ADP1

cells grown in LB and labelled with gold nanoparticles retained a noticeable feature of spontaneous Raman spectra of bacteria: the 1001 cm^{-1} phenylalanine/substituted benzene derivatives peak, which was usually missing in SERS spectra of this study. The reductant, sodium borohydride, was also tested for possible contamination. An alternative method was designed to generate silver nanoparticles without borohydride: (1) Sodium borohydride solution was replaced by 0.85% sodium chloride saline; (2) after residual silver nitrate solution was washed away, cells were suspends in UHQ water and exposed to UV light for 5 minutes. The resultant SERS spectrum is shown in Figure 4.9. Although the relative intensity of the SERS bands was changed, no significant difference was observed between the SERS spectra of this alternative labelling and normal labelling. In summary, culturing media and reagents may affect the signal-to-noise ratio of SERS spectra, but did not change any main features of them. Therefore, SERS signal observed in this study was likely to come from bacteria surface molecules.

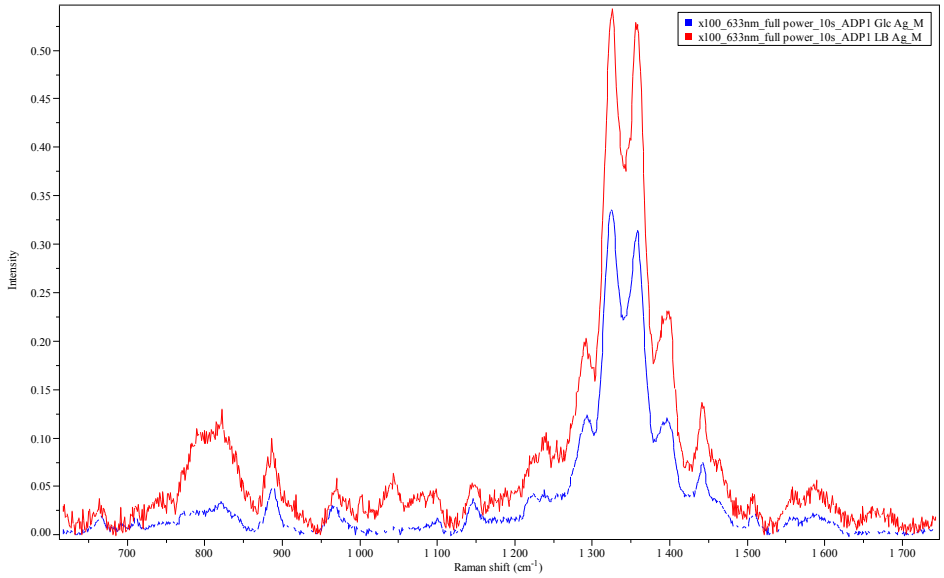

Figure 4.7 The effect of growth media on SERS spectra.
SERS spectrum of ADP1 grown in MM-glucose medium (blue) and LB broth (red) (silver nanoparticles, averaged and normalised spectra from raw data)

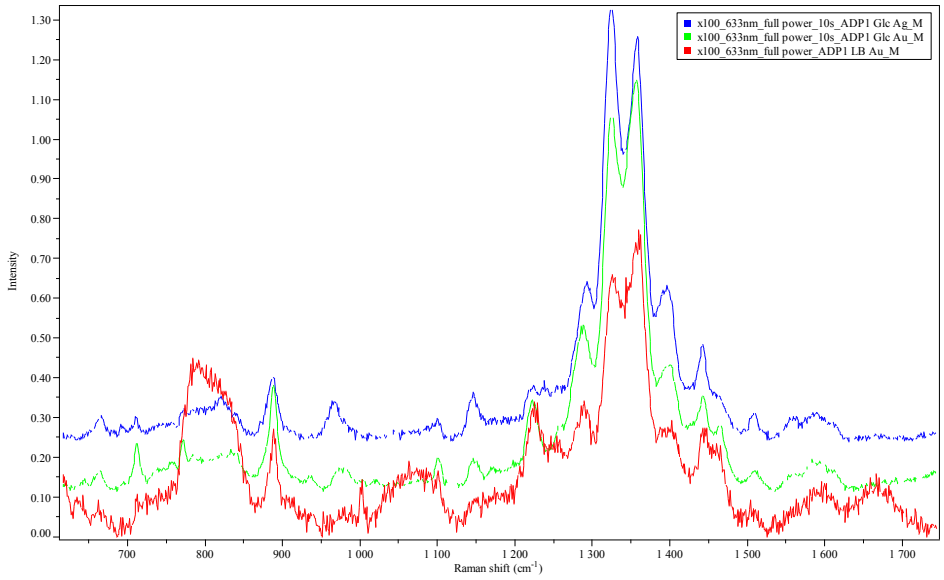

Figure 4.8 SERS signal from silver and gold nanoparticles.
The SERS spectrum of ADP1 cells labelled with silver nanoparticles (blue), gold nanoparticles (green) and LB-grown ADP1 labelled with gold nanoparticles (red) (averaged and normalised spectra from raw data)

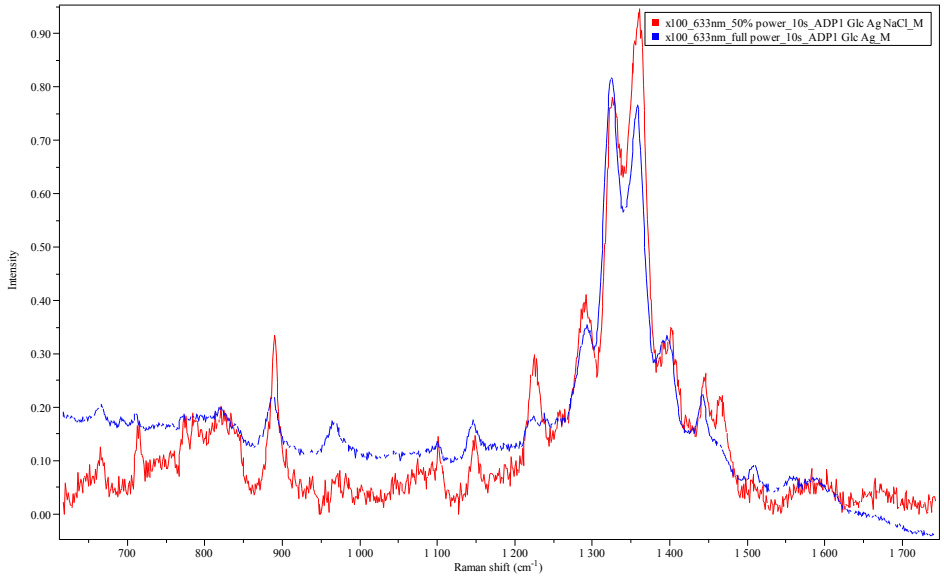

Figure 4.9 The effect of reductant on SERS spectra.
The SERS spectrum of normal labelling (blue) and NaCl labelling (red) (averaged and normalised spectra from raw data)

Figure 4.10, Figure 4.11 and Figure 4.12 compare SERS spectra between stable isotope labelled and unlabelled ADP1 and Strain2 cells. Raman red-shift was observed in the SERS spectra of ^{13}C-labelled bacteria as indicated by the red arrows in the figures. No significant red-shift was found in ^{15}N-labelled bacteria. However, the strongest bands were not affected by the stable isotope labelling.

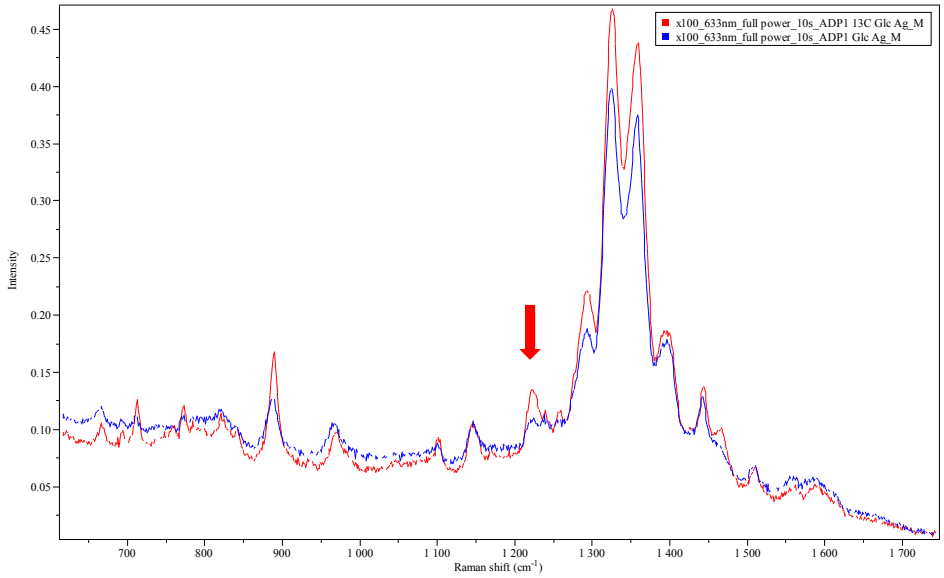

Figure 4.10 ^{13}C-Raman red-shift in SERS spectra.
The comparison of SERS spectra (averaged and normalised from raw data) between normal ADP1 cells (blue) and ADP1 cells cultured in ^{13}C-medium (red)

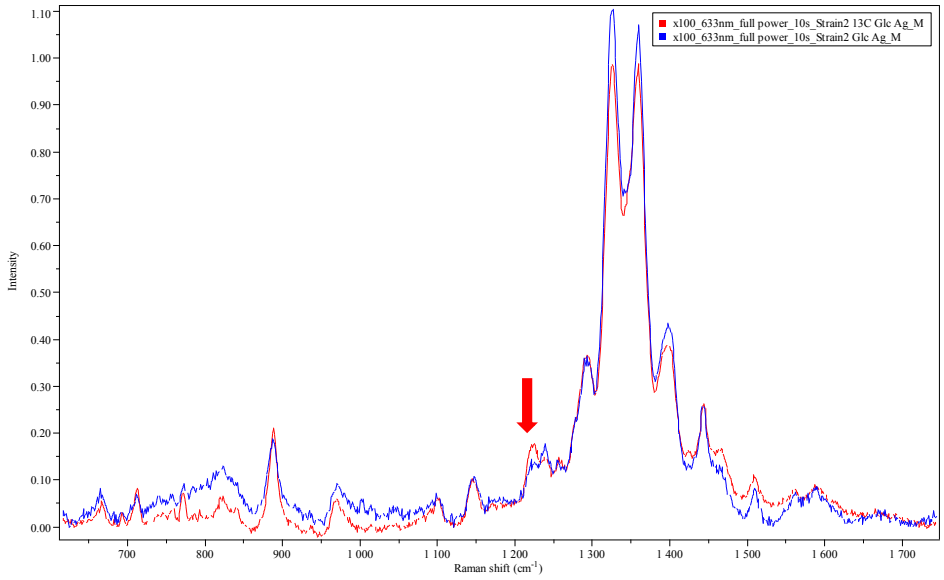

Figure 4.11 ^{13}C-Raman red-shift in SERS spectra.
The comparison of SERS spectra (averaged and normalised from raw data) between normal Strain2 cells (blue) and Strain2 cells cultured in ^{13}C-medium (red)

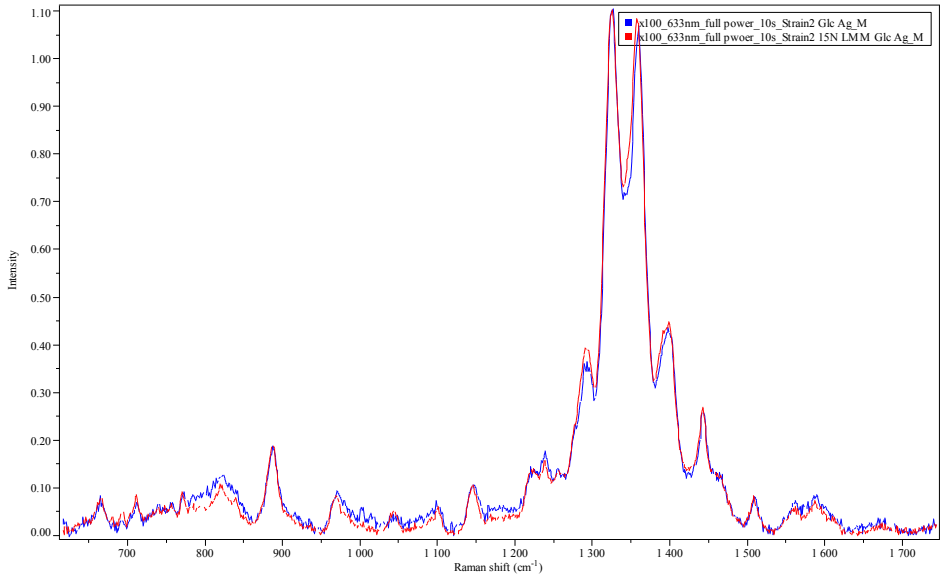

Figure 4.12 ^{15}N-Raman red-shift in SERS spectra.
The comparison of SERS spectra (averaged and normalised from raw data) between normal Strain2 cells (blue) and Strain2 cells cultured in ^{15}N-medium (red)

This study employed a SERS labelling method similar to Zeiri and co-workers' method, who suggested that the SERS signal was dominated by flavin molecules [73, 142]. However, SERS spectra in this study were not similar to the Raman spectrum of riboflavin (Figure 4.13). This study is consistent with Zeiri and co-workers's findings that SERS spectra of different bacterial species were very similar to each other, which indicates that silver and gold nanoparticles may have high affinity to specific biological molecules that present universally in different species.

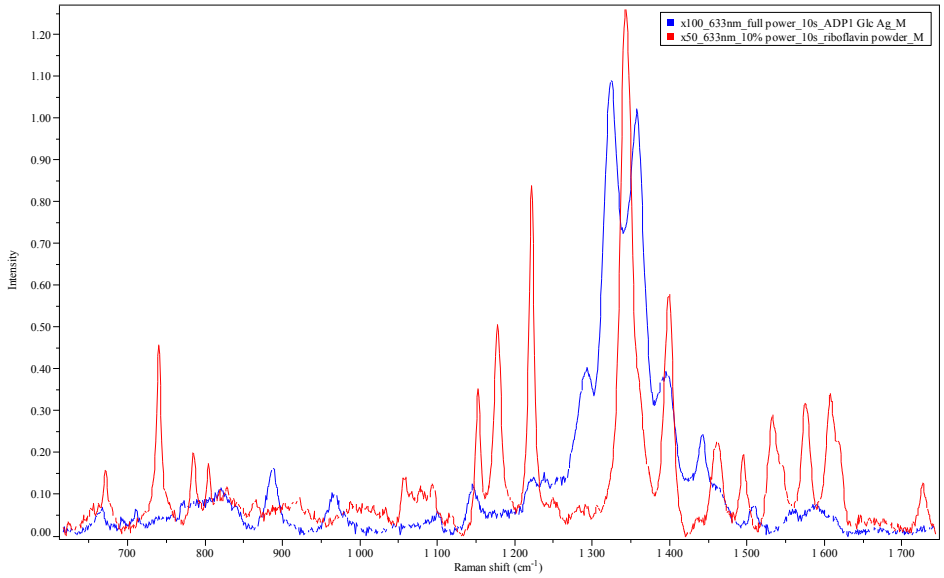

Figure 4.13 SERS spectra of ADP1 and the Raman spectrum of riboflavin. The comparison between ADP1 SERS spectrum (blue) and the spectrum of riboflavin powder (red) (averaged and normalised from raw data)

4.3.2 Bacteria labelled in Method 2

Silver nanoparticle colloidal solution made in Method 2 had a characteristic yellow colour of silver nanoparticles. After being mixed with bacteria cells, the solution turned to almost colourless and the pellet of cells turned from pale yellow to dark yellow, indicating that almost all the silver nanoparticles were absorbed on the bacteria surface. TEM images of the synthesised silver nanoparticles are shown in Figure 4.14. TEM images of *E. coli* strain DH5α labelled by the silver nanoparticles are shown in Figure 4.15. Silver nanoparticles had irregular shapes and sizes ranging from about 5 to 30 nm, and DH5α cells were coated by large number of silver nanoparticles.

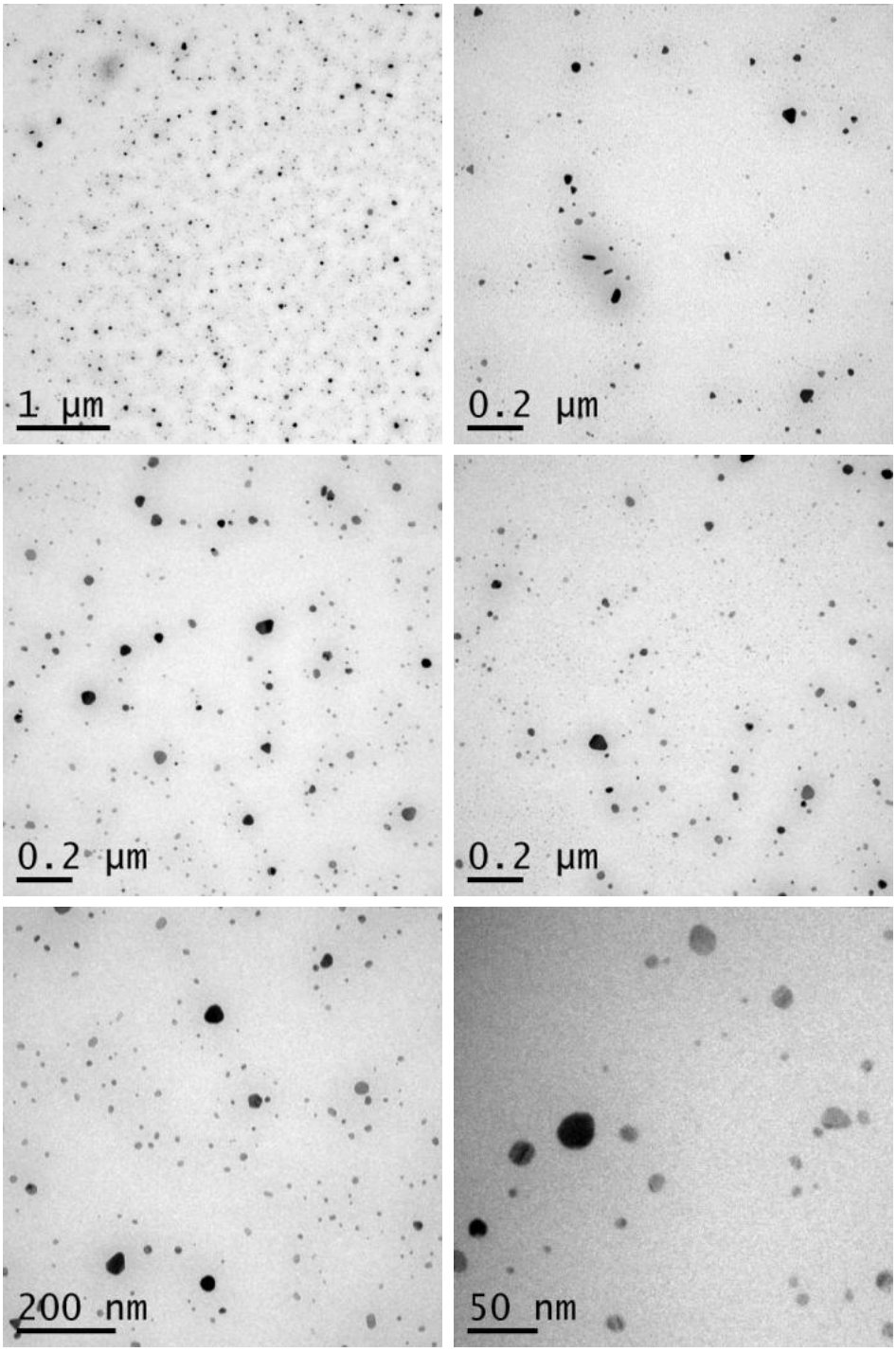

Figure 4.14 TEM images of silver nanoparticles synthesised in Method 2.

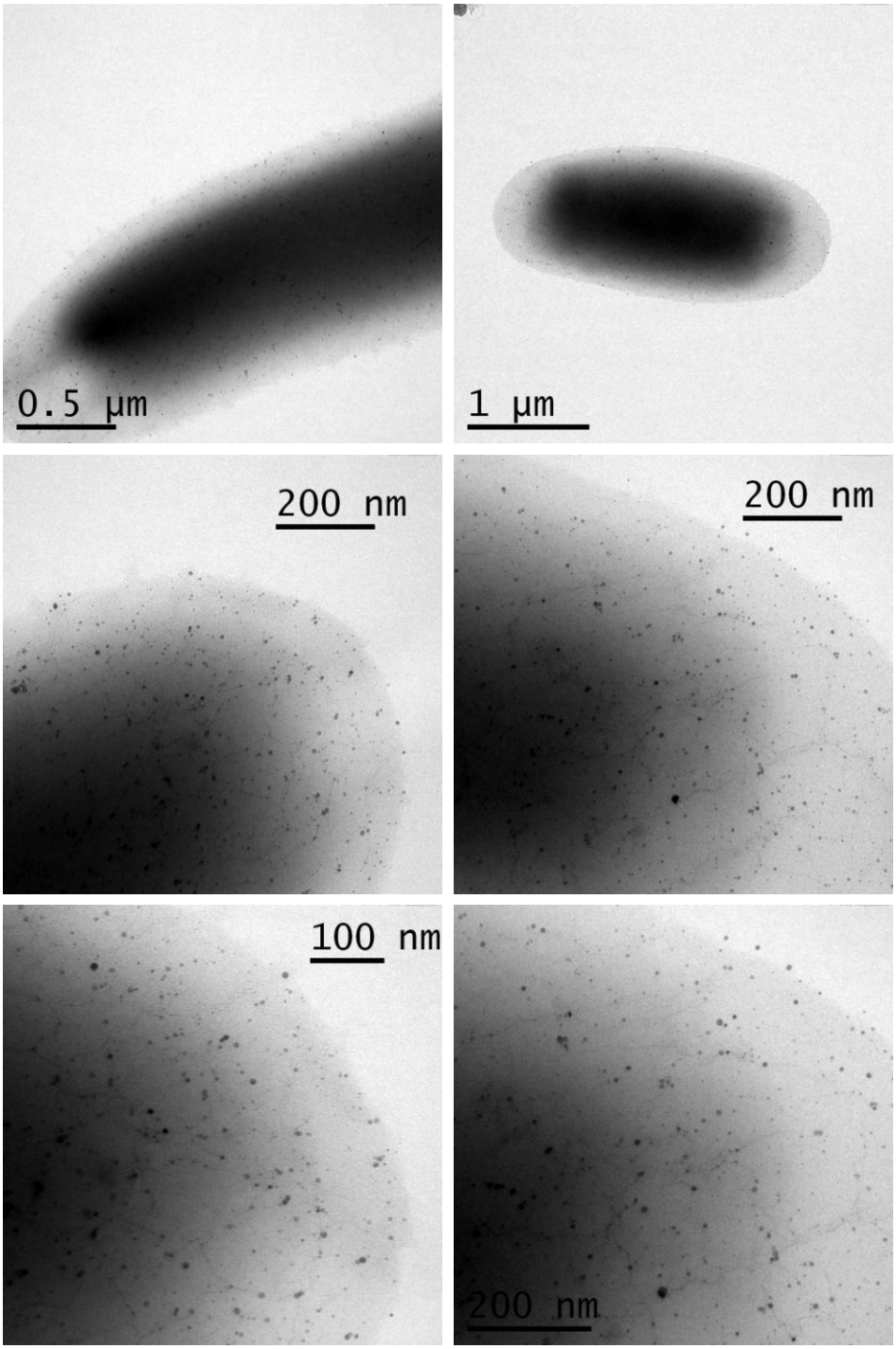

Figure 4.15 TEM images of DH5α cells labelled by silver nanoparticles in Method 2.

Zeta potential of the synthesised silver nanoparticles showed a very weak positive surface charge of 0.0131 mV (averaged from the three replicates in

Figure 4.16), which suggests that this colloid is not stable and should be synthesised and used fresh. Residual anions from the reduction of silver ions may absorb to the surface of nanoparticles and neutralise their positive surface charge.

However, Raman spectra of bacteria labelled by silver nanoparticles in Method 2 were featureless and without any band or peak.

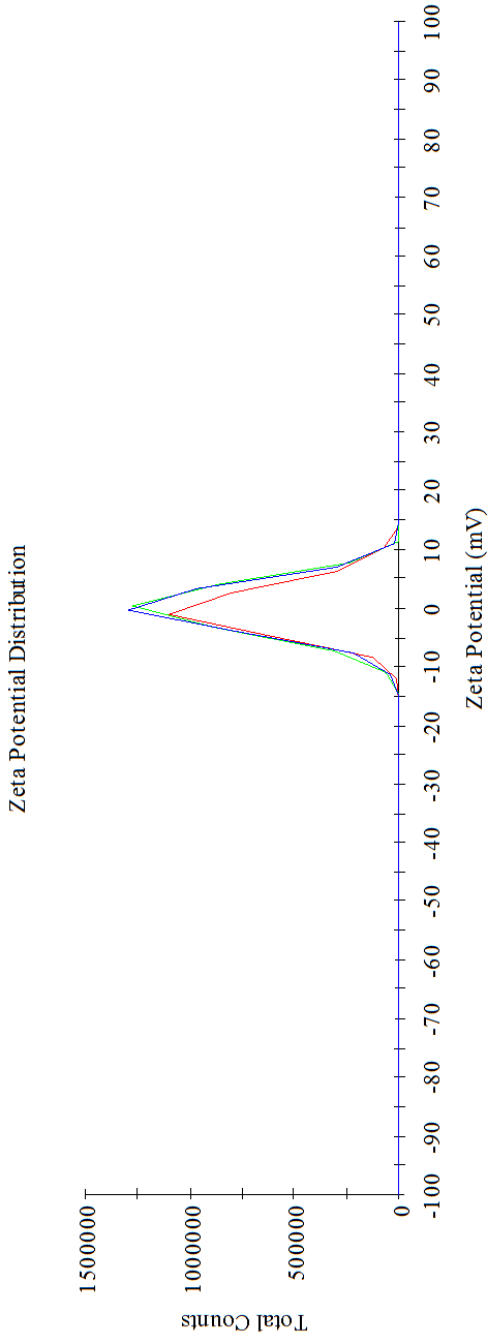

Figure 4.16 Zeta potential of synthesised silver nanoparticles.

4.4 Suggestion for future research

This chapter reports some preliminary results of SERS labelling attempt. Results of Method 1 show that silver nanoparticles were successfully

synthesised on the surface of bacteria and the resultant SERS spectra may represent certain biological molecules on bacteria surface. However, the main SERS bands were not red-shifted by ^{13}C- or ^{15}N-labelling, which raises the question of possible chemical contamination during the SERS labelling process. Further investigation is needed in order to: 1) rule out any possible chemical contamination, 2) assign these bands 3) explain the selective attachment of silver nanoparticles to specific bacteria surface molecules. Method 2 provides a rapid and simple protocol of one-pot room-temperature synthesis for cysteamine coated and positively charged silver nanoparticles. These nanoparticles showed very high affinity to *E. coli* cell surface but did not generate any meaningful spectra. Method 2 is expandable because the nanoparticles' surface amine groups can be covalently linked to biologically abundant carboxylic groups using commercially available kits, which often contain the combination of 1-ethyl-3-(3-dimethylaminopropyl) carbodiimide and N-hydroxysuccinimide. In order to assess the feasibility of using the nanoparticles in Method 2 for environmental microbiology research, a simple and well studied substance with known Raman spectrum should be used to substitute bacteria cells during the labelling. Uniform micrometer sized polymer beads may serve this purpose. Further study to improve Method 2 should also be made to produce nanoparticles with uniform size.

Chapter 5: Monitoring carbon flow in a food chain model and revealing metabolic pathways using stable isotope probing and Raman spectroscopy

5.1 Introduction

The combination of stable isotope probing (SIP) with Raman spectroscopy has been a novel and valuable addition to the methods available to researchers in microbiology [20, 22], microbial ecology [21, 58, 82] and clinical research [81]. Raman spectra of living organisms are the signatures of their chemical composition and indicate the identity, phenotypic features and physiological status of the sample [20]. Combined with SIP, Raman spectroscopy can quantify the ^{13}C content in single microbial cells [20]. The Raman-SIP method has been used to determine bacterial species involved in biodegradation processes [26, 57], reveal the extracellular activity of a human pathogen [81] and quantify carbon dioxide fixation at single-bacterium level [21]. The Raman-SIP method can potentially track carbon flow in a complex community in a quantitative and non-destructive manner. This study demonstrates that the Raman-SIP method can track carbon flow quantitatively in a model food chain that consists of an organic carbon source, bacteria and soil nematodes. From detailed examination of the spectral data, it is shown that the Raman-SIP method can provide another layer of information regarding the biochemical pathways leading to the

synthesis of crucial biological molecules. This study may bring a new research tool to microbial ecology and biophysical/biochemical science.

Soil bacteria form the basis of soil food webs and drive numerous soil processes, such as nutrient turnover, phytohormone production and pathogen suppression [183]. In the rhizosphere, bacteria are top-down regulated, and predation has important consequences on the structure and functioning of the microbial community [184]. Nematodes are amongst the main consumers of bacteria in terrestrial ecosystems. Understanding the nutrient flows between bacteria and nematodes is of central importance for the reconstruction of soil food webs and reliable prediction of nutrient cycles. Recently, SIP has revolutionised research on predator-prey interactions in soil, allowing the fate of ^{13}C-labelled substrates to be followed to bacteria [185], protozoa [186, 187] and meso- and macrofauna [188]. At microbial level, most SIP experiments use a combination of ^{13}C labelling and nucleic acid fractionation by ultracentrifugation. This method has greatly enriched our knowledge of microbial communities and can be used, for example, to investigate active root-associated communities [189] and uncover the complex links between bacteria, fungi and protozoa [185]. However, this method is destructive, time consuming and requires a high degree of labelling (usually 50% ^{13}C or more) to ensure efficient separation of ^{13}C- from ^{12}C-labelled nucleic acids and would therefore neglect organisms which incorporate the labelled substrate less quickly or grow at a slower rate. In contrast, Raman spectroscopy is non-destructive and requires

less time. As shown in this study, it also detects ^{13}C labelling in almost the entire range from 1.1 to 99 %.

The detection of ^{13}C-incorporation is achieved by measuring the isotopic shift (red-shift of Raman bands) caused by the slightly heavier ^{13}C-atoms. Raman red-shift was observed in single cells at many positions across the spectra which correspond to amide, nucleobases, phenylalanine, etc.; red-shifted bands are potential quantitative spectral markers for ^{13}C content of the sample [20]. However, owing to the complex nature of cells, many of those red-shifted Raman bands overlap with other bands and therefore quantitative spectral markers for ^{13}C content are very limited.

The Raman band of phenylalanine is a well established marker for ^{13}C-incorporation at single-cell level [26]. It is a sharp band at about 1001 cm^{-1} with limited interference from other Raman bands. It is almost universally observed in any type of cell. In this study, we report a new quantitative Raman spectral marker for ^{13}C in single nematodes. This marker appears at about 747 cm^{-1} in ^{12}C-nematode samples and it was assigned to thymine. The nature of the isotopic shifts of phenylalanine and thymine Raman bands are noticeably different. Through careful examination of this difference, this study reveals a new link between Raman spectra and biosynthetic pathways.

5.2 Materials and Methods

5.2.1 Bacteria and nematode growth conditions

Escherichia coli OP50 were maintained on lysogeny broth (LB) agar plates at 37 °C. Prior to the experiment, one colony was picked and grown overnight in OS minimal medium [190] supplemented with a mixture of ^{12}C- and ^{13}C-glucose (both from Sigma-Aldrich, St-Louis, USA) as the sole carbon source. We set up an isotopic gradient comprising 1.1 (natural abundance), 2.1, 6.0, 11, 21, 50, 89 and 99 % ^{13}C, at a total concentration of 25 mM glucose. To ensure reliable labelling, bacteria were grown overnight, and a 100 µL aliquot was used to start a new 10 mL culture at the same isotopic ratio. Bacteria were then pelleted by centrifugation (16,000 g, 2 min), washed three times in M9 buffer to remove remaining nutrients, and concentrated in 50 µL M9 buffer. M9-agar plates without carbon were seeded with the labelled *E. coli* and kept at 4°C until start of the experiment.

Caenorhabditis elegans were routinely grown in NGM plates seeded with *E. coli* OP50. Prior to experiments, eggs were scrapped down the plate and sterilised with 1 % NaClO for 5 min, and washed according to standard procedures. About 50 eggs were placed on each agar plate (three plates for each isotopic ratio and time point) and incubated at 20 °C in the dark. After 5, 10, 15 and 20 days, nematodes were washed off the plates with 1 mL M9 buffer; the worms were collected by gentle centrifugation (20 g, 1 min) and washed three times with M9 buffer to remove bacteria; worms were then

fixed in 1 % formaldehyde and analysed by Raman micro-spectroscopy as described below.

5.2.2 Raman micro-spectroscopy

Each nematode or bacteria sample suspension (5 - 10 µL) was spread on a calcium fluoride slide and allowed to air dry prior to Raman analysis. Raman spectra were acquired using a confocal Raman microscope (LabRAM HR, HORIBA Scientific, UK) equipped with an integrated Olympus microscope (model BX41). A 100 × magnifying dry objective (NA=0.90, Olympus, UK) was used to observe samples and acquire Raman signal. The laser beam was targeted on samples visually using an integrated camera and a motorised XYZ stage (0.1 µm step). Raman scattering was excited with a 532 nm Nd:YAG laser (Torus Laser, Laser Quantum, UK). The laser power on a sampling point was about 3.5 mW. Raman spectra were recorded by a -70 °C-cooled CCD detector (Andor, UK). The system was run with a confocal pinhole diameter of 100 µm, enabling a spatial resolution of approximately 1 µm. Each Raman spectrum was acquired between the range 2172 cm^{-1} and 557 cm^{-1}, with 1021 data points and spectral resolution of about 1.5 cm^{-1}. LabSpec software (HORIBA Scientific, UK) was used to control the Raman system and acquire Raman spectra. Acquisition times of Raman spectra were 5-10 s for nematodes and 30 s for bacteria. In each nematode sample, a few worms were randomly chosen and measured at multiple points alongside their bodies. Spectra smoothing was performed by the Savitsky–Golay smoothing method in

LabSpec. Microsoft Excel 2007 was used to process and analyse spectral data.

5.2.3 Calculation of the wavenumbers of phenylalanine Raman bands and thymine Raman spectra

The equilibrium geometry of the phenylalanine molecule was obtained at the B3LYP/6-31G** level of theory using the GAUSSIAN09 package [191]. Raman frequencies of phenylalanine were calculated in the harmonic approximation for the isotopomers 1 to 8 derived by $^{13}C/^{12}C$ substitution (Figure S5.4). The structure of thymine was optimised and checked using the same procedure. The Raman frequencies and intensity constants of the 32 possible isotopomers of thymine derived by $^{12}C/^{13}C$ substitution were calculated using the same method (Figure S5.6). The thymine Raman band was calculated by superposition of the 32 possible isotopomers of thymine. Each isotopomer was treated as an individual Raman band and these 32 bands were simulated using both Gaussian and Lorentzian lineshape functions.

The probability P_i of any isotopomer i of thymine was calculated using the following function:

$$P_i = (1-p)^{5-z_i} p^{z_i}$$

where p is the fractional ^{13}C content ($0 \leq p \leq 1$) and z_i is the number of ^{13}C-atoms in the isotopomer.

As described in the main text, any isotopomer *i* has a calculated Raman frequency b_i, and an intensity constant E_i. Their full width at half maximum (FWHM) was set to equal that of the observed thymine Raman bands at 1.1 % and 99 % ^{13}C, which is about 12 cm^{-1}. For any isotopomer *i* of thymine, the Gaussian function representing the individual Raman band is:

$$G_i(x) = a_i e^{-\frac{(x-b_i)^2}{2c^2}}$$

where,

$$c = \frac{FWHM}{2\sqrt{2\ln 2}}$$

If we assume that

$$\int_{-\infty}^{+\infty} G_i(x)\,dx = P_i E_i$$

and note that integral of the Gaussian function is:

$$\int_{-\infty}^{+\infty} G_i(x)\,dx = a_i c\sqrt{2\pi}$$

the pre-exponential factor is:

$$a_i = \frac{P_i E_i}{c\sqrt{2\pi}}$$

Similarly, the Lorentzian function representing the Raman band of isotopomer *i* is:

$$L_i(x) = \frac{d_i \frac{FWHM}{2}}{\pi\left[(x - b_i)^2 + \left(\frac{FWHM}{2}\right)^2\right]}$$

If we assume that

$$\int_{-\infty}^{+\infty} L_i(x)\, dx = P_i E_i$$

and note that the integral of the Lorentzian function is:

$$\int_{-\infty}^{+\infty} L_i(x)\, dx = d_i$$

we derive:

$$d_i = P_i E_i$$

Finally, Raman spectra of thymine at six ^{13}C levels (p = 1.1, 11, 21, 50, 89, 99 %) were simulated using:

$$Raman(x)_p = \sum_{i=1}^{32} G_i(x)$$

or

$$Raman(x)_p = \sum_{i=1}^{32} L_i(x)$$

Simulated Raman spectra based on both Gaussian and Lorentzian functions were plotted using Microsoft Excel 2007 (Figure 5.5A and Figure 5.5B).

5.3 Results

5.3.1 Using Raman red-shift to track carbon flow in a model predator-prey system

In this study, *Escherichia coli* were labelled with 1.1 to 99 % ^{13}C by growing them on ^{13}C-labelled glucose. ^{13}C-labelled bacteria were then fed to the nematode model strain *Caenorhabditis elegans*. It has been previously demonstrated that Raman spectroscopy is a reliable, quantitative and simple method to detect carbon flow from carbon substrates to single bacteria cells [21, 81]. ^{13}C-labelling of bacteria from 1.1 to 99 % is shown in Figure 5.1A. As shown in Figure 5.1B, Raman spectra of nematodes fed by ^{13}C-bacteria showed distinctive red-shift similar to that of bacteria [20]. This result indicates that Raman spectra of single nematodes are a good measurement for ^{13}C-incorporation at single-organism level, and can therefore track the nutrition flow from carbon source, via microbial cells, up to multicellular predators.

A (*E. coli*)

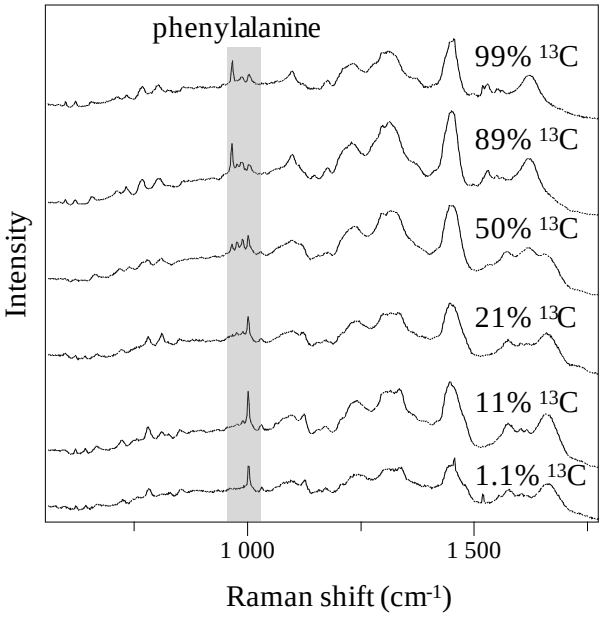

B (*C. elegans*)

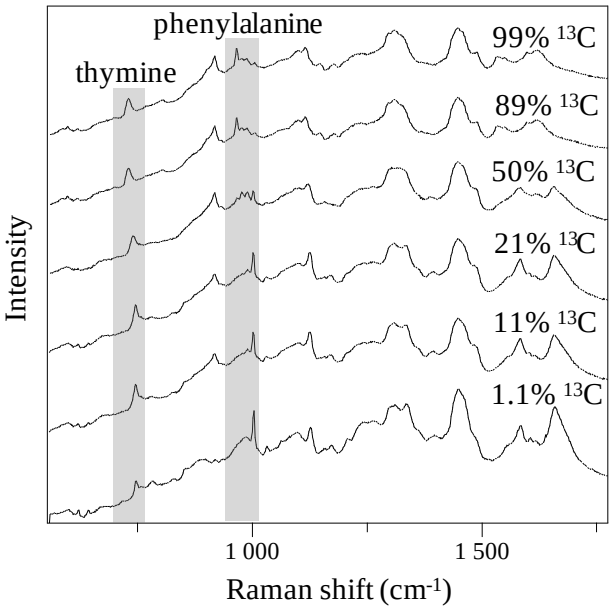

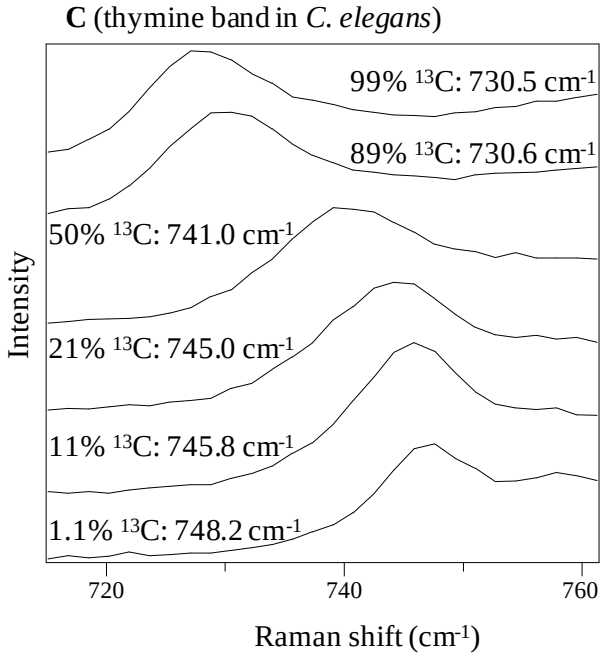

Figure 5.1 Using Raman spectra to track carbon flow in a food chain.
Examples of Raman spectra of ^{13}C-labelled *E. coli* (A) and *C. elegans* fed by the labelled *E. coli* (B). Shaded areas are the red-shirted phenylalanine and thymine bands (A and B); the gradual red-shift of the thymine band (C) can potentially quantify ^{13}C content of *C. elegans*.

Many Raman bands in the spectra of nematodes are visibly red-shifted, but the majority of them also overlap with other bands. In this study, only phenylalanine and thymine bands (shaded areas in Figure 5.1B) are readily usable for quantifying ^{13}C content in *C. elegans*. However, a broad and strong band appeared at the same position as phenylalanine. This unidentified band could be significantly reduced by photobleaching using the Raman probing laser in about 10 s; but a raised baseline with a rounded shape is still seen in the shaded area of phenylalanine in Figure 5.1B. This interfering band possibly arises from autofluorescence or the fixation procedure for nematode samples. In order to correlate the phenylalanine band with ^{13}C content, the intensity of phenylalanine band must be derived

from baseline-corrected Raman spectra. Without a strong indication of the nature of the background Raman signal forming the 'baseline', baseline correction is usually done by so-called 'rubber band' baseline subtraction, which is arbitrary and introduces unnecessary uncertainties. Furthermore, quantifying ^{13}C content using the phenylalanine band is based on its band intensity, which is usually seen as semi-quantitative in Raman spectroscopy. Owing to the difficulties listed above, the correlation between the red-shift of the phenylalanine band and ^{13}C content is relatively weak (with R^2 values < 0.9 in linear regression) and unreliable because it was calculated from heavily processed spectra which still contain the unidentified interfering band.

In contrast, the thymine Raman band, the new quantitative ^{13}C spectral marker reported in this study, is almost immune to all of the problems associated with the phenylalanine band. It peaks at about 747 cm^{-1} in ^{12}C-nematode samples (with 1.1% natural abundance of ^{13}C) and was assigned to thymine in a number of studies [192-198]. Raman spectra of deoxynucleotides (dATP, dTTP, dGTP and dCTP, 100 mM, Sigma-Aldrich, UK) also support this band assignment (Figure S5.1). The thymine Raman band moved gradually towards lower wavenumber with increasing ^{13}C content (Figure 5.1C). Therefore, by finding the position of the thymine band of a nematode sample, one can determine the extent of ^{13}C incorporation quantitatively, without using the band intensity.

If a statistically sound relationship is established between the position

(wavenumber) of the thymine band and the ^{13}C content, one can use it to determine the ^{13}C content of a single organism based on the non-destructive and easy-to-use technique of Raman spectroscopy. As seen in Figure 5.2, linear regression resulted in a good linear relationship between the position of the thymine band and the ^{13}C content in single *C. elegans*. In samples which underwent 5, 10 and 15 days of incubation, R^2 values are 0.95 - 0.97. Therefore, quantitative detection of ^{13}C-incorporation ranging from 1.1 to 99 % in *C. elegans* can be achieved at single-organism level. A previous showed that the ^{13}C content of a biological molecule is a good quantitative indicator for the ^{13}C content of the whole cell [21].

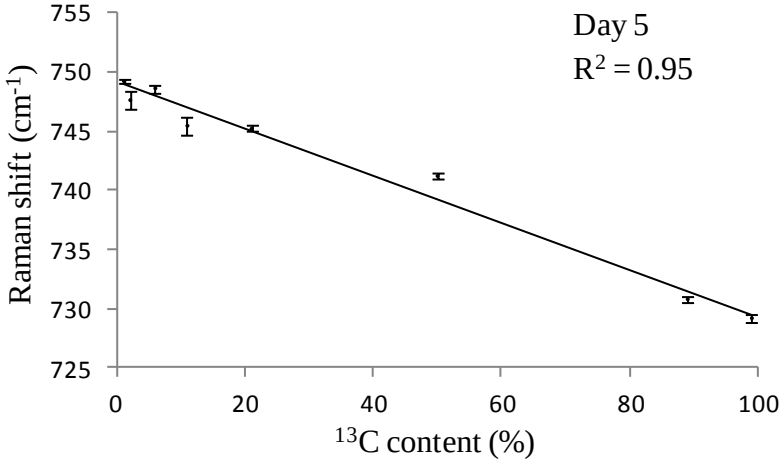
Day 5
$R^2 = 0.95$
Raman shift (cm^{-1})
755
750
745
740
735
730
725
0
20
40
60
80
100
^{13}C content (%)

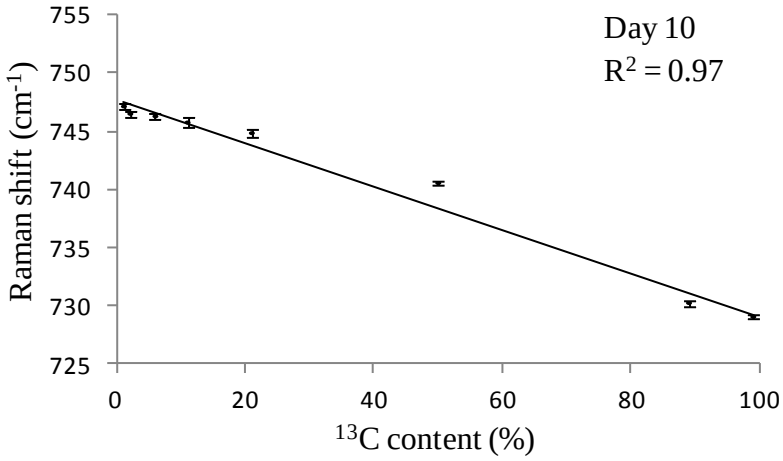
Day 10
$R^2 = 0.97$
Raman shift (cm^{-1})
755
750
745
740
735
730
725
0
20
40
60
80
100
^{13}C content (%)

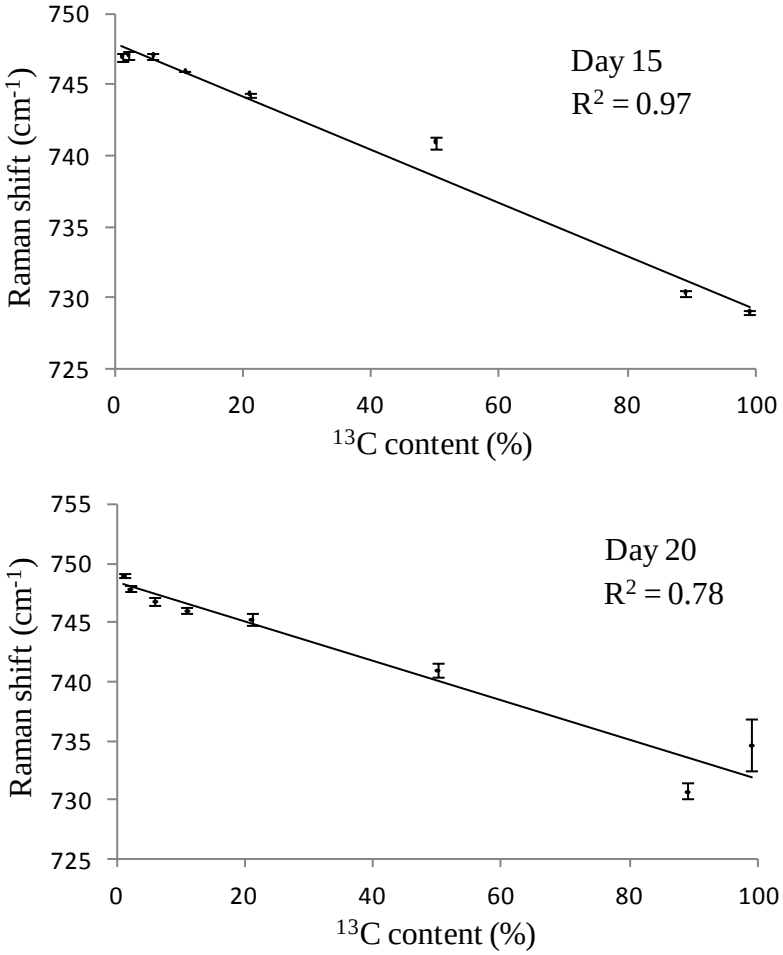

Figure 5.2 Linear relationship between Raman red-shift and ^{13}C content.
The linear relationship between the position (wavenumber) of the thymine Raman bands and the ^{13}C content of C. elegans. Error bars show the standard error of Raman band positions at each ^{13}C level.

It is worth noting that the red-shift of the thymine band has a very different 'red-shift mode' from that of the phenylalanine band as previously described [26]. A '^{13}C-phenylalanine band' at about 965 cm^{-1} appears from the ^{13}C containing cells. The '^{12}C-phenylalanine band' at about 1001 cm^{-1} does not disappear or move in the presence of ^{13}C; instead, with increasing ^{13}C content, it loses intensity whilst the '^{13}C-phenylalanine band' gains intensity. Therefore, ^{13}C content can be correlated to the ratio or difference

between these two intensities. In addition, we observed two extra Raman bands between the '^{13}C-phenylalanine band' and the '^{12}C-phenylalanine band' in *E. coli* grown in 50% ^{13}C media (Figure 5.3A); in these spectra, all four bands have almost identical intensities. A similar four-band feature has been observed previously [26].

For thymine, however, no new band was observed from ^{13}C-labelled samples. The thymine band moves gradually with increasing ^{13}C content (Figure 5.1C and Figure 5.2). In the entire range of ^{13}C % used in this study, there was always only one thymine band without obvious band splitting.

This difference in 'red-shift mode' may result from different biosynthetic pathways of phenylalanine and thymine. There are a large number of phenylalanine and thymine molecules in living cells; in any given molecule of phenylalanine or thymine, each carbon atom can be ^{12}C or ^{13}C, resulting in different isotopomers. There are 9 and 5 carbon atoms in phenylalanine and thymine, respectively. If we allow for the free rotation of the aromatic ring about its sigma bond with the 'alanine' moiety, there are 320 (2^9-12*2^4) different isotopomers for phenylalanine. Thymine has 32 (2^5) different isotopomers. Phenylalanine and thymine are synthesised by particular pathways, therefore the number of permitted isotopomers may be smaller than the upper bounds of 320 and 32 for phenylalanine and thymine, respectively. Each isotopomer has in principle a different Raman frequency (usually reported as a wavenumber). A Raman spectrum of a single bacterium or part of a nematode contains the contribution from all of the molecules within its focal point; and each detected molecule may be any

one of the permitted isotopomers. We can reasonably assume that every molecule contributes to the spectrum equally. Therefore, the shape of a Raman band encodes the shape of the probability distribution of the isotopomers and the observed difference in the 'red-shift mode' of phenylalanine and thymine indicates that their probability distributions of isotopomers may have very different shapes.

5.3.2 Proposed mechanism for the 'red-shift mode' of the phenylalanine Raman band

In order to determine the permitted isotopomers of phenylalanine, we can start tracking carbon atoms from glycolysis. The flow of carbon atoms in the biosynthesis of phenylalanine is shown in Figure S5.2A [199]. Although phenylalanine may be synthesised from other precursors by different reactions, as glucose was the sole carbon source and Raman spectra were taken shortly after the start of incubation, it is reasonable to assume that the biosynthesis of phenylalanine mainly relies on the input of carbon atoms from glycolysis. One glucose 6-phosphate (G6P) molecule and two phosphoenolpyruvate (PEP 1 and PEP 2) molecules provide carbon atoms to the biosynthesis of phenylalanine. Erythrose 4-phosphate (E4P) inherits four carbon atoms from G6P. One carbon atom that originates from a PEP molecule is removed during the synthesis ('PEP 1' in Figure 5.3B and Figure S5.2A). Therefore, E4P, PEP 1 and PEP 2 provide four, two and three carbon atoms to phenylalanine, respectively. The destination of the carbon atoms is shown in Figure 5.3B. As seen in Figure 5.3B, E4P, PEP 1 and PEP 2 provide three 'modules' to form phenylalanine and glucose is the

common precursor of all of the three 'modules'. Since a mixed glucose source was given as the sole carbon source, each one of the E4P, PEP 1 and PEP 2 molecules is randomly all-^{12}C or all-^{13}C. E4P, PEP 1 and PEP 2 should be independent from each other. Therefore, the number of permitted isotopomers of phenylalanine is $2^3 = 8$. These isotopomers are shown in Figure 5.3B, Figure 5.3C, Figure 5.3D and Figure 5.3E. The aromatic ring of phenylalanine, however, has only four isotopic forms. The phenylalanine Raman band corresponds to a ring mode of phenylalanine and therefore the key atoms that affect its Raman frequency are the aromatic carbon atoms. As seen in Figure 5.3, we hypothesise that the eight permitted isotopomers can be divided into four groups and assigned to the four observed phenylalanine Raman bands: Band 1 corresponds to all-^{12}C aromatic rings; Band 2 corresponds to $^{12}C_4{}^{13}C_2$ aromatic rings; Band 3 corresponds to $^{12}C_2{}^{13}C_4$ aromatic rings; Band 4 corresponds to all-^{13}C aromatic rings. This hypothesis explains the origin of the four different phenylalanine Raman bands in isotopically partially labelled *E. coli* (Figure 5.3A).

A Phenylalanine Raman bands in *E. coli*

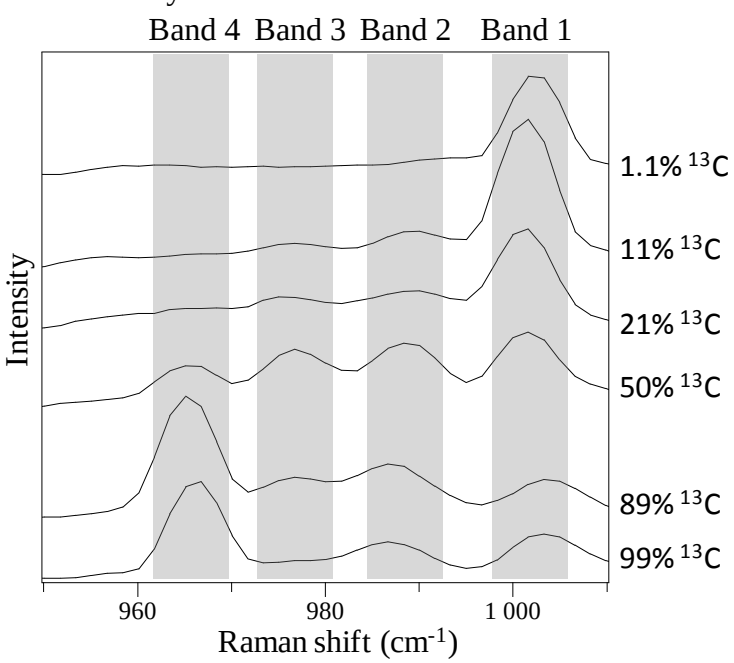

B (Band 1)

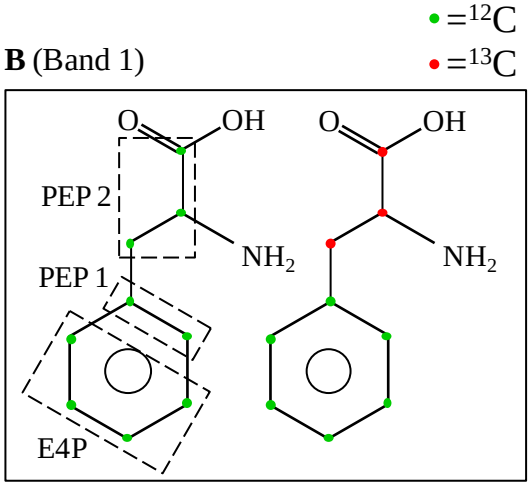

C (Band 2)

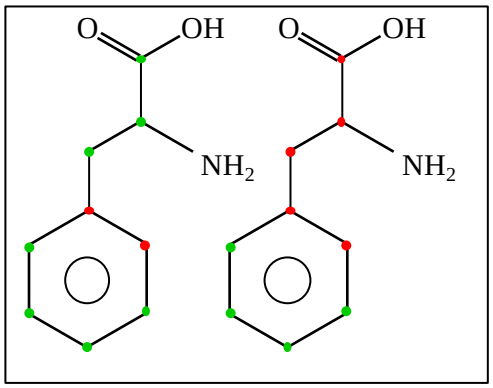

D (Band 3)

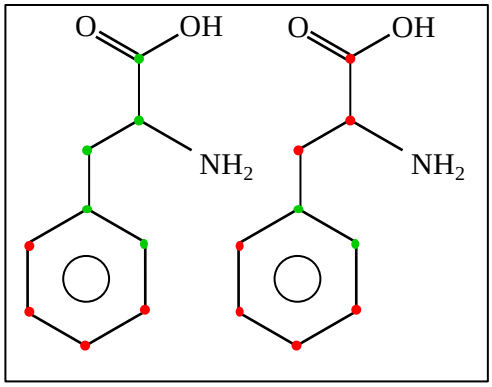

E (Band 4)

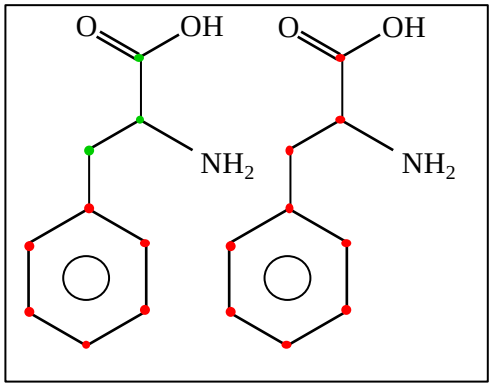

Figure 5.3 The assignment of the four phenylalanine Raman bands.
Four phenylalanine Raman bands were observed in *E. coli*, including the full-^{12}C band (Band 1) and the full-^{13}C band (Band 4) (A); there are eight permitted isotopomers of phenylalanine; they are assigned to the four Raman bands (B-E); the origin of carbon atoms is shown (B).

In order to test this hypothesis, Raman frequencies of the permitted isotopomers of phenylalanine were calculated using a quantum chemical procedure based on density functional theory. The geometric structure of an isolated phenylalanine molecule (Figure S5.3) was optimised and confirmed as a local minimum on the potential energy surface by diagonalisation of the Hessian matrix. The vibrational mode of interest is the Raman-active 'ring-breathing' mode (Movie 1 in Appendix). Conformers in which the aromatic ring has rotated about the sigma bond connecting it to the remainder of the

molecule have in principle different Raman frequencies (isotopomers marked ‘a’ and ‘b’ in Figure S5.4) but the results show that this effect is negligible (± 0.2 cm^{-1}). Figure S5.4 shows Raman frequencies of the permitted isotopomers. The ring-breathing mode appears at 1017 cm^{-1} and 980 cm^{-1} for all-^{12}C and all-^{13}C isotopomers, i.e., with a frequency overestimation of 1.5 %, which is within the typical uncertainty for this level of theory [200] and the simplified model of *in vivo* phenylalanine as an isolated species. The results are clustered in four groups, as isotopic substitution in the C_3 backbone has negligible effect on the Raman frequency of the ring-breathing mode, and this allows unambiguous assignment of the four experimental peaks (Figure 5.4). This assignment is independent from the precision level of theory: for example, calculations with the Hartree-Fock method, which neglects electron correlation, give identical trends and peak assignments.

As described before, ‘red-shift modes’ of phenylalanine and thymine are manifestations of their different probability distributions of isotopomers. The aromatic ring in phenylalanine has four permitted isotopomers, giving the probability distribution a four-peak shape. The Raman frequencies of these isotopomers are well separated; therefore this four-peak probability distribution manifests itself as a four-peak Raman spectrum.

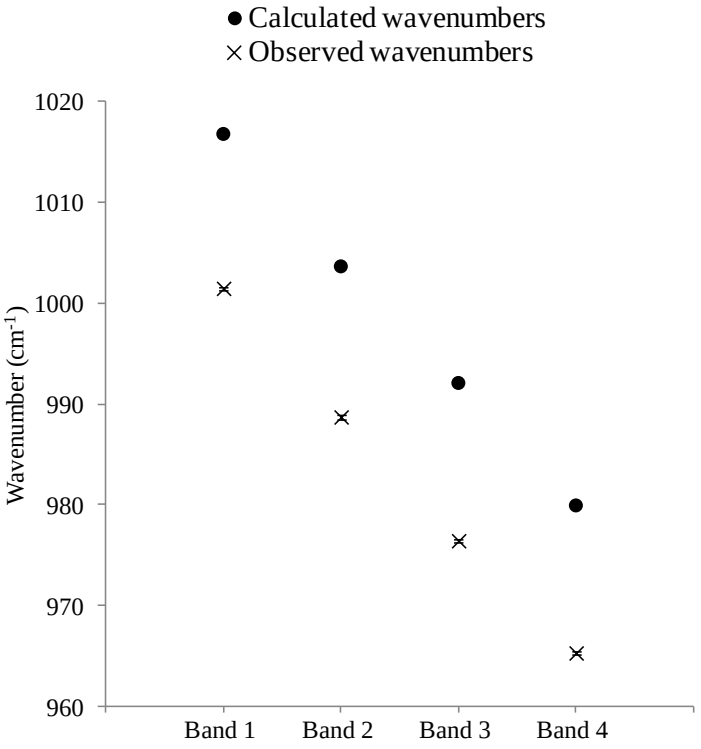

Figure 5.4 Calculated and observed Raman band positions of the four phenylalanine Raman bands.
Error bars show the standard error of the observed wavenumbers.

5.3.3 Proposed mechanism for the 'red-shift mode' of the thymine Raman band

The origin of carbon atoms in the biosynthesis of thymine is more complex than that of phenylalanine. Here we attempt to demonstrate how increased complexity of the thymine biosynthesis ultimately leads to a 'red-shift mode' differing from that of phenylalanine. *De novo* synthesis of deoxythymidylate (dTMP) with deoxyuridylate (dUMP) as its immediate precursor will be used as a typical pathway to demonstrate our hypothesis (Figure S5.2B) [199]. Oxaloacetate, carbamoyl phosphate and N^5, N^{10}-methylenetetrahydrofolate provide three, one and one carbon atom(s),

respectively. Carbamoyl phosphate is a one-carbon molecule of bicarbonate origin and therefore can randomly contribute a ^{12}C or ^{13}C to the thymine biosynthesis. The carbon atom that N^5, N^{10}-methylenetetrahydrofolate contributes could originate from a number of biological molecules; therefore we consider it to be random. The remaining three carbon atoms come from oxaloacetate, an intermediate in the citric acid cycle. From examination of this cycle, we conclude that oxaloacetate also contains random ratios of ^{13}C and ^{12}C. In the citric acid cycle, oxaloacetate's precursors are succinate and fumarate. In succinate, the two methylene carbon atoms are not distinguishable, neither are the two carboxylic carbon atoms; in fumarate, the two alkene carbon atoms are not distinguishable, neither are the two carboxylic carbon atoms. ^{12}C and ^{13}C can randomly enter the cycle in the form of acetyl coenzyme A; they can also randomly leave the cycle in the form of CO_2 owing to the cyclic nature of these reactions and the symmetries of succinate and fumarate. As a result, oxaloacetate can leave the citric acid cycle and enter the biosynthesis of thymine with any number of ^{12}C and ^{13}C. Therefore, thymine molecules can carry a random number of ^{12}C and ^{13}C.

One can divide a phenylalanine molecule into three 'modules' and trace their origin to glucose, the sole carbon source in growth media (Figure 5.3B). However, the origin of carbon atoms in thymine is highly diverse and 'tracing' them would be difficult, if not impossible. We hypothesise that, owing to complexity in the origin of carbon atoms, all 32 possible isotopomers of thymine are permitted.

Based on this hypothesis, Raman spectra of thymine can be calculated and compared to observation. The structure of the isolated thymine molecule (Figure S5.5) was optimised using the same method as for phenylalanine. The mode of interest here is the asymmetric 'ring-breathing' vibration (Movie 2 in Appendix). This mode appears at 737 cm^{-1} for the all-^{12}C isotopomer, indicating a discrepancy of 1.3 %, which is within the uncertainties associated with the level of theory and the simplified model of *in vivo* thymine as an isolated species. The average isotopic shift per ^{13}C substitution at sites a, b, c, d, e is -4, -1, -3,- 6 and -0.1 cm^{-1}, respectively (Figure S5.5). The Raman band of thymine can be seen as the superposition of the Raman bands of all permitted isotopomers. Each isotopomer has a distinct calculated Raman frequency (Figure S5.6) and intensity. In order to calculate the thymine Raman band, a probability for each isotopomer is also needed. The carbon atom provided by carbamoyl phosphate can seen as independent from that provided by N^5, N^{10}-methylenetetrahydrofolate. These two carbon atoms can be also seen as independent from oxaloacetate. The three carbon atoms of oxaloacetate, as described before, can be seen as independent from each other as the result of the citric acid cycle. Therefore, the probability of each isotopomer, as a function of ^{13}C %, can be calculated based on the hypothesis that the isotopic nature of carbon atoms in thymine is the result of the combination of five independent statistical events. Gaussian and Lorentzian functions were used to calculate Raman bands of the 32 isotopomers with four parameters: observed full width at half maximum (FWHM), isotopomer probability, calculated Raman frequency

and calculated relative intensity. The Raman spectra were simulated by adding the 32 Gaussian or Lorentzian functions together (Figure 5.5A and Figure 5.5B). Band position (wavenumber) of the calculated thymine Raman spectra were compared with observed values (Figure 5.5C). Calculated Raman spectra exhibit a linear red-shift with increasing ^{13}C content, and no obvious band splitting is seen. This simulation matches the observed 'red-shift mode' of the thymine band. Gaussian and Lorentzian functions produced virtually identical results. The simulated Raman red-shift of thymine band indicates that the hypothesis described before is likely to be the underlying mechanism for the observed Raman 'red-shift mode' of thymine.

A

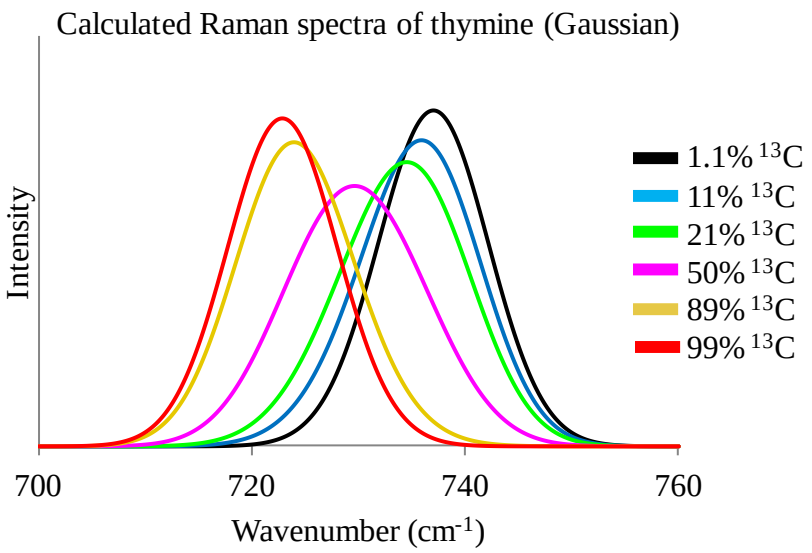
Calculated Raman spectra of thymine (Gaussian)
Intensity
700
720
740
760
Wavenumber (cm-1)
1.1% 13C
11% 13C
21% 13C
50% 13C
89% 13C
99% 13C

B

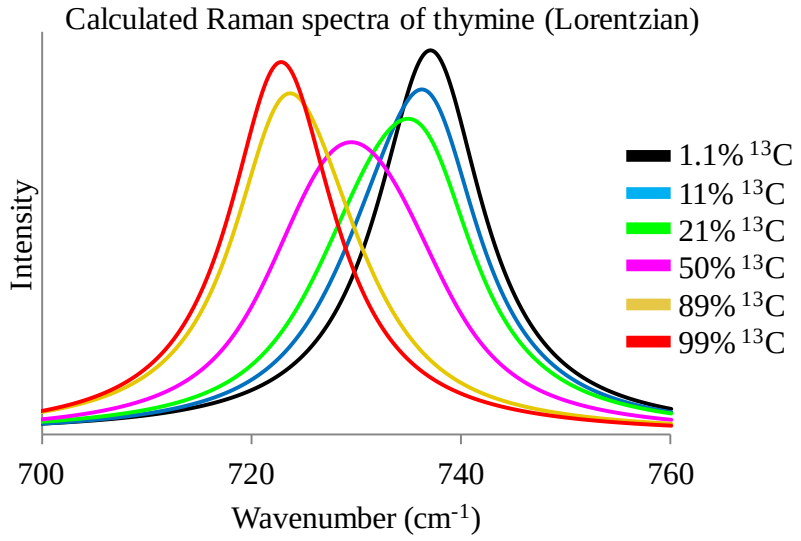
Calculated Raman spectra of thymine (Lorentzian)
Intensity
700
720
740
760
Wavenumber (cm-1)
1.1% 13C
11% 13C
21% 13C
50% 13C
89% 13C
99% 13C

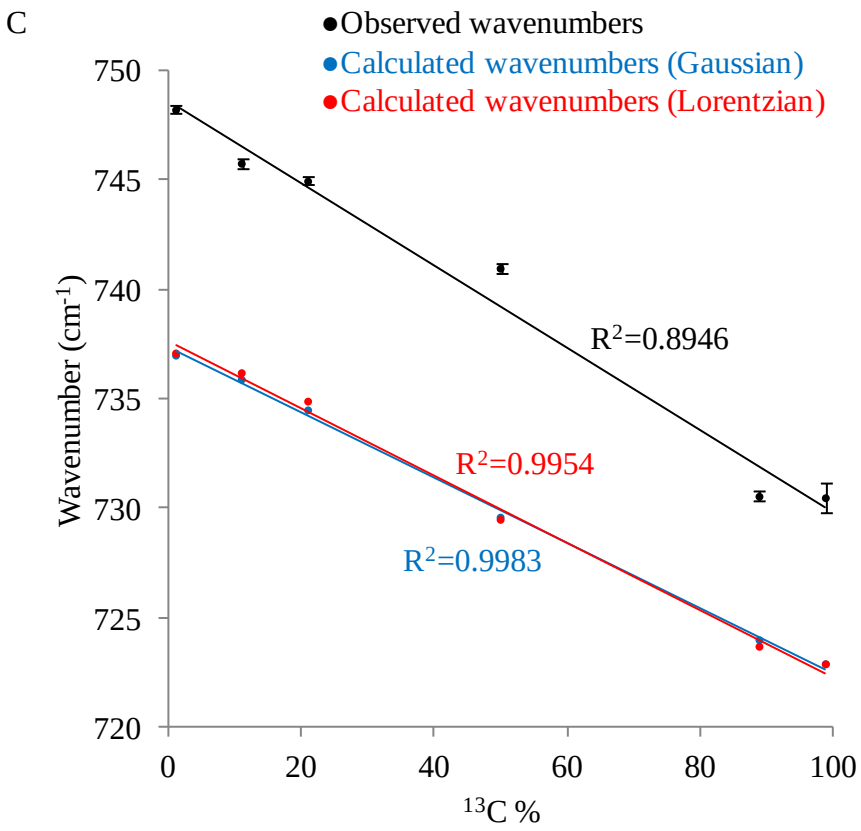

Figure 5.5 Simulated and observed Raman red-shift of the thymine Raman band.
Simulated thymine Raman spectra using Gaussian and Lorentzian functions show similar gradual red-shift with increasing carbon-13 content (A and B); a comparison of the Raman red-shift was drawn between the simulated and observed spectra with error bars showing the standard error of the observed wavenumbers (Day 5-20) (C).

5.4 Discussion

This study describes a novel Raman spectral marker which enables the monitoring of carbon flow from a carbon source, via microorganisms, to single predatory nematodes in a non-destructive and quantitative manner. This marker is the thymine Raman band, which has a different 'red-shift mode' from another important Raman spectral marker, the phenylalanine

band. Mechanisms accounting for this difference are proposed in this study, revealing a dependence of the Raman red-shift on biochemistry. This study provides researchers with a new and accurate technique for quantifying ^{13}C-incorporation at single-cell level, which is supported by quantum chemical calculation. As discussed in detail above, the red-shift and shapes of Raman bands may encode information about biosynthetic pathways. By revealing this hidden relationship, this study also proves the concept that Raman spectroscopy and the Raman-SIP method can be a simple but powerful technique to probe the complex biochemical reaction networks.

The slope of the linear regression line for observed red-shift shows that a ± 5.3 % change in ^{13}C % will shift the thymine band by ± 1 cm^{-1} (Figure 5.5C). Therefore, when the thymine Raman band is used to determine single cells' ^{13}C content, 5.3 % can be seen as the resolution of ^{13}C % measurement with the present equipment. It could be further improved by using a better spectrometer and finer grating. In comparison with other methods which measure the isotopic incorporation, such as mass spectrometry, secondary ion mass spectrometry and ultracentrifugation, this resolution is competitive.

Based on the collection of Raman spectra in our laboratory, the thymine Raman band is observed in *C. elegans*, Chinese hamster ovary (CHO) cells, human embryonic stem cells, and some protists. It is usually absent from bacteria. Interestingly, the thymine band appears in a strain of *Pseudomonas* and this strain is known to have an accumulation of DNA absorbed on its surface [80]. The absence of the thymine band from bacteria may be a result of their relatively small genomes and consequently smaller number of

copies of thymine molecules in each cell. *E. coli* K-12 has a genome size of 4.6 M [201]; *C. elegans* has a genome size of 97 M [202]; sequence data of CHO cells and human are on Gb level [203, 204]. In addition, thick bacterial cell wall may attenuate both the Raman probing lasers and the thymine Raman signal. The almost universally observed phenylalanine Raman band will still serve as a quantitative spectral marker for ^{13}C content at single-cell level but when the thymine band is available, it will be more reliable since that Raman wavenumbers are more accurate than Raman band intensities.

5.5 Supplementary figures

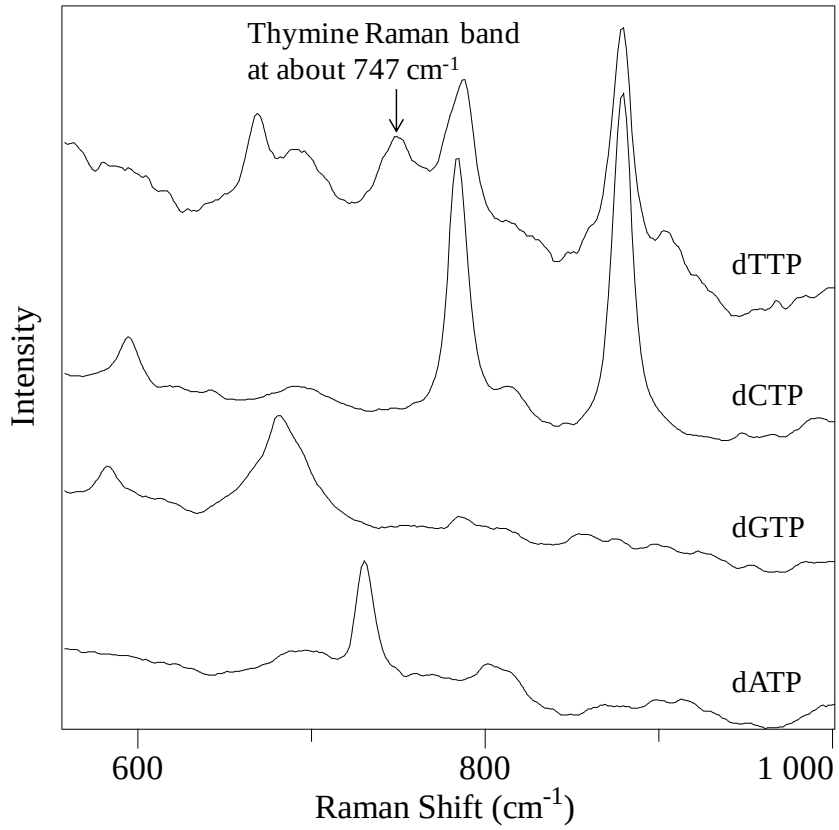

Figure S5.1 Raman spectra of dNTP.
The Raman band at about 747 cm^{-1}, assigned to thymine, was observed only in dTTP (100 mM dNTP, Sigma-Aldrich).

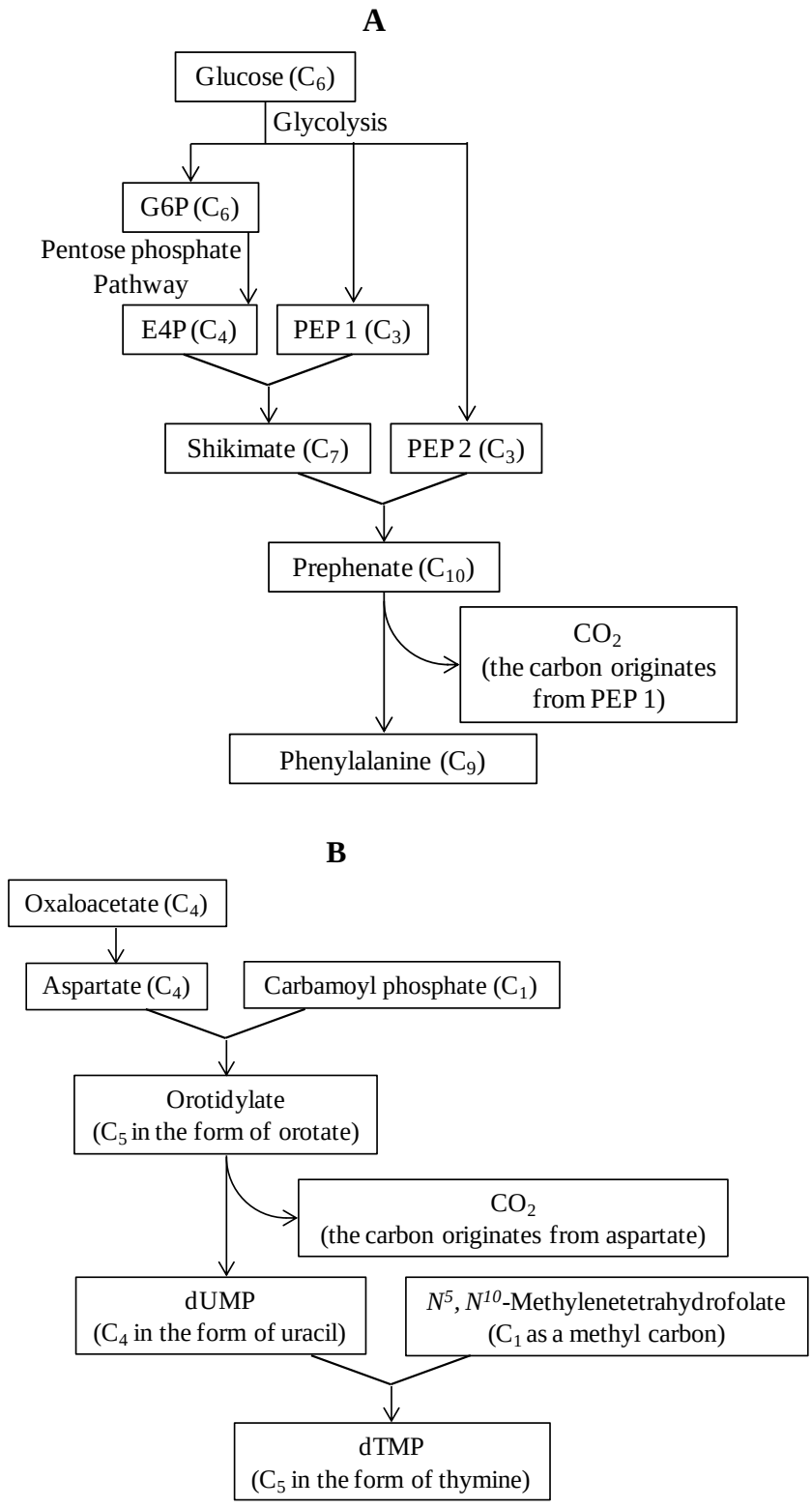

Figure S5.2 The flow of carbon atoms in the biosynthesis of phenylalanine (A) and thymine (B).

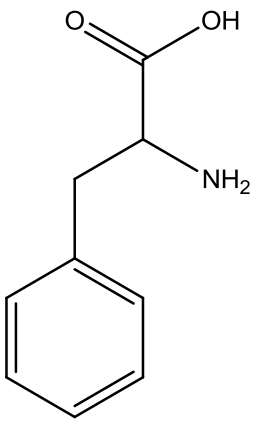

Figure S5.3 Structure of phenylalanine.

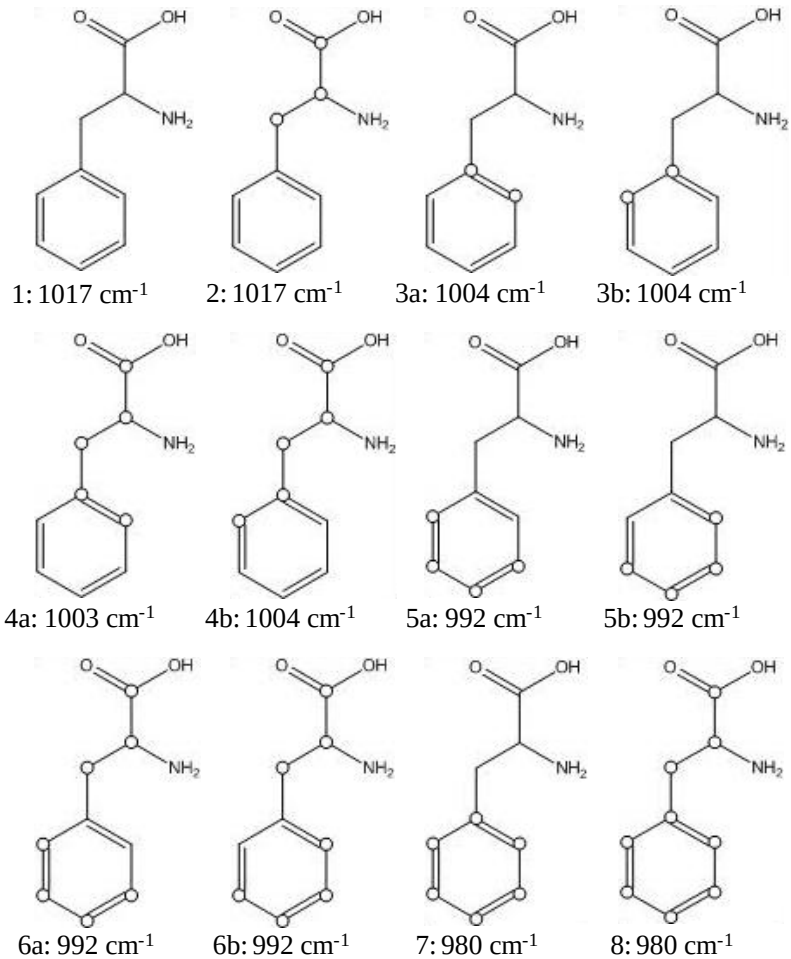

Figure S5.4 Calculated isotopic shift of phenylalanine.
The positions of ^{13}C-atoms are labelled by hollow circles.

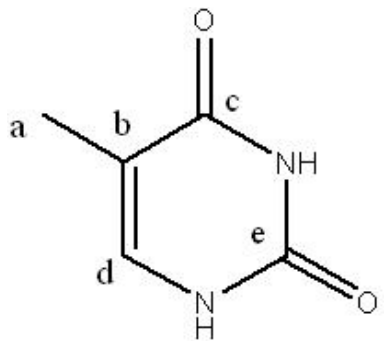

Figure S5.5 Structure of thymine with carbon sites denoted.

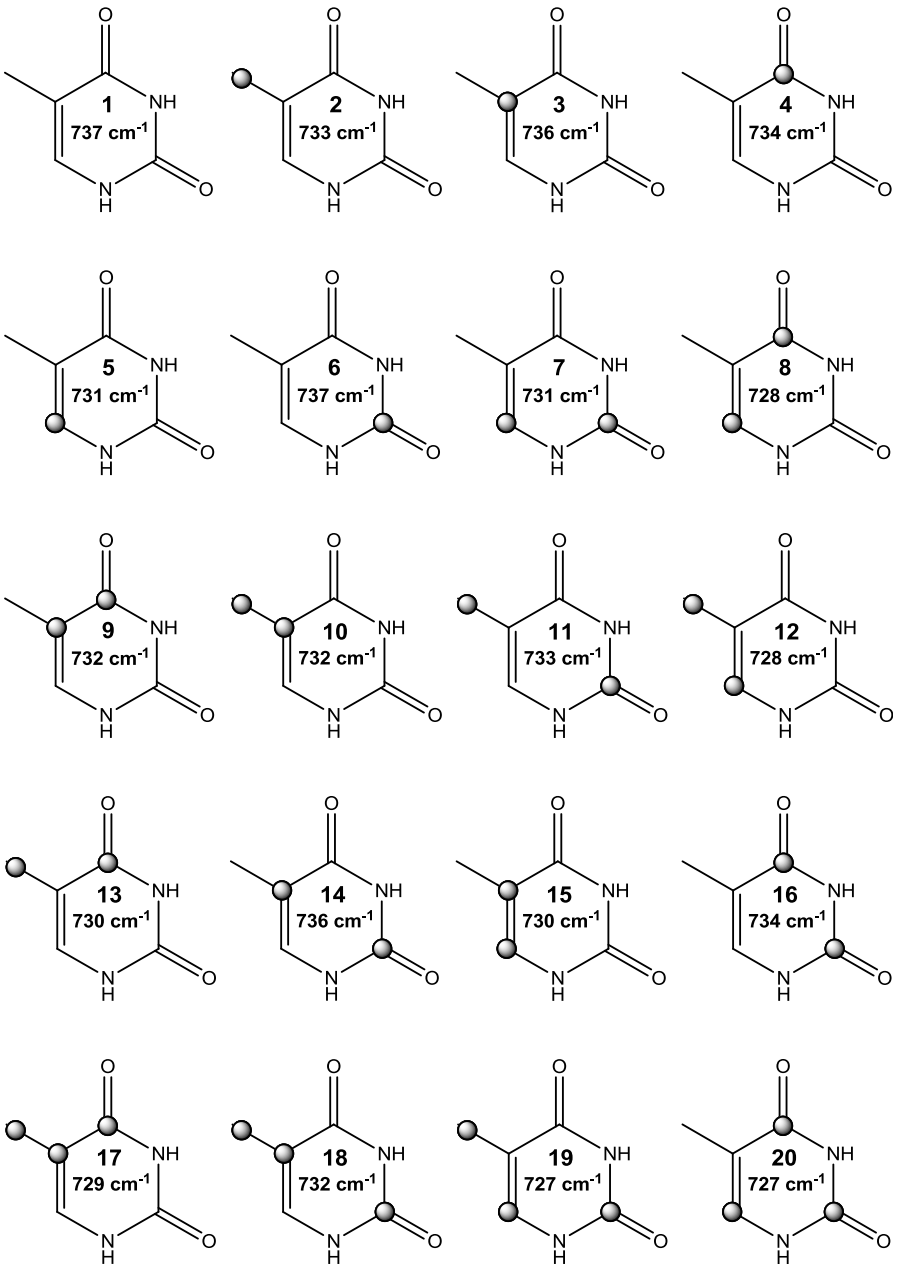
1
737 cm-1
2
733 cm-1
3
736 cm-1
4
734 cm-1
5
731 cm-1
6
737 cm-1
7
731 cm-1
8
728 cm-1
9
732 cm-1
10
732 cm-1
11
733 cm-1
12
728 cm-1
13
730 cm-1
14
736 cm-1
15
730 cm-1
16
734 cm-1
17
729 cm-1
18
732 cm-1
19
727 cm-1
20
727 cm-1

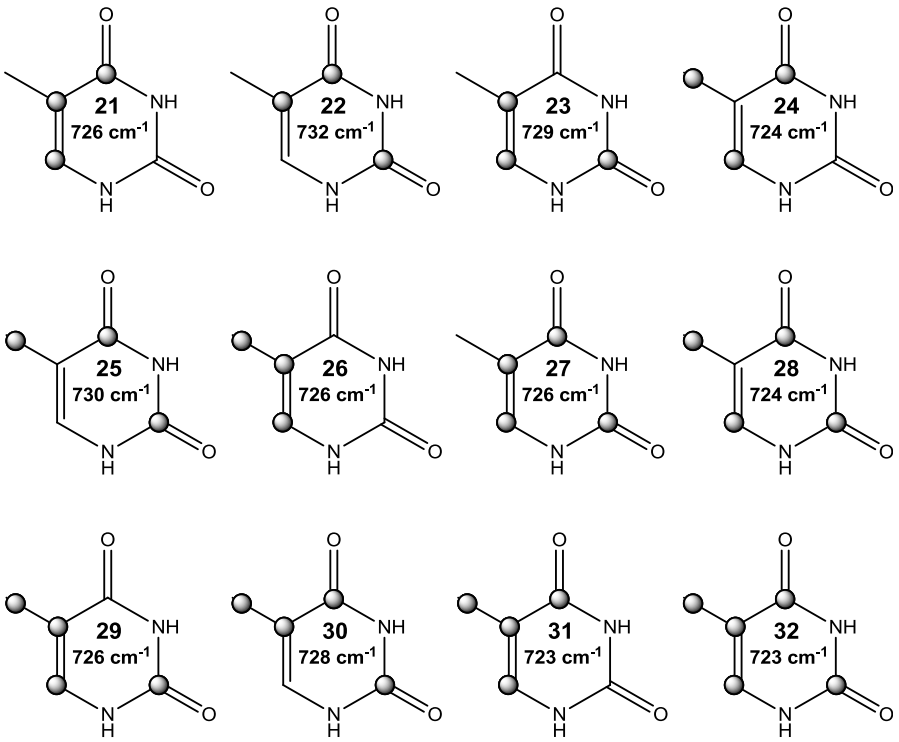

Figure S5.6 The 32 isotopomers of thymine.
The positions of ^{13}C-atoms are labelled by shaded spheres.

Chapter 6: Raman activated cell counting for profiling carbon dioxide fixing microorganisms

6.1 Introduction

Photosynthetic microorganisms are one of the major sinks of atmospheric CO_2 and the main primary producers in marine ecosystems. Photosynthetic microorganisms may also harbour many previously unknown genes encoding enzymes and other biological products with high values in biotechnology industry and renewable energy research. They are a vastly diverse group of microorganisms that consists of prokaryotic and eukaryotic species. Like other environmental microorganisms, most of them do not grow in laboratories. Therefore, researchers have to study individual cells in order to gain an unbiased view of photosynthetic microbial communities.

The technological advances in Raman spectroscopy and microfluidic device are of particular interest for the increasingly important single-cell research [85, 205, 206]. The characterisation of individual microorganisms is being used by more researchers in order to study unculturable microorganisms and phenotypic variation within isogenic populations [21, 57, 94, 207, 208]. However, owing to the small size and heterogeneity of many naturally occurring cells, developing high-throughput single-cell techniques remains a challenge. Raman spectroscopy offers a unique opportunity for single-cell analysis because it provides an intrinsic and label-free chemical profile of a

single cell with sub-micrometre spatial resolution. When combined with a microfluidic device system, Raman spectroscopy may be used to build a high-throughput Raman activated cell sorting (RACS) system to survey natural microbial communities without artificial interference such as fluorescent labelling or the insertion of reporting genes.

Raman spectra are generated by detecting inelastically scattered light from a sample. Analogous to infrared spectra, the bands in Raman spectra match the vibrational frequencies of the chemical bonds present in the sample. A Raman spectrum of a single microorganism contains a large number of bands due to the complex chemical composition of a cell; therefore, it can serve as the chemical fingerprint of a cell, which differs depending on the species and physiological states of cells [44, 82]. Visible and near-infrared lasers are usually used in Raman spectroscopy for biological samples. They do not cause any significant chemical or biological change in interrogated cells, which can be recovered for cultivation or DNA analysis [27, 85].

However, Raman scattering is a relatively weak process that occurs once in every 10^6 - 10^8 incident photons [20]. In order to acquire a Raman spectrum that has a reasonably high signal-to-noise ratio from a single microbial cell, a spontaneous Raman spectrum usually requires at least 4 to 5 s with a well optimised confocal Raman microscope [22]. An acquisition time of a few seconds is difficult to achieve in a microfluidic device because it is difficult to stabilise a slow flow rate that maintains a cell within the Raman detection region for such a long time. Even if it is technically possible, the throughput

of the resultant RACS system would be very low, precluding it from useful applications.

Reducing the Raman spectrum acquisition time is thus vital to achieve high-throughput RACS systems. Surface-enhanced Raman scattering (SERS) and resonance Raman (RR) spectroscopy are widely used to enhance the Raman signal and reduce the Raman spectrum acquisition time. SERS is mainly an electromagnetic enhancement that occurs in the vicinity (about < 10 nm) of gold/silver nanoparticles or patterned surfaces [37, 38, 137]. SERS has been proven to enhance the Raman signal by up to a factor of 10^{14} and is able to detect single molecules [209]. SERS has been combined with microfluidic devices for several applications [210-213]. The RR effect can enhance the Raman signal from RR-active molecules by up to six orders of magnitude [31]. RR spectroscopy has shown great potential as a rapid label-free imaging technique for photosynthetic microorganisms [21]. The RR enhancement requires no special treatment of the sample, while SERS experiments usually involve treating microorganisms with gold or silver nanoparticles.

Carotenoids are highly diverse (over 600 types in carotenoid groups) and RR-active molecules. Nearly all photosynthetic microorganisms contain carotenoids that are essential for light harvesting, singlet oxygen quenching, and the structure of a photosynthetic pigment-protein complex [21]. Due to the greatly enhanced Raman signature of carotenoids in photosynthetic cells, a Raman spectrum of a single cell, recorded with a 1 ms acquisition time, may be used to quantify CO_2 fixation of the cell [21].

In this study, a combination of RR spectroscopy and microfluidic device is reported to perform Raman activated cell counting. Figure 6.1 shows the schematic illustration of the platform. We profiled an artificially mixed microbial community to quantify the ratio of ^{12}C- and ^{13}C-containing cells. This study paves the way toward the development of a high-throughput RACS system that can characterise photosynthetic microbial communities and isolate photosynthetic cells of interest [22].

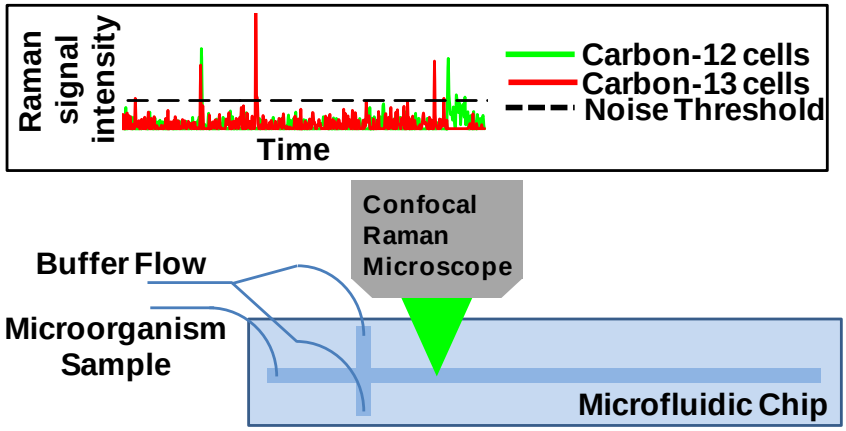

Figure 6.1 Schematic representation of the RR-microfluidic cell counting system.

6.2 Experimental Methods

6.2.1 Chemicals, microbial strain, and growth conditions

All chemicals and growth media used in this study were purchased from Sigma-Aldrich UK unless otherwise stated. *Synechocystis* sp. PCC 6803 was used as the model strain in this study. *Synechocystis* sp. PCC 6803 was grown in BG-11 media supplemented with 5 mM ^{12}C- or ^{13}C-sodium bicarbonate as the sole carbon source. The cell concentrations of ^{12}C- and

^{13}C-cells were counted by fluorescence microscopy before mixing them for Raman measurement. Naturally dissolved CO_2 in BG-11 media was removed by a degasification step prior to the incubation of the PCC 6803 strain, as previously described [21]. The *Synechocystis* sp. PCC 6803 strain was grown at 30 °C and 50 μmol photons $m^{-2}s^{-1}$ on an orbital shaker (150 RPM) for 4 days (Innova 44 illuminated rotary incubator, New Brunswick Scientific, Cambridge, UK).

6.2.2 Fabrication and operation of the microfluidic devices

The microfluidic chip was fabricated using a conventional soft-lithographic technique [214]. The chip was fabricated in polydimethylsiloxane (PDMS), where two-dimensional hydrodynamic focusing was implemented, whose design is shown in Figure 6.2. Laminar microfluidic flow was achieved by pressure-driven flow using syringe pumps (Pico Plus, Harvard Apparatus). The microfluidic channel had a height of 50 μm and a width of 100 μm (Figure 6.2). Cells were injected into the chip through the sample inlet, and the buffer solution (water) was injected into the chip through the buffer inlet. The ratio of the flow rate of the sample stream to that of the buffer stream was fixed at 1:4. The total flow rate at the Raman detection region was 17.7 nL / min. At the flow-focusing region, which is designed as a cross junction, the sample stream was hydrodynamically focused to the centre of the main channel by the higher flow rate of the buffer stream.

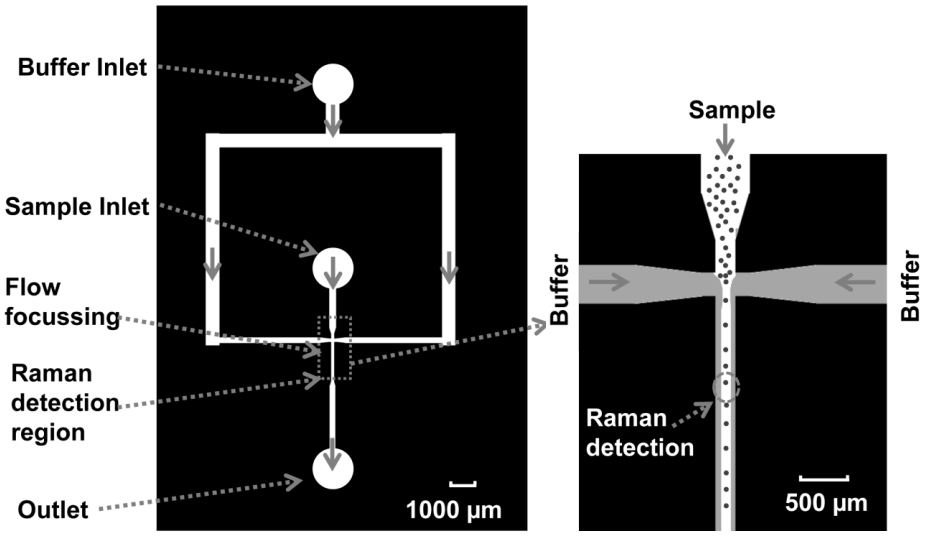

Figure 6.2 Schematic representation of the microfluidic chip used in this study.
Channels are shown in white. The buffer streams focused the sample stream into a nearly single-cell flow. Inset: hydrodynamic focusing and Raman detection region (cell shown in the figure are not to scale). Cells were injected into the microfluidic chip through the sample inlet, and buffer solution (water) was injected through the buffer inlet to achieve two-dimensional hydrodynamic focusing before the Raman detection region. At the Raman detection region, the channel had a width of 100 µm and height of 50 µm. The total flow rate at the Raman detection region was 17.7 nL/min, and the ratio of the flow rate of the sample stream to that of the buffer stream was 1:4.

6.2.3 Total cell counting of the ^{12}C- and ^{13}C-cells

In order to determine the ratio of the numbers of the ^{12}C- and ^{13}C-cells in the mixed sample, the number of cells in both samples was determined before being mixed for the RR-microfluidic device experiment. Twenty microlitre of ^{12}C- and ^{13}C-cell suspension was dried separately onto two 0.2 µm membrane filters (Millipore, U.S.A.) by a vacuum filtration device. The images of the cells on the membrane filters were recorded by a fluorescence microscope (Carl Zeiss, UK) with Cy5 fluorescence filter and a 40× dry objective (NA = 0.60, Carl Zeiss, UK). Twenty images of non-overlapping

views were recorded for each sample. The number of cells in each image was manually counted in ImageJ software (http://rsb.info.nih.gov/ij/).

6.2.4 Raman activated cell counting of the ^{12}C- and ^{13}C-cells

The mixture of the ^{12}C- and ^{13}C-cells (the mixing ratio was 1:1 by volume) was washed with phosphate buffered saline three times before loading into the microfluidic device. RR spectra were acquired consecutively when the cells were flowing through the Raman detection region of the microfluidic channel. RR spectra were acquired using a confocal Raman microscope (LabRAM HR, HORIBA Scientific, UK) equipped with a 532 nm Nd:YAG laser (Torus Laser, Laser Quantum, UK) and a 50× air-dry objective (NA = 0.55, Leica Microsystems, UK). The laser beam was targeted to the centre of the microfluidic channel. The laser power on a single cell was about 18 mW. The detector was a CCD detector kept at -70 °C (Andor Technology, UK). The confocal pinhole was 100 μm. Each Raman spectrum was acquired between 2172 and 557 cm^{-1}, with a spectral resolution of about 1.5 cm^{-1}. LabSpec software (HORIBA Scientific, U.K.) was used to control the Raman system and acquire Raman spectra. Raman spectra were acquired and recorded every 36.6 ms, including the acquisition time of 10 ms. There was about 26.6 ms in every Raman signal recording cycle for the system to process and save data. Detected cells were differentiated based on the position of the ν1 RR band of carotenoids (Figure 6.3). Cells containing ^{13}C had distinctively red-shifted RR bands.

6.3 Results and Discussion

The photosynthetic cells of *Synechocystis* sp. PCC 6803 were driven by the syringe pump to flow through the Raman detection area of the microfluidic channel, while the confocal Raman microscope acquired Raman spectra consecutively about 27 times per second. *Synechocystis* sp. PCC 6803 cells were 1 - 2 μm spherical cells and were hydrodynamically converged to the middle of the microfluidic channel. Discrimination of ^{12}C- or ^{13}C-cells was done by determining the position of the ν1 RR band (Figure 6.3). The ν1 RR bands of ^{13}C-cells shifted distinctively to lower wavenumbers, which can serve as a quantitative marker of single cells' ^{13}C content [21].

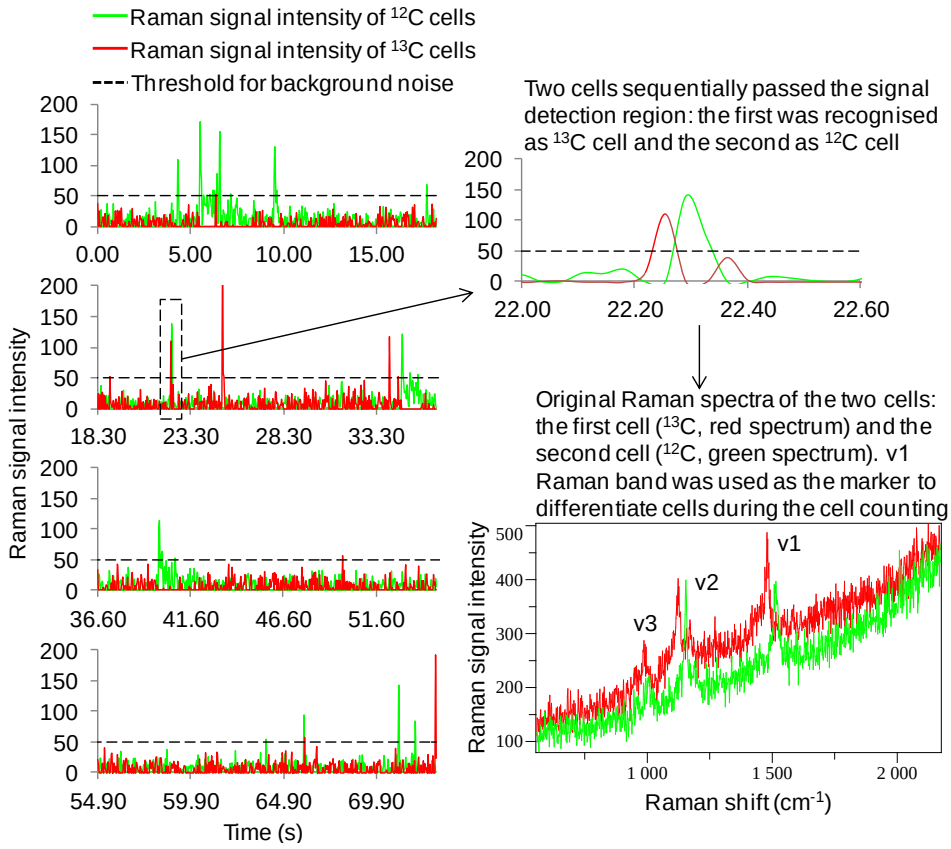

Figure 6.3 An example of the RR-microfluidic counting of photosynthetic microorganisms.
As the cells of the model strain *Synechocystis* sp. PCC 6803 flow through the Raman detection area of the microfluidic device, RR spectra were acquired consecutively about 27 times per second. The v1 RR band was used to differentiate ^{12}C- and ^{13}C-cells. The intensity of this band was plotted against the time axis and displayed in green and red for ^{12}C- and ^{13}C-cells, respectively. A part of the figure near 23.3 s was enlarged to show a ^{13}C-cell and ^{12}C-cell passed through the Raman detection area sequentially only about 0.1 s apart from each other; the untreated RR spectra of the two cells show a distinctive red-shift of all of the carotenoids RR bands.

The total numbers of ^{12}C- and ^{13}C-cells counted separately by fluorescence microscopy were 1125 and 762, respectively. Because the fluorescence microscopic counting was performed using the same procedure for both samples and they were mixed 1:1 by volume afterward, the real ratio of the number of ^{12}C-cells to that of ^{13}C-cells was 1.48. This ratio was measured at

1.56 (316 ^{12}C-cells and 203 ^{13}C-cells) in the RR-microfluidic device counting. The counting result of the RR-microfluidic device is therefore 95 % accurate in this instance compared to fluorescence microscopic counting, which is an accurate reference method. The good agreement proves the concept that the combination of RR spectroscopy and microfluidic device can be a novel method to rapidly profile the ^{13}C distribution in photosynthetic microbial communities in a non-destructive manner.

If a photosynthetic microbial community is given $^{13}CO_2$ as the sole carbon source, this method will be able to rapidly monitor the uptake of $^{13}CO_2$ and the kinetics of CO_2 fixation. Because of the non-destructive nature of this method, measured cells can be further used in nucleic acid amplification or cultivation. The CO_2 fixation data provided by this method will be easily comparable among different photosynthetic microbial communities to investigate the effects of environmental factors on the CO_2 fixation such as temperature, lighting condition, water salinity, depth of water, etc. RR spectroscopy is very sensitive to stable isotope labelling; therefore, a small amount of sample (e.g., 50 μL of seawater) is needed to achieve the kinetic monitoring of photosynthetic microbial communities. In contrast to other methods that are also sensitive enough to detect ^{13}C-incorporation at single-cell level, for example, nanometre scale secondary ion mass spectrometry (NanoSIMS), RR spectroscopy does not require any special sample preparation; it is also non-destructive, easier to operate, and inexpensive.

The method reported in this study is intended to serve as a proof of concept and a stepping stone toward the proposed high-throughput RACS system

[22]. The flow velocity inside the microfluidic chip in the RACS should be ideally adjusted to equal the quotient of the diameter of the confocal Raman sampling volume divided by the Raman spectrum acquisition time. One millisecond has been proven to be enough to record Raman spectra that differentiate ^{13}C-single cells from ^{12}C-single cells [21]. Considering the time needed for recording data, communication between different parts of the instrument etc., measuring and sorting two cells per second is a conservative estimation of the throughput of the proposed RACS system. We can then potentially measure and sort up to 14,400 single cells in 2 h, which are sufficient to characterise a photosynthetic microbial community and enough replicates of different species can be collected from them. The main technical difficulty in developing such RACS systems is the reliable synchronisation of the Raman spectrometer, the controlling computer, and the sorting mechanism (e.g. optical force sorting, pressure-driven closure of the microfluidic channel). There is scope for improving the efficiency of the hydrodynamic focusing in the microfluidic chip. As described above, the ratio of the flow rate of the buffer channel (water) to that of the sample channel (cell suspension) was set to 4:1. This was done to balance between the efficiency of data recovery (detecting a large number of cells) and the data quality (good signal-to-noise ratio). A higher ratio of flow rates will focus cells more tightly to the centre of the channel; therefore, more cells will flow through the focal area of the laser, and more cells will be recorded. One can usually achieve a higher ratio of flow rates by increasing the flow rate of the buffer channel because the flow rate of the sample channel is

usually already very low, and reducing it caused unstable flow with the experimental devices used in this study. However, increasing the buffer flow will decrease the time during which a cell remains within the focal area of the laser and therefore reduce the quality of the resulting spectrum. One can reduce the spectrum acquisition time to match this shortened time, but it is unlikely that the signal-to-noise ratio will improve without upgrading the optical part of the system. With advancement in microfluidic technology, it will be possible to use more sophisticated microfluidic devices to achieve a more stable flow at a slower flow rate.

In summary, this study reports a novel method that combines RR spectroscopy and microfluidic devices in order to rapidly profile the ^{13}C content in photosynthetic microbial communities. This provides the foundation for developing a high-throughput RACS system to monitor and sort single cells of natural photosynthetic microbial communities without cultivation bias.

Chapter 7: Quantitative measurement of nitrogen-15 uptake in *Ruegeria pomeroyi* DSS-3 single cells by Raman spectroscopy

7.1 Introduction

Nitrogen cycling by microorganisms plays an important role in the global nitrogen cycle and agricultural production, for example, symbiotic rhizobia provide plant growth a vital nitrogen source, cyanobacteria are believed to be the major nitrogen fixing microorganisms in marine environments [215]. There is a large diversity in bacteria and archaea that make significant contributions to the transformation of nitrogen compounds, e.g. fixation, ammonium oxidation and denitrification [216]. Microorganisms also utilise organic nitrogen compounds as their nitrogen and carbon sources [217]. However, as majority of microorganisms in natural environments are unculturable, it is necessary to employ culture-independent methods to study microorganisms that are involved in nitrogen transformation.

Metagenomics methods are widely used in environmental microbiology because it circumvents the growth of microorganisms by directly analysing the combined genome sequences of the microbial communities [13, 18]. A recent study concluded that bacterial flavin-containing monooxygenase can function as trimethylamine monooxygenase (TMM) in marine microorganisms [218]. TMM genes were found to be widely distributed in a

major group of marine microorganisms, the *Roseobacter* clade bacteria, which indicates that methylated amines (MAs) may be important nitrogen, carbon and energy sources for marine microbial ecosystems [218]. However, there is still a lack of easily accessed direct evidence to evaluate the significance of MAs for marine microbial communities.

Stable isotope probing (SIP) is widely used to label environmental microorganisms that incorporate certain compounds of interest [129]. Stable isotope-labelled compounds are chemically similar to their naturally occurring counterparts, therefore are used in the incubation of environmental samples under nearly natural conditions. The separation and identification of stable isotope-labelled microorganisms are usually done by one or more of the following methods: separation and sequencing of community nucleic acids that contain stable isotopes, mass spectrometry based methods such as nanometre scale secondary ion mass spectrometry (NanoSIMS), Raman spectroscopy [58, 129, 219, 220]. Nucleic acids based methods mix the genetic materials from the microbial community and usually cannot differentiate microorganisms with difference levels of stable isotope labelling (for example, the separation of microorganisms containing 30 % stable isotopes from ones that contain 60 %). NanoSIMS and Raman spectroscopy can quantify the content of stable isotopes in single microorganisms, making them ideal for researchers to study the nitrogen flow in microbial communities. NanoSIMS has higher sensitivity and spatial resolution at nanometre level, but Raman spectroscopy requires much

simpler experimental procedures and is suitable for measuring large number of single cells in environmental samples [21].

The combination of ^{13}C-SIP with Raman spectroscopy has been used in a number of studies [21, 26, 81, 221]. Distinctive isotopic shifts in vibrational frequencies caused by heavier ^{13}C-atoms can be used as the marker for the incorporation of ^{13}C-labelled substance. Some Raman bands, such as the phenylalanine band, can be used to quantify the percentage of ^{13}C in the sample [26]. However, the application of ^{15}N-Raman-SIP spectroscopy in environmental microbiology is limited as a suitable band has not been found to serve as the quantitative spectral marker for ^{15}N-incorporation. Using a strain in marine *Roseobacter* clade, this study demonstrates that by using multivariate analysis, whole Raman spectra may be used to quantify single microbial cells' ^{15}N content.

7.2 Materials and Methods

7.2.1 Bacterial strain and growth conditions

Ruegeria pomeroyi DSS-3 (ATCC number: 700808) is a marine *Roseobacter* model strain. It was grown as previously described [218]. The sole nitrogen source in the media was monomethylamine (MMA). Different ^{15}N levels were achieved by adding ^{14}N-MMA and ^{15}N-MMA to the media to a total concentration of 2 mM. Taking into account the natural abundance

of ^{15}N, the 6 different percentages of ^{15}N used in this study were 0.37, 10, 20, 49, 74 and 98 %.

7.2.2 Raman micro-spectroscopy

Samples were collected from culture media by centrifugation (3000 RCF, 5 min). Pelleted cells were then washed three times by water and air-dried on calcium fluoride slides. Single-cell Raman spectra were acquired by a confocal Raman microscope (LabRAM HR, HORIBA Scientific, UK). A 100 × dry objective (NA = 0.90, Olympus, UK) was used to focus probing laser on single cells and collect Raman signal. The confocal Raman microscope was equipped with a motorised XYZ stage (0.1 μm step size). Raman spectra were taken with a 532 nm Nd:YAG laser (Torus Laser, Laser Quantum, UK). The laser power was about 35 mW on a single cell. The diameter of the confocal pinhole was set to 50 μm. Each Raman spectrum was acquired between 558 cm^{-1} and 2173 cm^{-1}, with 1021 data points and a spectral resolution of 1.5 cm^{-1}. Acquisition time was 30 s. LabSpec software (HORIBA Scientific, UK) was used for controlling the Raman microscope and spectral data pre-treatment. At least twelve randomly chosen single cells were measured on each ^{15}N level.

7.2.3 Raman spectra analysis

All Raman spectra were smoothed and normalised in LabSpec software before statistical analysis. Spectra were smoothed by Savitsky-Golay smoothing method; smoothing parameters were: degree 2 and size 7.

Whole-spectrum normalisation was performed to normalise the total integral peak area of each spectrum to a fixed value.

The pre-treated spectral data were imported to MATLAB (version R200011A, MathWorks, MA, USA) for multivariate analysis. Principle component (PCA) was employed to reduce the dimensionality of the multivariate data, whilst retaining the variance and was performed prior to canonical variate analysis (PC-CVA) [222]. In this study, PC-CVA models were built with *a priori* knowledge of the ^{15}N content in the biological replicates. Cross-validation was performed in order to ensure these models were not over- or under-trained. Nine of the biological replicates were employed for model training with the remaining three replicates projected into the model for cluster validation purposes, as previously reported [40]. Circles in the PC-CVA score plots represent the 95 % χ^2 confidence region constructed around each group mean based upon the χ^2 distribution with two degrees of freedom [223].

Partial least square regression (PLSR) [224] is a multivariate linear regression method and was performed to predict ^{15}N content of single bacterium based on Raman spectra. As for PC-CVA, the PLSR models were calibrated with nine of the twelve biological replicates and the remaining replicates were used as an independent test set to validate the model and establish whether the models could generalise.

7.3 Results and Discussion

Principle component analysis (PCA) was employed to reduce the dimensionality of Raman spectral data whilst retaining the majority of variance in the data set. Based on the results of the unsupervised PCA, a supervised method, canonical variate analysis (CVA) was used to study the clustering of data. CVA minimises the variance within groups (same ^{15}N %) whilst maximises variance between groups (different ^{15}N %). A calibration line between Raman spectra and ^{15}N % was found by partial least square regression (PLSR). PLSR is a multivariate regression method that is suitable to treat data with large variance which is irrelevant to the calibration line [225]. Raman spectra have relatively large spectrum-to-spectrum and replicate-to-replicate variance which can be caused by irrelevant factors such as bacteria cell size, the position of laser focal point or penetration depth. These factors are irrelevant to ^{15}N % but can cause significant difference in the intensity of Raman bands.

Averaged Raman spectra of *Ruegeria pomeroyi* DSS-3 grown in media with different ^{15}N % are shown in Figure 7.1. Raman red-shift cased by the incorporation of ^{15}N can be seen in some part of the spectra but was less obvious than the typical red-shift of ^{13}C [20]. Most of the ^{15}N-red-shift also overlaps with other Raman bands and it was difficult to use a single Raman band to mark the isotope uptake.

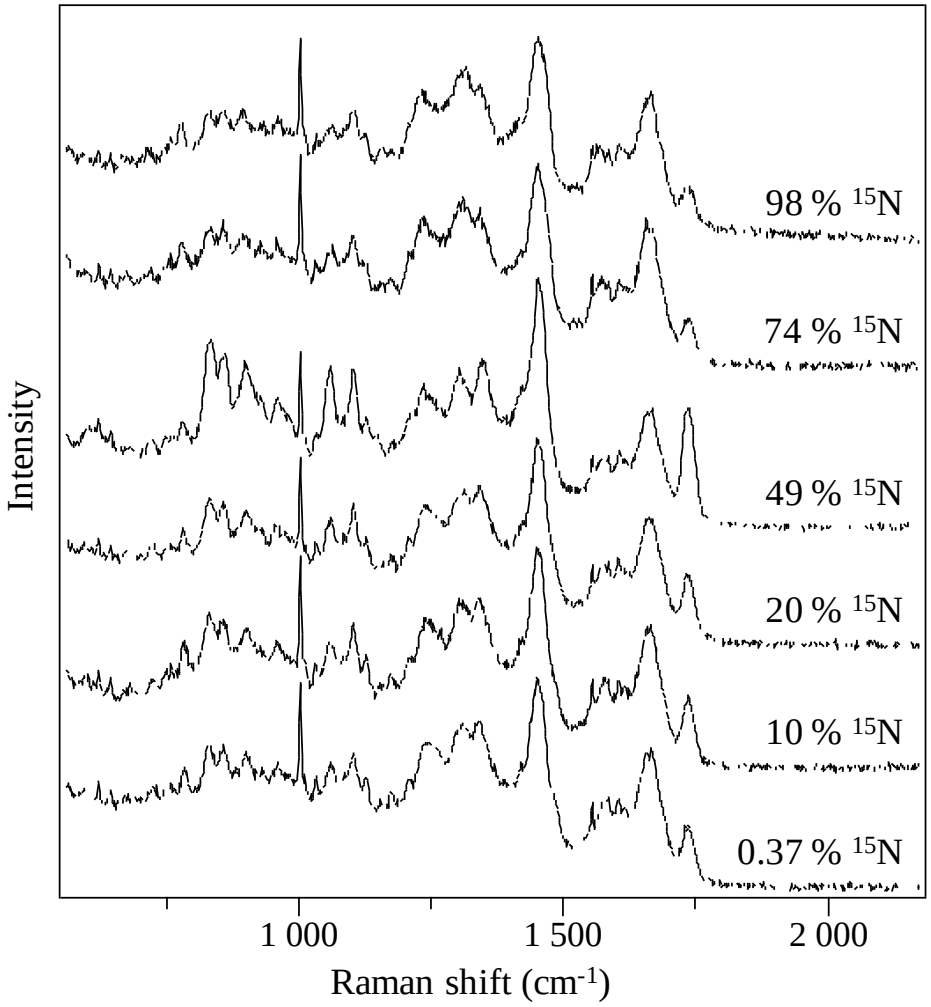

Figure 7.1 Raman spectra of *Ruegeria pomeroyi* DSS-3 grown in media with different ^{15}N content.

As seen in Figure 7.2, the first axis in PC-CVA (PC-CV 1) accounts for the greatest variance in the spectral data. The scores in PC-CV 1 also show a trend that it is correlated with ^{15}N %. Large differences in ^{15}N content, e.g. 0.37 % and 49 % (denoted as 00 and 50 in Figure 7.2), were well separated by PC-CV 1 in Figure 7.2. However, the PC-CVA model was not able to differentiate smaller differences in ^{15}N content, especially between the ones below 20%. Raman bands with significant contribution (outside of the circle

in Figure 7.3) to the PC-CVA model can be seen in Figure 7.3. The most of the listed wavenumbers can be assigned to the following groups of biological molecules: bases in nucleotides, amide, nucleic acids and amino acids (e.g. tyrosine) [20]. They are all abundant nitrogen-containing molecules in living cells, indicating that the variance in PC-CV 1 and PC-CV 2 is caused by different ^{15}N content and the PC-CVA did not amplify irrelevant variance between different groups.

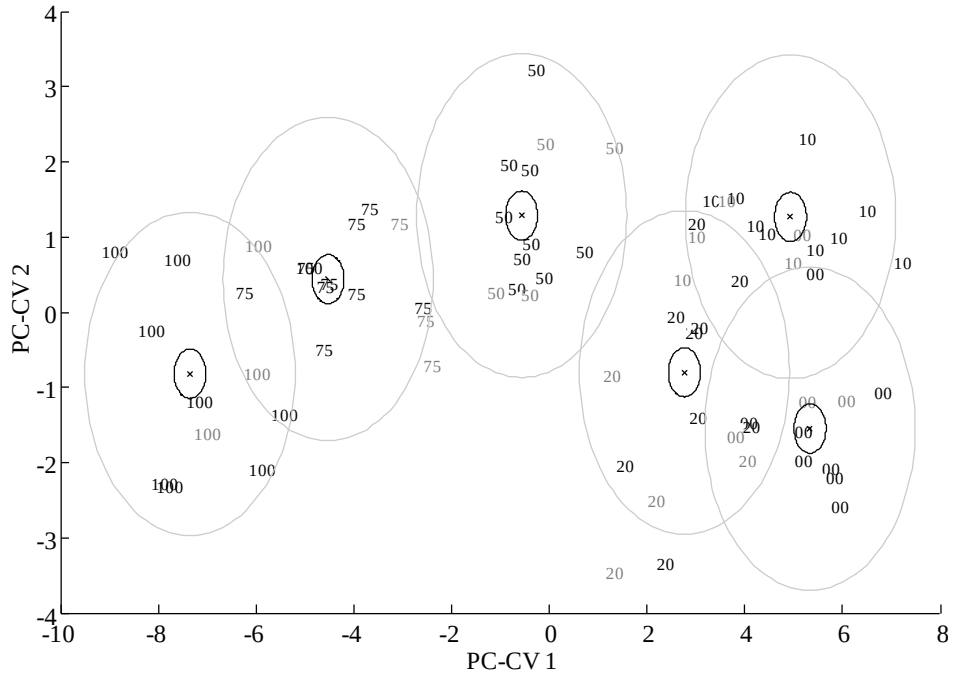

Figure 7.2 PC-CVA result of single-cell Raman spectra.
PC-CVA scores plot for Raman spectra of *Ruegeria pomeroyi* DSS-3 grown in media with different ^{15}N content. PCs 1 - 5 were used by the algorithm with the *a priori* knowledge of the biological replicates. The points shown in black represent the 9 biological replicates used to train the PC-CVA models. Points shown in grey represent the three biological replicates used to validate the PC-CVA model. Black circles represent the 95% confidence interval about the group centroid, and grey circles the 95% confidence region about the group sample population.

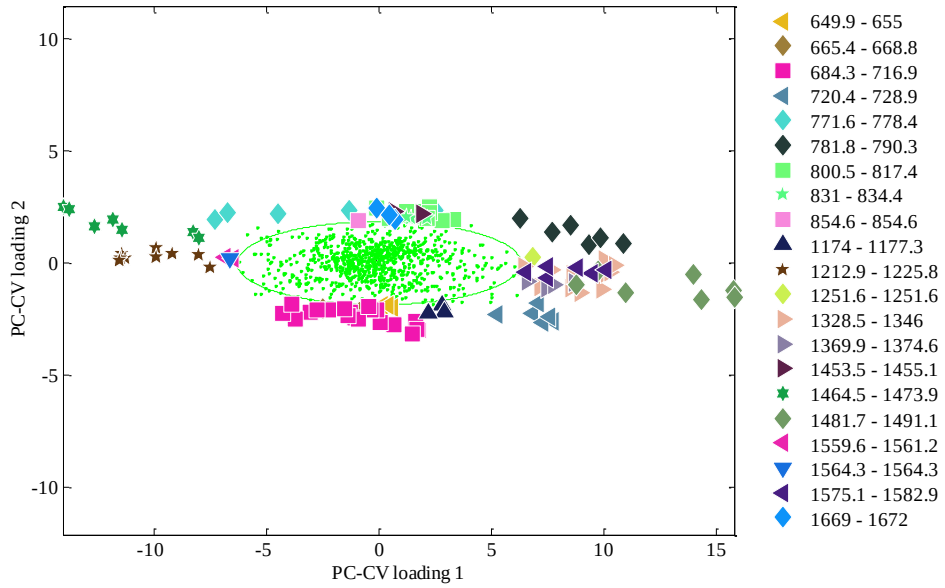

Figure 7.3 PC-CVA loading plots of PC-CVA axis 1 and 2.
Contiguous spectral regions falling beyond 2 standard deviations from the mean are encoded by symbols detailed in the figure legend.

The PC-CVA is a clustering method. The linear relationship between the ^{15}N % and Raman spectra was explored through the use of PLSR (Figure 7.4). Figure 7.4 shows that a good linear relationship was found and cross validation points fall close to this calibration line. For the *Roseobacter* strain used in this study, ^{15}N % of single bacteria cells can be measured by Raman spectroscopy with an accuracy of 94.34 %. Raman bands that have significant contribution (outside of the circle in Figure 7.5) the PLSR model were listed in Figure 7.5, the assignment of which is similar to that described before in PC-CVA.

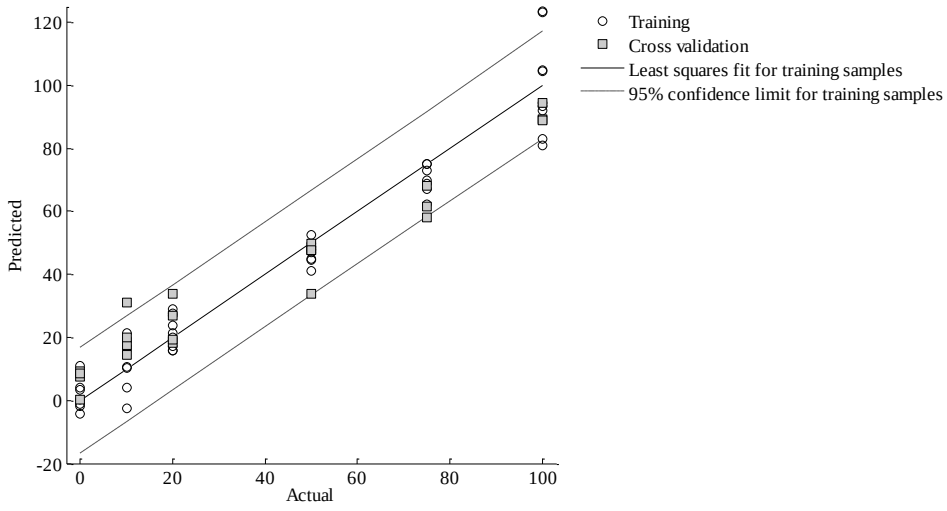

Figure 7.4 PLSR model for single-cell Raman spectra.
RLSR model for single-cell Raman spectra of *Ruegeria pomeroyi* DSS-3 grown in media with different ^{15}N content. The model was trained with Raman spectral data using nine of the biological replicates and validated using the three remaining biological replicates. The PLSR model was built using 3 factors.

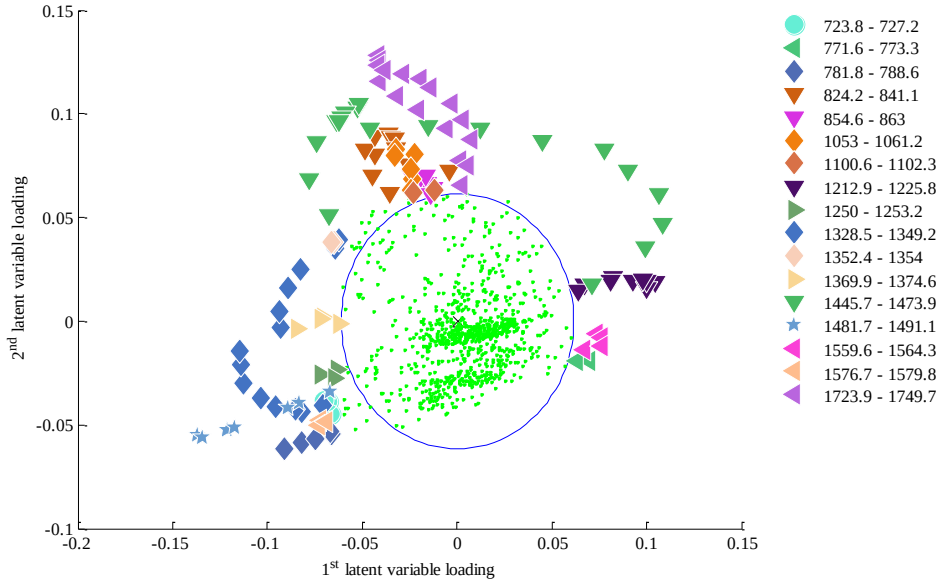

Figure 7.5 PLSR loadings plot of the first two latent variables.
Circle represents the boundary of 2 standard deviations. Wavenumbers of Raman bands that have significant contribution were listed in the figure legend.

The results of PC-CVA and PLSR show that Raman red-shift caused by ^{15}N-incorportation in single bacterium, although not visibly apparent, can be extracted by multivariate analysis. One can use PLSR to construct a linear model to calculate ^{15}N % in single bacteria cells with high accuracy. These results were derived from a strain in the naturally abundant marine *Roseobacter* clade which may input a significant amount of nitrogen into marine ecosystem through the consumption of methylated amines. Therefore, Raman spectroscopy may be a suitable method to rapidly map nitrogen uptake in microbial communities in a quantitative and non-destructive manner and with single-cell precision. The main challenge in achieving such goal is the generalisation of the linear model in PLSR or similar multivariate analysis. Raman red-shift caused by ^{15}N may not

happen at the same wavenumber or to the same extent in different species because of their different biochemical pathways to convert nitrogen compounds. A future study encompassing a relatively large number of representative species is needed to establish a more general linear model to measure nitrogen incorporation in single cells.

Chapter 8: Summary and suggestion for future research

This Ph.D. thesis focuses on the development of novel techniques based on Raman spectroscopy for the application in environmental microbiology. Raman spectroscopy offers a unique opportunity for researchers to look into the microbial world in a non-destructive and quantitative manner, avoiding the problem of unculturable microorganisms. When combined with stable isotope probing (SIP), Raman spectroscopy is a very powerful research tool in this field. However, naturally weak Raman signal and difficulties in interpreting complex Raman spectra hinder it from being employed widely in biological research, because most biological molecules exist in small quantities and the *a priori* knowledge of biological samples may be unavailable. This thesis aims to resolve these problems by enhancing Raman signal and simplifying data interpretation.

Two Raman signal enhancement methods, resonance Raman (RR) spectroscopy and surface enhanced Raman scattering (SERS), were investigated in this thesis for possible applications in environmental microbiology. SIP and the resultant Raman red-shift can be used to identify individual cells that can incorporate any compounds of choice. It also greatly simplifies the Raman data analysis because Raman red-shift unambiguously signifies the uptake of ^{13}C-labelled compounds. Another strategy to analysis Raman spectra, multivariate analysis, was also used in

this thesis to treat spectra with less obvious red-shift caused by ^{15}N incorporation.

The study on SIP-RR spectroscopy found that RR spectroscopy can be used to measure CO_2 fixation activities in single photosynthetic microorganisms. It also demonstrated the potential of the functional imaging technique based on RR spectra. The most significant discovery made in this study was that one can very rapidly and non-destructively measure photosynthetic single cells' ^{13}C content. To the best of my knowledge, the alternative methods to achieve similar results are all based on mass spectrometry, and are usually much more complicated techniques. As discussed in this thesis, mass spectrometry is not preferable for screening large number of environmental microorganisms because it is destructive, time-consuming and expensive. With this method, one can image photosynthetic communities and identify CO_2 fixers automatically, therefore such technique can be used in combination with a laser microdissection system to separate cells of interest and perform many further experiments, e.g. DNA sequencing. This thesis also demonstrated the combination of RR and microfluidic device, which provided a working solution for researchers to easily measure the CO_2 uptake in photosynthetic microbial communities. However, the microfluidic device has not yet included a sorting mechanism to separate cells of interest from other organisms. Researchers can detect and profile the dynamics of CO_2 uptake, but the results can only describe the whole community because of the lack of sorting mechanism. Prototype sorting chips were tested in the laboratory with unsatisfactory results. The main challenge encountered was

the accurate control (starting, stopping and diverging) of cells in a micrometer sized flow. It is foreseeable that such a lab-on-a-chip microfluidic device can be made because accurate cell sorting has been achieved in many other instruments, e.g. flow cytometry, optical tweezers, etc. Environmental microbiologists can use such device to sort sample taken from different locations at different time and correlate the uptake of carbon source, CO_2 or other ^{13}C labelled compounds, to individual species with quantitative results (uptake speed or rate). Metagenomics methods cannot provide such information and mass spectrometry methods would destroy cells whose genetic materials could be sequenced. Therefore, Raman sorting can provide a better understanding of microbial ecology in photosynthetic microbial communities.

However, questions about the non-photosynthetic microorganisms cannot be addressed by SIP-RR Raman sorting technique because there is no strong RR enhancement to exploit and the rich information contained in Raman spectra simply takes too long to obtain. As an example, engineers often seek the contributing species in a bio-reactor or wastewater treatment plant. In principle, using optical tweezers, one can take a Raman spectrum from each single cell and manually 'pick out' single cells that incorporate ^{13}C labelled compounds, e.g. a water pollutants analogue, then culture or sequence those single cells. However, usually only a small fraction of the total community is of research interest, it is nearly impossible to accumulate enough cells and draw convincing conclusions by blind searching and manual handling single cells from a large number of environmental microorganisms and particulate

materials. Therefore, a study attempted to synthesise SERS-active nanoparticles that can universally label microorganism was reported in this thesis. SERS enhancement can be combined with SIP and expand the application of the microfluidic device mentioned above to any microorganisms. SERS is the strongest known Raman signal enhancement mechanism. This thesis proved that one can label the surface of the tested microorganisms with silver nanoparticles by two different methods. However, the resulting SERS spectra could not be used as the sorting criteria in a microfluidic device. The difficulty lies in the lack of understanding of the interaction between nanoparticles and the surface molecules of microorganisms, and the SERS effect itself. The SERS spectra reported in this thesis were difficult to explain because of these reasons. Further investigation should focus on finding a highly specific interaction between nanoparticles and certain universally present molecules on the surface of microorganisms. Because microorganisms' surface contains many different molecules, any non-specific labelling by SERS-active nanoparticles is likely to result in unpredictable spectra, or featureless spectra, like the ones observed in this thesis, due to the fact that the signal from too many different molecules is enhanced and superimposed. Researchers need to know what SERS spectra to expect to be able to programme a computer to identify Raman red-shift automatically, and a specific labelling of one type of surface molecules would serve such purpose. Furthermore, if such labelling is possible, one can multi-label cells with different nanoparticles, similar to cells stained by multiple fluorescent

dyes, making SERS Raman sorting method a more powerful multiplex assay. Self-evidently, it requires a multidisciplinary team with knowledge in the physics of SERS effect, the synthesis and functionalisation of nanoparticles, biochemistry and microfluidics to build a SERS microfluidic cell sorting device.

SIP has been a pillar of new techniques developed in this thesis. It connects single cells to the chemical compounds they consume and simplifies Raman data analysis because of the distinct Raman red-shift. However, such seemingly simple phenomenon had its unexplored aspects. Firstly, a new quantitative Raman spectral marker for ^{13}C incorporation, thymine Raman band, was found which may greatly extend the application of Raman-SIP method. Quantitative monitoring of carbon flow in a model food chain was made possible thanks to the new spectral marker. Secondly and probably more importantly, the intriguing difference in the Raman red-shift between thymine and phenylalanine reveals that the pattern of Raman red-shift is directly affected by the biosynthetic pathways of these two molecules. These findings resolve the mystery of the previously unexplained 'four bands' feature observed in phenylalanine's Raman red-shift; they also show that Raman-SIP method may reveal information about organisms' biochemical pathways. It is a standard practice in organic chemistry to start a synthesis with isotope labelled compounds and observe the fate of the isotopic atoms by NMR or Raman spectroscopy to study the reaction mechanism. The author would like to point out that the same principle applies to biological systems as well as proven by this thesis. This study

may stimulate the development of a new class of methods to study the biochemical pathways and reaction mechanisms of biological systems by non-destructive and simple Raman spectroscopy.

Nitrogen is another crucial element of biological significance. A study in this thesis explored the possibility of using Raman-SIP method and multivariate analysis to quantify single cells' ^{15}N content. With the initial success with a representative species, this study may be a start point to establish a general method to study nitrogen cycle with Raman spectroscopy.

For any newly developed technique, the reproducibility of measurement is of key importance. The reproducibility of Raman data acquisition cannot be described by a single diagram because Raman spectra are multidimensional data. However, the reproducibility of Raman data for each specific purpose in different studies in this thesis is represented by error bars in all the figures where applicable. They are all excellent or at least acceptable, for example, error bars are almost invisible in Figure 3.3 because of its high reproducibility.

In summary, this thesis contributed new knowledge and technical advancement to environmental microbiology and Raman spectroscopy. Some findings, for example, in RR spectroscopy and Raman-biochemical pathways, may find immediate applications in biological research. Other results, for example, in SERS, RACS and ^{15}N-Raman-SIP, may need more extensive further investigation to materialise the intended techniques.

Acknowledgements

I would like to thank my Ph.D. supervisor Dr. Wei Huang. Wei is a pioneer in his field of research, a hard working scientist and a helpful supervisor. I received comprehensive training for academic research from Wei. He also encourages his students to collaborate with scientists from different disciplines, which is particularly beneficial for young researchers. I want to thank all my colleagues in the Kroto Research Institute for helping me with my experiments, my thesis and my English. I also want to thank the University of Sheffield for offering me a scholarship.

I am very grateful to my wife and my parents for giving me support and advice.

I want to acknowledge the great work done by all the co-authors.

The past four years have been a wonderful experience, and I want to thank everyone who provided me support but I haven't named here.

References

1. Jones, J.G., *Effect of environmental-factors on estimated viable and total populations of planktonic bacteria in lakes and experimental enclosures.* Freshwater Biology, 1977. **7**(1): p. 67-91.
2. Kogure, K., Simidu, U., and Taga, N., *Tentative direct microscopic method for counting living marine-bacteria.* Canadian Journal of Microbiology, 1979. **25**(3): p. 415-420.
3. Kogure, K., Simidu, U., and Taga, N., *Distribution of viable marine-bacteria in neritic seawater around Japan.* Canadian Journal of Microbiology, 1980. **26**(3): p. 318-323.
4. Ferguson, R.L., Buckley, E.N., and Palumbo, A.V., *Response of marine bacterioplankton to differential filtration and confinement.* Applied and Environmental Microbiology, 1984. **47**(1): p. 49-55.
5. Torsvik, V., Goksoyr, J., and Daae, F.L., *High diversity in DNA of soil bacteria.* Applied and Environmental Microbiology, 1990. **56**(3): p. 782-787.
6. Ellis, R.J., *et al.*, *Cultivation-dependent and -independent approaches for determining bacterial diversity in fleavy-metal-contaminated soil.* Applied and Environmental Microbiology, 2003. **69**(6): p. 3223-3230.
7. Wagner, M., *et al.*, *Probing activated-sludge with oligonucleotides specific for proteobacteria - inadequacy of culture-dependent methods for describing microbial community structure.* Applied and Environmental Microbiology, 1993. **59**(5): p. 1520-1525.
8. Rappe, M.S. and Giovannoni, S.J., *The uncultured microbial majority.* Annual Review of Microbiology, 2003. **57**: p. 369-394.
9. Rolph, H.J., *et al.*, *Molecular identification of microorganisms from endodontic infections.* Journal of Clinical Microbiology, 2001. **39**(9): p. 3282-3289.
10. Munson, M.A., *et al.*, *Molecular analysis of the microflora associated with dental caries.* Journal of Clinical Microbiology, 2004. **42**(7): p. 3023-3029.
11. Zengler, K., *Central Role of the Cell in Microbial Ecology.* Microbiology and Molecular Biology Reviews, 2009. **73**(4): p. 712-729.
12. Lewis, K., *Persister cells, dormancy and infectious disease.* Nature Reviews Microbiology, 2007. **5**(1): p. 48-56.
13. Scholz, M.B., Lo, C.C., and Chain, P.S., *Next generation sequencing and bioinformatic bottlenecks: the current state of metagenomic data analysis.* Current Opinion in Biotechnology, 2012. **23**(1): p. 9-15.

14. Handelsman, J., *Metagenomics: Application of genomics to uncultured microorganisms.* Microbiology and Molecular Biology Reviews, 2004. **68**(4): p. 669-+.
15. Riesenfeld, C.S., Schloss, P.D., and Handelsman, J., *Metagenomics: Genomic analysis of microbial communities.* Annual Review of Genetics, 2004. **38**: p. 525-552.
16. Ekkers, D.M., *et al.*, *The great screen anomaly-a new frontier in product discovery through functional metagenomics.* Applied Microbiology and Biotechnology, 2012. **93**(3): p. 1005-1020.
17. Streit, W.R., Daniel, R., and Jaeger, K.E., *Prospecting for biocatalysts and drugs in the genomes of non-cultured microorganisms.* Current Opinion in Biotechnology, 2004. **15**(4): p. 285-290.
18. Desai, N., *et al.*, *From genomics to metagenomics.* Current Opinion in Biotechnology, 2012. **23**(1): p. 72-6.
19. Suenaga, H., *Targeted metagenomics: a high-resolution metagenomics approach for specific gene clusters in complex microbial communities.* Environmental Microbiology, 2012. **14**(1): p. 13-22.
20. Huang, W.E., *et al.*, *Shining Light on the Microbial World: The Application of Raman Microspectroscopy*, in *Advances in Applied Microbiology, Vol 70*. 2010, Elsevier Academic Press Inc: San Diego. p. 153-186.
21. Li, M., *et al.*, *Rapid resonance Raman microspectroscopy to probe carbon dioxide fixation by single cells in microbial communities.* ISME Journal, 2012. **6**(4): p. 875-885.
22. Li, M., *et al.*, *Single cell Raman spectroscopy for cell sorting and imaging.* Current Opinion in Biotechnology, 2012. **23**(1): p. 56-63.
23. Meier, R.J., *Vibrational spectroscopy: a 'vanishing' discipline?* Chemical Society Reviews, 2005. **34**(9): p. 743-752.
24. Schultz, Z.D. and Levin, I.W., *Vibrational spectroscopy of biomembranes.* Annual Review of Analytical Chemistry, 2011. **4**(1): p. 343-66.
25. Maquelin, K., *et al.*, *Identification of medically relevant microorganisms by vibrational spectroscopy.* Journal of Microbiological Methods, 2002. **51**(3): p. 255-271.
26. Huang, W.E., *et al.*, *Raman-FISH: combining stable-isotope Raman spectroscopy and fluorescence in situ hybridization for the single cell analysis of identity and function.* Environmental Microbiology, 2007. **9**(8): p. 1878-1889.
27. Huang, W.E., Ward, A.D., and Whiteley, A.S., *Raman tweezers sorting of single microbial cells.* Environmental Microbiology Reports, 2009. **1**(1): p. 44-49.
28. Kim, H., *et al.*, *Resonance Raman and surface- and tip-enhanced Raman spectroscopy methods to study solid catalysts and heterogeneous catalytic reactions.* Chemical Society Reviews, 2010. **39**(12): p. 4820-4844.

29. Atkins, P. and de Paula, J., *Atkins' Physical Chemistry*. 7th ed. 2002, Oxford: Oxford University Press.
30. Ferraro, J.R., Nakamoto, K., and Brown, C.W., *Introductory Raman spectroscopy*. 2nd ed. 2003, Amsterdam ; Boston: Academic Press. xiii, 434 p.
31. Robert, B., *Resonance Raman spectroscopy.* Photosynthesis Research, 2009. **101**(2-3): p. 147-155.
32. Michaels, A.M., Jiang, J., and Brus, L., *Ag nanocrystal junctions as the site for surface-enhanced Raman scattering of single Rhodamine 6G molecules.* Journal of Physical Chemistry B, 2000. **104**(50): p. 11965-11971.
33. Kneipp, K., *et al.*, *Detection and identification of a single DNA base molecule using surface-enhanced Raman scattering (SERS).* Physical Review E, 1998. **57**(6): p. R6281-R6284.
34. Xu, H.X., *et al.*, *Electromagnetic contributions to single-molecule sensitivity in surface-enhanced Raman scattering.* Physical Review E, 2000. **62**(3): p. 4318-4324.
35. Kneipp, K., *et al.*, *Single molecule detection using surface-enhanced Raman scattering (SERS).* Physical Review Letters, 1997. **78**(9): p. 1667-1670.
36. Michaels, A.M., Nirmal, M., and Brus, L.E., *Surface enhanced Raman spectroscopy of individual rhodamine 6G molecules on large Ag nanocrystals.* Journal of the American Chemical Society, 1999. **121**(43): p. 9932-9939.
37. Willets, K.A. and Van Duyne, R.P., *Localized surface plasmon resonance spectroscopy and sensing.* Annual Review of Physical Chemistry, 2007. **58**: p. 267-297.
38. Tong, L.M., Zhu, T., and Liu, Z.F., *Approaching the electromagnetic mechanism of surface-enhanced Raman scattering: from self-assembled arrays to individual gold nanoparticles.* Chemical Society Reviews, 2011. **40**(3): p. 1296-1304.
39. Choo-Smith, L.P., *et al.*, *Investigating microbial (micro)colony heterogeneity by vibrational spectroscopy.* Applied and Environmental Microbiology, 2001. **67**(4): p. 1461-1469.
40. Jarvis, R.M. and Goodacre, R., *Discrimination of bacteria using surface-enhanced Raman spectroscopy.* Analytical Chemistry, 2004. **76**(1): p. 40-47.
41. Maquelin, K., *et al.*, *Rapid identification of Candida species by confocal Raman micro spectroscopy.* Journal of Clinical Microbiology, 2002. **40**(2): p. 594-600.
42. Maquelin, K., *et al.*, *Raman spectroscopic method for identification of clinically relevant microorganisms growing on solid culture medium.* Analytical Chemistry, 2000. **72**(1): p. 12-19.
43. Chan, J.W., *et al.*, *Reagentless identification of single bacterial spores in aqueous solution by confocal laser tweezers Raman spectroscopy.* Analytical Chemistry, 2004. **76**(3): p. 599-603.
44. Huang, W.E., *et al.*, *Raman microscopic analysis of single microbial cells.* Analytical Chemistry, 2004. **76**(15): p. 4452-4458.

45. Huang, W.E., Ude, S., and Spiers, A.J., *Pseudomonas fluorescens SBW25 biofilm and planktonic cells have differentiable Raman spectral profiles.* Microbial Ecology, 2007. **53**(3): p. 471-474.
46. Rosch, P., *et al.*, *Chemotaxonomic identification of single bacteria by micro-Raman spectroscopy: Application to clean-room-relevant biological contaminations.* Applied and Environmental Microbiology, 2005. **71**(3): p. 1626-1637.
47. Xie, C., *et al.*, *Identification of single bacterial cells in aqueous solution using confocal laser tweezers Raman spectroscopy.* Analytical Chemistry, 2005. **77**(14): p. 4390-4397.
48. Goodacre, R., *et al.*, *Rapid identification of urinary tract infection bacteria using hyperspectral whole-organism fingerprinting and artificial neural networks.* Microbiology-SGM, 1998. **144**: p. 1157-1170.
49. Maquelin, K., *et al.*, *Rapid epidemiological analysis of Acinetobacter strains by Raman spectroscopy.* Journal of Microbiological Methods, 2006. **64**(1): p. 126-131.
50. Schuster, K.C., Urlaub, E., and Gapes, J.R., *Single-cell analysis of bacteria by Raman microscopy: spectral information on the chemical composition of cells and on the heterogeneity in a culture.* Journal of Microbiological Methods, 2000. **42**(1): p. 29-38.
51. Neugebauer, U., *et al.*, *Towards a detailed understanding of bacterial metabolism - Spectroscopic characterization of Staphylococcus epidermidis.* Chemphyschem, 2007. **8**(1): p. 124-137.
52. Singer, A.C., *et al.*, *Insight into pollutant bioavailability and toxicity using Raman confocal microscopy.* Journal of Microbiological Methods, 2005. **60**(3): p. 417-422.
53. Hermelink, A., *et al.*, *Phenotypic heterogeneity within microbial populations at the single-cell level investigated by confocal Raman microspectroscopy.* Analyst, 2009. **134**(6): p. 1149-1153.
54. Carey, P.R., *Resonance Raman-spectroscopy in biochemistry and biology.* Quarterly Reviews of Biophysics, 1978. **11**(3): p. 309-370.
55. Beja, O., *et al.*, *Bacterial rhodopsin: Evidence for a new type of phototrophy in the sea.* Science, 2000. **289**(5486): p. 1902-1906.
56. Daniel, R., *The metagenomics of soil.* Nature Reviews Microbiology, 2005. **3**(6): p. 470-478.
57. Huang, W.E., *et al.*, *Resolving Genetic Functions within Microbial Populations: In Situ Analyses Using rRNA and mRNA Stable Isotope Probing Coupled with Single-Cell Raman-Fluorescence In Situ Hybridization.* Applied and Environmental Microbiology, 2009. **75**(1): p. 234-241.
58. Wagner, M., *Single-cell ecophysiology of microbes as revealed by Raman microspectroscopy or secondary ion mass spectrometry imaging.* Annual Review of Microbiology, 2009. **63**: p. 411-429.
59. van Manen, H.J., *et al.*, *Single-cell Raman and fluorescence microscopy reveal the association of lipid bodies with phagosomes*

in leukocytes. Proceedings of the National Academy of Sciences of the United States of America, 2005. **102**(29): p. 10159-10164.
60. Nyquist, R.A., *Interpreting infrared, Raman, and nuclear magnetic resonance spectra*. 2001, San Diego: Academic Press.
61. De Gelder, J., *et al.*, *Reference database of Raman spectra of biological molecules.* Journal of Raman Spectroscopy, 2007. **38**(9): p. 1133-1147.
62. Schuster, K.C., *et al.*, *Multidimensional information on the chemical composition of single bacterial cells by confocal Raman microspectroscopy.* Analytical Chemistry, 2000. **72**(22): p. 5529-5534.
63. Ramser, K., *et al.*, *Resonance Raman spectroscopy of optically trapped functional erythrocytes.* Journal of Biomedical Optics, 2004. **9**(3): p. 593-600.
64. Wood, B.R., *et al.*, *Resonance Raman spectroscopy of red blood cells using near-infrared laser excitation.* Analytical and Bioanalytical Chemistry, 2007. **387**(5): p. 1691-1703.
65. Wen, Z.Q., Armstrong, A., and Thomas, G.J., *Demonstration by ultraviolet resonance Raman spectroscopy of differences in DNA organization and interactions in filamentous viruses Pf1 and fd.* Biochemistry, 1999. **38**(10): p. 3148-3156.
66. Moore, B.D., *et al.*, *Rapid and ultra-sensitive determination of enzyme activities using surface-enhanced resonance Raman scattering.* Nature Biotechnology, 2004. **22**(9): p. 1133-1138.
67. Hunter, N., *The purple phototrophic bacteria*. 2008, Springer New York, NY: Springer Dordrecht.
68. Evans, C.L. and Xie, X.S., *Coherent Anti-Stokes Raman Scattering Microscopy: Chemical Imaging for Biology and Medicine.* Annual Review of Analytical Chemistry, 2008. **1**: p. 883-909.
69. Petrov, G.I., *et al.*, *Comparison of coherent and spontaneous Raman microspectroscopies for noninvasive detection of single bacterial endospores.* Proceedings of the National Academy of Sciences of the United States of America, 2007. **104**(19): p. 7776-7779.
70. Min, W., *et al.*, *Coherent Nonlinear Optical Imaging: Beyond Fluorescence Microscopy.* Annual Review of Physical Chemistry, 2011. **62**: p. 507-530.
71. Camden, J.P., *et al.*, *Controlled Plasmonic Nanostructures for Surface-Enhanced Spectroscopy and Sensing.* Accounts of Chemical Research, 2008. **41**(12): p. 1653-1661.
72. Nie, S.M. and Emery, S.R., *Probing single molecules and single nanoparticles by surface-enhanced Raman scattering.* Science, 1997. **275**(5303): p. 1102-1106.
73. Zeiri, L., *et al.*, *Surface-enhanced Raman spectroscopy as a tool for probing specific biochemical components in bacteria.* Applied Spectroscopy, 2004. **58**(1): p. 33-40.
74. Cooper, J.M., Sirimuthu, N.M.S., and Syme, C.D., *Monitoring the Uptake and Redistribution of Metal Nanoparticles during Cell*

Culture Using Surface-Enhanced Raman Scattering Spectroscopy. Analytical Chemistry, 2010. **82**(17): p. 7369-7373.
75. Bailo, E. and Deckert, V., *Tip-enhanced Raman scattering.* Chemical Society Reviews, 2008. **37**(5): p. 921-930.
76. Hennigan, S.L., *et al.*, *Detection of Mycoplasma pneumoniae in simulated and true clinical throat swab specimens by nanorod array-surface-enhanced Raman spectroscopy.* PLoS One, 2010. **5**(10): p. e13633.
77. Kneipp, J., *et al.*, *Gold nanolenses generated by laser ablation-efficient enhancing structure for surface enhanced Raman scattering analytics and sensing.* Analytical Chemistry, 2008. **80**(11): p. 4247-4251.
78. Huang, W.E., *et al.*, *Single-cell Raman spectral profiles of Pseudomonas fluorescens SBW25 reflects in vitro and in planta metabolic history.* Microbial Ecology, 2007. **53**(3): p. 414-425.
79. Schmid, U., *et al.*, *Gaussian mixture discriminant analysis for the single-cell differentiation of bacteria using micro-Raman spectroscopy.* Chemometrics and Intelligent Laboratory Systems, 2009. **96**(2): p. 159-171.
80. Andrews, J.S., *et al.*, *Biofilm formation in environmental bacteria is influenced by different macromolecules depending on genus and species.* Environmental Microbiology, 2010. **12**(9): p. 2496-2507.
81. Haider, S., *et al.*, *Raman microspectroscopy reveals long-term extracellular activity of chlamydiae.* Molecular Microbiology, 2010. **77**(3): p. 687-700.
82. Hall, E.K., *et al.*, *Looking inside the box: using Raman microspectroscopy to deconstruct microbial biomass stoichiometry one cell at a time.* ISME Journal, 2011. **5**(2): p. 196-208.
83. Autissier, P., *et al.*, *Evaluation of a 12-Color Flow Cytometry Panel to Study Lymphocyte, Monocyte, and Dendritic Cell Subsets in Humans.* Cytometry Part A, 2010. **77A**(5): p. 410-419.
84. Bendall, S.C., *et al.*, *Single-Cell Mass Cytometry of Differential Immune and Drug Responses Across a Human Hematopoietic Continuum.* Science, 2011. **332**(6030): p. 687-696.
85. Lau, A.Y., Lee, L.P., and Chan, J.W., *An integrated optofluidic platform for Raman-activated cell sorting.* Lab on a Chip, 2008. **8**(7): p. 1116-1120.
86. Camp, C.H., *et al.*, *Label-free flow cytometry using multiplex coherent anti-Stokes Raman scattering (MCARS) for the analysis of biological specimens.* Optics Letters, 2011. **36**(12): p. 2309-2311.
87. Walter, A., *et al.*, *Towards a fast, high specific and reliable discrimination of bacteria on strain level by means of SERS in a microfluidic device.* Lab on a Chip, 2011. **11**(6): p. 1013-1021.
88. Chitsaz, H., *et al.*, *Efficient de novo assembly of single-cell bacterial genomes from short-read data sets.* Nature Biotechnology, 2011. **29**(10): p. 915-U214.

89. Furlani, E.P., *Magnetophoretic separation of blood cells at the microscale.* Journal of Physics D-Applied Physics, 2007. **40**(5): p. 1313-1319.
90. MacDonald, M.P., Spalding, G.C., and Dholakia, K., *Microfluidic sorting in an optical lattice.* Nature, 2003. **426**(6965): p. 421-424.
91. Kim, U., *et al.*, *Multitarget Dielectrophoresis Activated Cell Sorter.* Analytical Chemistry, 2008. **80**(22): p. 8656-8661.
92. Kang, Y., *et al.*, *Transcript amplification from single bacterium for transcriptome analysis.* Genome Research, 2011. **21**(6): p. 925-935.
93. Cialla, D., *et al.*, *Raman to the limit: tip-enhanced Raman spectroscopic investigations of a single tobacco mosaic virus.* Journal of Raman Spectroscopy, 2009. **40**(3): p. 240-243.
94. De Luca, A.C., *et al.*, *Online Fluorescence Suppression in Modulated Raman Spectroscopy.* Analytical Chemistry, 2010. **82**(2): p. 738-745.
95. Okuno, M., *et al.*, *Quantitative CARS Molecular Fingerprinting of Single Living Cells with the Use of the Maximum Entropy Method.* Angewandte Chemie-International Edition, 2010. **49**(38): p. 6773-6777.
96. Kong, L.B., *et al.*, *Monitoring the Kinetics of Uptake of a Nucleic Acid Dye during the Germination of Single Spores of Bacillus Species.* Analytical Chemistry, 2010. **82**(20): p. 8717-8724.
97. Hermelink, A., Stammler, M., and Naumann, D., *Observation of content and heterogeneity of poly-beta-hydroxybutyric acid (PHB) in Legionella bozemanii by vibrational spectroscopy.* Analyst, 2011. **136**(6): p. 1129-1133.
98. Day, J.P.R., *et al.*, *Quantitative Coherent Anti-Stokes Raman Scattering (CARS) Microscopy.* Journal of Physical Chemistry B, 2011. **115**(24): p. 7713-7725.
99. Kong, L.B., *et al.*, *Rapid confocal Raman imaging using a synchro multifoci-scan scheme for dynamic monitoring of single living cells.* Applied Physics Letters, 2011. **98**(21).
100. Jiao, N., *et al.*, *Microbial production of recalcitrant dissolved organic matter: long-term carbon storage in the global ocean.* Nature Reviews Microbiology, 2010. **8**(8): p. 593-599.
101. Singh, B.K., *et al.*, *Microorganisms and climate change: terrestrial feedbacks and mitigation options.* Nature Reviews Microbiology, 2010. **8**(11): p. 779-790.
102. Amann, R.I., Ludwig, W., and Schleifer, K.H., *Phylogenetic identification and in-situ detection of individual microbial-cells without cultivation.* Microbiological Reviews, 1995. **59**(1): p. 143-169.
103. Venter, J.C., *et al.*, *Environmental genome shotgun sequencing of the Sargasso Sea.* Science, 2004. **304**(5667): p. 66-74.
104. Beja, O., *et al.*, *Proteorhodopsin phototrophy in the ocean.* Nature, 2001. **411**(6839): p. 786-789.
105. Weller, R., *et al.*, *Uncultivated cyanobacteria, chloroflexus-like inhabitants, and spirochete-like inhabitants of a hot-spring*

microbial mat. Applied and Environmental Microbiology, 1992. **58**(12): p. 3964-3969.
106. Karl, D.M., *Microbiological oceanography - Hidden in a sea of microbes.* Nature, 2002. **415**(6872): p. 590-591.
107. Crump, B.C., *et al.*, *Respiratory succession and community succession of bacterioplankton in seasonally anoxic estuarine waters.* Applied and Environmental Microbiology, 2007. **73**(21): p. 6802-6810.
108. Stepanauskas, R. and Sieracki, M.E., *Matching phylogeny and metabolism in the uncultured marine bacteria, one cell at a time.* Proceedings of the National Academy of Sciences of the United States of America, 2007. **104**(21): p. 9052-9057.
109. Tripp, H.J., *et al.*, *Metabolic streamlining in an open-ocean nitrogen-fixing cyanobacterium.* Nature, 2010. **464**(7285): p. 90-94.
110. Zehr, J.P., *et al.*, *Globally Distributed Uncultivated Oceanic N-2-Fixing Cyanobacteria Lack Oxygenic Photosystem II.* Science, 2008. **322**(5904): p. 1110-1112.
111. Jardillier, L., *et al.*, *Significant CO2 fixation by small prymnesiophytes in the subtropical and tropical northeast Atlantic Ocean.* ISME Journal, 2010. **4**(9): p. 1180-1192.
112. Lorenz, P. and Eck, J., *Metagenomics and industrial applications.* Nature Reviews Microbiology, 2005. **3**(6): p. 510-516.
113. Bode, H.B. and Muller, R., *The impact of bacterial genomics on natural product research.* Angewandte Chemie-International Edition, 2005. **44**(42): p. 6828-6846.
114. Fortman, J.L. and Sherman, D.H., *Utilizing the power of microbial genetics to bridge the gap between the promise and the application of marine natural products.* Chembiochem, 2005. **6**(6): p. 960-978.
115. Wu, H.W., *et al.*, *In vivo lipidomics using single-cell Raman spectroscopy.* Proceedings of the National Academy of Sciences of the United States of America, 2011. **108**(9): p. 3809-3814.
116. Krebs, R.A., *et al.*, *Resonance Raman characterization of proteorhodopsin's chromophore environment.* Journal of Physical Chemistry B, 2003. **107**(31): p. 7877-7883.
117. Garcia-Asua, G., *et al.*, *Carotenoid diversity: a modular role for the phytoene desaturase step.* Trends in Plant Science, 1998. **3**(11): p. 445-449.
118. Tracewell, C.A., *et al.*, *Resonance Raman spectroscopy of carotenoids in Photosystem II core complexes.* Photosynthesis Research, 2005. **83**(1): p. 45-52.
119. Tracewell, C.A., *et al.*, *Characterization of carotenoid and chlorophyll photooxidation in photosystem II.* Biochemistry, 2001. **40**(1): p. 193-203.
120. Szalontai, B., *et al.*, *Structure and interactions of phycocyanobilin chromophores in phycocyanin and allophycocyanin from an analysis of their resonance Raman-spectra.* Biochemistry, 1994. **33**(39): p. 11823-11832.

121. Pandey, A., Andersen, J.S., and M., M., *Use of Mass Spectrometry to Study Signaling Pathways.* Science's STKE, 2000.
122. Gust, D., *et al.*, *The photochemistry of carotenoids - some photosynthetic and photomedical aspects*, in *Carotenoids in Human Health*, L.M. Canfield, Krinsky, N.I., and Olson, J.A., Editors. 1993, New York Acad Sciences: New York. p. 32-47.
123. Rimai, L., Heyde, M.E., and Gill, D., *Vibrational-spectra of some carotenoids and related linear polyenes - Raman spectroscopic study.* Journal of the American Chemical Society, 1973. **95**(14): p. 4493-4501.
124. Zhang, J., *The diversity and biotechnological application of marine microbes producing Omega-3 fatty acids*. 2011, Newcastle University: Newcastle, UK.
125. Stanier, R.Y. and Cohenbazire, G., *Phototropic prokaryotes - cyanobacteria.* Annual Review of Microbiology, 1977. **31**: p. 225-274.
126. Radajewski, S., *et al.*, *Stable-isotope probing as a tool in microbial ecology.* Nature, 2000. **403**(6770): p. 646-649.
127. Manefield, M., *et al.*, *RNA stable isotope probing, a novel means of linking microbial community function to Phylogeny.* Applied and Environmental Microbiology, 2002. **68**(11): p. 5367-5373.
128. Chen, Y. and Murrell, J.C., *When metagenomics meets stable-isotope probing: progress and perspectives.* Trends in Microbiology, 2010. **18**(4): p. 157-163.
129. Dumont, M.G. and Murrell, J.C., *Stable isotope probing - linking microbial identity to function.* Nature Reviews Microbiology, 2005. **3**(6): p. 499-504.
130. Sorokin, D.Y., *et al.*, *Thioalkalimicrobium aerophilum gen. nov., sp nov and Thioalkalimicrobium sibericum sp nov., and Thioalkalivibrio versutus gen. nov., sp nov., Thioalkalivibrio nitratis sp nov and Thioalkalivibrio denitrificans sp nov., novel obligately alkaliphilic and obligately chemolithoautotrophic sulfur-oxidizing bacteria from soda lakes.* International Journal of Systematic and Evolutionary Microbiology, 2001. **51**: p. 565-580.
131. Walsh, D.A., *et al.*, *Metagenome of a Versatile Chemolithoautotroph from Expanding Oceanic Dead Zones.* Science, 2009. **326**(5952): p. 578-582.
132. Fleischmann, M., Hendra, P.J., and McQuillan, A.J., *Raman spectra of pyridine adsorbed at a silver electrode.* Chemical Physics Letters, 1974. **26**(2): p. 163-166.
133. Jeanmaire, D.L. and Vanduyne, R.P., *Surface Raman spectroelectrochemistry .1. Heterocyclic, aromatic, and aliphatic-amines adsorbed on anodized silver electrode.* Journal of Electroanalytical Chemistry, 1977. **84**(1): p. 1-20.
134. Albrecht, M.G. and Creighton, J.A., *Anomalously intense Raman-spectra of pyridine at a silver electrode.* Journal of the American Chemical Society, 1977. **99**(15): p. 5215-5217.

135. Otto, A., *et al.*, *Surface-enhanced Raman-scattering.* Journal of Physics-Condensed Matter, 1992. **4**(5): p. 1143-1212.
136. Moskovits, M., *Surface-enhanced spectroscopy.* Reviews of Modern Physics, 1985. **57**(3): p. 783-826.
137. Moskovits, M., *Surface-enhanced Raman spectroscopy: a brief retrospective.* Journal of Raman Spectroscopy, 2005. **36**(6-7): p. 485-496.
138. Jarvis, R.M., *et al.*, *Surface-enhanced Raman scattering from intracellular and extracellular bacterial locations.* Analytical Chemistry, 2008. **80**(17): p. 6741-6746.
139. Culha, M., *et al.*, *Characterization of Thermophilic Bacteria Using Surface-Enhanced Raman Scattering.* Applied Spectroscopy, 2008. **62**(11): p. 1226-1232.
140. Wilson, R., *et al.*, *Surface. enhanced Raman signatures of pigmentation of cyanobacteria from within geological samples in a spectroscopic-microfluidic flow cell.* Analytical Chemistry, 2007. **79**(18): p. 7036-7041.
141. Naja, G., *et al.*, *Raman-based detection of bacteria using silver nanoparticles conjugated with antibodies.* Analyst, 2007. **132**(7): p. 679-686.
142. Zeiri, L., *et al.*, *Silver metal induced surface enhanced Raman of bacteria.* Colloids and Surfaces a-Physicochemical and Engineering Aspects, 2002. **208**(1-3): p. 357-362.
143. Jarvis, R.M. and Goodacre, R., *Characterisation and identification of bacteria using SERS.* Chemical Society Reviews, 2008. **37**(5): p. 931-936.
144. Alexander, T.A. and Le, D.M., *Characterization of a commercialized SERS-active substrate and its application to the identification of intact Bacillus endospores.* Applied Optics, 2007. **46**(18): p. 3878-3890.
145. Chu, H.Y., Huang, Y.W., and Zhao, Y.P., *Silver nanorod arrays as a surface-enhanced Raman scattering substrate for foodborne pathogenic bacteria detection.* Applied Spectroscopy, 2008. **62**(8): p. 922-931.
146. Efrima, S. and Zeiri, L., *Understanding SERS of bacteria.* Journal of Raman Spectroscopy, 2009. **40**(3): p. 277-288.
147. Zhang, X., *et al.*, *Surface-enhanced Raman spectroscopy biosensors: excitation spectroscopy for optimisation of substrates fabricated by nanosphere lithography.* IEE Proceedings Nanobiotechnology, 2005. **152**(6): p. 195-206.
148. GarciaVidal, F.J. and Pendry, J.B., *Collective theory for surface enhanced Raman scattering.* Physical Review Letters, 1996. **77**(6): p. 1163-1166.
149. Kneipp, K., *et al.*, *Population pumping of excited vibrational states by spontaneous surface-enhanced Raman scattering.* Physical Review Letters, 1996. **76**(14): p. 2444-2447.
150. Kneipp, K., Kneipp, H., and Kneipp, J., *Surface-enhanced Raman scattering in local optical fields of silver and gold nanoaggregatess -*

From single-molecule Raman spectroscopy to ultrasensitive probing in live cells. Accounts of Chemical Research, 2006. **39**(7): p. 443-450.
151. Vosgrone, T. and Meixner, A.J., *Surface- and resonance-enhanced micro-raman spectroscopy of xanthene dyes: From the ensemble to single molecules.* Chemphyschem, 2005. **6**(1): p. 154-163.
152. Jordan, P., *et al.*, *Surface-enhanced resonance Raman scattering in optical tweezers using co-axial second harmonic generation.* Optics Express, 2005. **13**(11): p. 4148-4153.
153. Johannessen, C., White, P.C., and Abdali, S., *Resonance raman optical activity and surface enhanced resonance raman optical activity analysis of cytochrome c.* Journal of Physical Chemistry A, 2007. **111**(32): p. 7771-7776.
154. Graham, D. and Faulds, K., *Quantitative SERRS for DNA sequence analysis.* Chemical Society Reviews, 2008. **37**(5): p. 1042-1051.
155. Kneipp, K., *et al.*, *Surface-enhanced non-linear Raman scattering at the single-molecule level.* Chemical Physics, 1999. **247**(1): p. 155-162.
156. Kneipp, J., Kneipp, H., and Kneipp, K., *Two-photon vibrational spectroscopy for biosciences based on surface-enhanced hyper-Raman scattering.* Proceedings of the National Academy of Sciences of the United States of America, 2006. **103**(46): p. 17149-17153.
157. Stockle, R.M., *et al.*, *Nanoscale chemical analysis by tip-enhanced Raman spectroscopy.* Chemical Physics Letters, 2000. **318**(1-3): p. 131-136.
158. Anderson, M.S., *Locally enhanced Raman spectroscopy with an atomic force microscope.* Applied Physics Letters, 2000. **76**(21): p. 3130-3132.
159. Pettinger, B., *et al.*, *Nanoscale probing of adsorbed species by tip-enhanced Raman spectroscopy.* Physical Review Letters, 2004. **92**(9): p. 4.
160. Neugebauer, U., *et al.*, *Characterization of bacterial growth and the influence of antibiotics by means of UV resonance Raman spectroscopy.* Biopolymers, 2006. **82**(4): p. 306-311.
161. Premasiri, W.R., *et al.*, *Characterization of the Surface Enhanced Raman Scattering (SERS) of bacteria.* Journal of Physical Chemistry B, 2005. **109**(1): p. 312-320.
162. Patel, I.S., *et al.*, *Barcoding bacterial cells: a SERS-based methodology for pathogen identification.* Journal of Raman Spectroscopy, 2008. **39**(11): p. 1660-1672.
163. Kao, P., *et al.*, *Surface-enhanced Raman detection on metalized nanostructured poly(p-xylylene) films.* Advanced Materials, 2008. **20**(18): p. 3562-+.
164. Sujith, A., *et al.*, *Surface enhanced Raman scattering analyses of individual silver nanoaggregates on living single yeast cell wall.* Applied Physics Letters, 2008. **92**(10): p. -.

165. Shanmukh, S., *et al., Rapid and sensitive detection of respiratory virus molecular signatures using a silver nanorod array SERS substrate.* Nano Letters, 2006. **6**(11): p. 2630-2636.
166. Sheng, R.S., Ni, F., and Cotton, T.M., *Determination of purine-bases by reversed-phase high-performance liquid-chromatography using real-time surface-enhanced Raman-spectroscopy.* Analytical Chemistry, 1991. **63**(5): p. 437-442.
167. Vodinh, T., Houck, K., and Stokes, D.L., *Surface-enhanced Raman gene probes.* Analytical Chemistry, 1994. **66**(20): p. 3379-3383.
168. Isola, N.R., Stokes, D.L., and Vo-Dinh, T., *Surface enhanced Raman gene probe for HIV detection.* Analytical Chemistry, 1998. **70**(7): p. 1352-1356.
169. Cao, Y.W.C., Jin, R.C., and Mirkin, C.A., *Nanoparticles with Raman spectroscopic fingerprints for DNA and RNA detection.* Science, 2002. **297**(5586): p. 1536-1540.
170. Chen, Z., *et al., Protein microarrays with carbon nanotubes as multicolor Raman labels.* Nature Biotechnology, 2008. **26**(11): p. 1285-1292.
171. Carey, P.R., *Spectroscopic characterization of distortion in enzyme complexes.* Chemical Reviews, 2006. **106**(8): p. 3043-3054.
172. Kneipp, J., *et al., Optical probing and imaging of live cells using SERS labels.* Journal of Raman Spectroscopy, 2009. **40**(1): p. 1-5.
173. Keren, S., *et al., Noninvasive molecular imaging of small living subjects using Raman spectroscopy.* Proceedings of the National Academy of Sciences of the United States of America, 2008. **105**(15): p. 5844-5849.
174. Vo-Dinh, T., Yan, F., and Wabuyele, M.B., *Surface-enhanced Raman scattering for medical diagnostics and biological imaging.* Journal of Raman Spectroscopy, 2005. **36**(6-7): p. 640-647.
175. Yu, M.X., *et al., Luminescent Gold Nanoparticles with pH-Dependent Membrane Adsorption.* Journal of the American Chemical Society, 2011. **133**(29): p. 11014-11017.
176. Lu, W.T., *et al., Gold Nano-Popcorn-Based Targeted Diagnosis, Nanotherapy Treatment, and In Situ Monitoring of Photothermal Therapy Response of Prostate Cancer Cells Using Surface-Enhanced Raman Spectroscopy.* Journal of the American Chemical Society, 2010. **132**(51): p. 18103-18114.
177. Caro, C., *et al., Thiol-immobilized silver nanoparticle aggregate films for surface enhanced Raman scattering.* Journal of Raman Spectroscopy, 2008. **39**(9): p. 1162-1169.
178. Sharma, A., *et al., Antibody immobilized cysteamine functionalized-gold nanoparticles for aflatoxin detection.* Thin Solid Films, 2010. **519**(3): p. 1213-1218.
179. Rong, H.T., *et al., On the importance of the headgroup substrate bond in thiol monolayers: A study of biphenyl-based thiols on gold and silver.* Langmuir, 2001. **17**(5): p. 1582-1593.

180. Zhang, D.Y., *et al., Whole-cell bacterial bioreporter for actively searching and sensing of alkanes and oil spills.* Microbial Biotechnology, 2012. **5**(1): p. 87-97.
181. Song, Y.Z., *et al., Ultrasound-mediated DNA transfer for bacteria.* Nucleic Acids Research, 2007. **35**(19): p. 9.
182. Bechtel, D.B. and Bulla, L.A., *Electron-microscope study of sporulation and parasporal crystal-formation in Bacillus-thuringiensis.* Journal of Bacteriology, 1976. **127**(3): p. 1472-1481.
183. Lugtenberg, B. and Kamilova, F., *Plant-Growth-Promoting Rhizobacteria.* Annual Review of Microbiology, 2009. **63**: p. 541-556.
184. Jousset, A., *Ecological and evolutive implications of bacterial defences against predators.* Environmental Microbiology, 2012. **14**(8): p. 1830-43.
185. Lueders, T., *et al., Stable isotope probing of rRNA and DNA reveals a dynamic methylotroph community and trophic interactions with fungi and protozoa in oxic rice field soil.* Environmental Microbiology, 2004. **6**(1): p. 60-72.
186. Murase, J. and Frenzel, P., *A methane-driven microbial food web in a wetland rice soil.* Environmental Microbiology, 2007. **9**(12): p. 3025-3034.
187. Kuppardt, S., Chatzinotas, A., and Kastner, M., *Development of a Fatty Acid and RNA Stable Isotope Probing-Based Method for Tracking Protist Grazing on Bacteria in Wastewater.* Applied and Environmental Microbiology, 2010. **76**(24): p. 8222-8230.
188. Pollierer, M.M., *et al., The underestimated importance of belowground carbon input for forest soil animal food webs.* Ecology Letters, 2007. **10**(8): p. 729-736.
189. Haichar, F.E., *et al., Plant host habitat and root exudates shape soil bacterial community structure.* ISME Journal, 2008. **2**(12): p. 1221-1230.
190. Schnider-Keel, U., *et al., Autoinduction of 2,4-diacetylphloroglucinol biosynthesis in the biocontrol agent Pseudomonas fluorescens CHA0 and repression by the bacterial metabolites salicylate and pyoluteorin.* Journal of Bacteriology, 2000. **182**(5): p. 1215-1225.
191. Frisch, M.J., *et al., Gaussian 09.* 2010, Gaussian, Inc.: Wallingford, CT, U. S. A.
192. Duguid, J., *et al., Raman Spectral Studies of Nucleic-Acids .44. Raman-Spectroscopy of DNA-Metal Complexes .1. Interactions and Conformational Effects of the Divalent-Cations - Mg, Ca, Sr, Ba, Mn, Co, Ni, Cu, Pd, and Cd.* Biophysical Journal, 1993. **65**(5): p. 1916-1928.
193. Duguid, J.G., *et al., Raman Spectroscopy of DNA-Metal Complexes .2. The Thermal Denaturation of DNA in the Presence of Sr2+, Ba2+, Mg2+, Ca2+, Mn2+, Co2+, Ni2+, and Cd2+.* Biophysical Journal, 1995. **69**(6): p. 2623-2641.

194. Duguid, J.G., *et al.*, *DNA Melting Investigated by Differential Scanning Calorimetry and Raman Spectroscopy.* Biophysical Journal, 1996. **71**(6): p. 3350-3360.
195. Fodor, S.P.A., Starr, P.A., and Spiro, T.G., *Raman Spectroscopic Elucidation of DNA Backbone Conformations for Poly(dG-dT).Poly(dA-dC) and Poly(dA-dT).Poly(dA-dT) in CsF Solution.* Biopolymers, 1985. **24**(8): p. 1493-1500.
196. Deng, H., *et al.*, *Dependence of the Raman Signature of Genomic B-DNA on Nucleotide Base Sequence.* Biopolymers, 1999. **50**(6): p. 656-666.
197. Benevides, J.M., Overman, S.A., and Thomas, G.J., *Raman, polarized Raman and ultraviolet resonance Raman spectroscopy of nucleic acids and their complexes.* Journal of Raman Spectroscopy, 2005. **36**(4): p. 279-299.
198. Mathlouthi, M., Seuvre, A.M., and Koenig, J.L., *FT-IR and Laser-Raman Spectra of Constituents of Nucleic-Acids .3. FT IR and Laser-Raman Spectra of Thymine and Thymidine.* Carbohydrate Research, 1984. **134**(1): p. 23-38.
199. Stryer, L., *Biochemistry*. 4th ed. 1995, New York: W.H. Freeman. xxxiv, 1064 p.
200. Irikura, K.K., Johnson, R.D., and Kacker, R.N., *Uncertainties in scaling factors for ab initio vibrational frequencies.* Journal of Physical Chemistry A, 2005. **109**(37): p. 8430-8437.
201. Blattner, F.R., *et al.*, *The complete genome sequence of Escherichia coli K-12.* Science, 1997. **277**(5331): p. 1453-&.
202. C elegans Sequencing Consortium, *Genome sequence of the nematode C-elegans: A platform for investigating biology.* Science, 1998. **282**(5396): p. 2012-2018.
203. Xu, X., *et al.*, *The genomic sequence of the Chinese hamster ovary (CHO)-K1 cell line.* Nature Biotechnology, 2011. **29**(8): p. 735-U131.
204. Lander, E.S., *et al.*, *Initial sequencing and analysis of the human genome.* Nature, 2001. **409**(6822): p. 860-921.
205. Jess, P.R.T., *et al.*, *Dual beam fibre trap for Raman microspectroscopy of single cells.* Optics Express, 2006. **14**(12): p. 5779-5791.
206. Ramser, K., *et al.*, *A microfluidic system enabling Raman measurements of the oxygenation cycle in single optically trapped red blood cells.* Lab on a Chip, 2005. **5**(4): p. 431-436.
207. Ferguson, A.S., *et al.*, *Microbial analysis of soil and groundwater from a gasworks site and comparison with a sequenced biological reactive barrier remediation process.* Journal of Applied Microbiology, 2007. **102**(5): p. 1227-1238.
208. Valm, A.M., *et al.*, *Systems-level analysis of microbial community organization through combinatorial labeling and spectral imaging.* Proceedings of the National Academy of Sciences of the United States of America, 2011. **108**(10): p. 4152-4157.

209. Kneipp, J., Kneipp, H., and Kneipp, K., *SERS - a single-molecule and nanoscale tool for bioanalytics.* Chemical Society Reviews, 2008. **37**(5): p. 1052-1060.
210. Liu, G.L. and Lee, L.P., *Nanowell surface enhanced Raman scattering arrays fabricated by soft-lithography for label-free biomolecular detections in integrated microfluidics.* Applied Physics Letters, 2005. **87**(7).
211. Park, T., *et al.*, *Highly sensitive signal detection of duplex dye-labelled DNA oligonucleotides in a PDMS microfluidic chip: confocal surface-enhanced Raman spectroscopic study.* Lab on a Chip, 2005. **5**(4): p. 437-442.
212. Chen, L.X. and Choo, J.B., *Recent advances in surface-enhanced Raman scattering detection technology for microfluidic chips.* Electrophoresis, 2008. **29**(9): p. 1815-1828.
213. Ackermann, K.R., Henkel, T., and Popp, J., *Quantitative online detection of low-concentrated drugs via a SERS microfluidic system.* Chemphyschem, 2007. **8**(18): p. 2665-2670.
214. McDonald, J.C., *et al.*, *Fabrication of microfluidic systems in poly(dimethylsiloxane).* Electrophoresis, 2000. **21**(1): p. 27-40.
215. Zehr, J.P., *Nitrogen fixation by marine cyanobacteria.* Trends in Microbiology, 2011. **19**(4): p. 162-173.
216. Jetten, M.S.M., *The microbial nitrogen cycle.* Environmental Microbiology, 2008. **10**(11): p. 2903-2909.
217. Chen, Y., *Comparative genomics of methylated amine utilization by marine Roseobacter clade bacteria and development of functional gene markers (tmm, gmaS).* Environmental Microbiology, 2012.
218. Chen, Y., *et al.*, *Bacterial flavin-containing monooxygenase is trimethylamine monooxygenase.* Proceedings of the National Academy of Sciences of the United States of America, 2011. **108**(43): p. 17791-17796.
219. Friedrich, M.W., *Stable-isotope probing of DNA: insights into the function of uncultivated microorganisms from isotopically labeled metagenomes.* Current Opinion in Biotechnology, 2006. **17**(1): p. 59-66.
220. Musat, N., *et al.*, *Detecting metabolic activities in single cells, with emphasis on nanoSIMS.* Fems Microbiology Reviews, 2012. **36**(2): p. 486-511.
221. van Manen, H.J., Lenferink, A., and Otto, C., *Noninvasive Imaging of Protein Metabolic Labeling in Single Human Cells Using Stable Isotopes and Raman Microscopy.* Analytical Chemistry, 2008. **80**(24): p. 9576-9582.
222. Manly, B.F.J., *Multivariate Statistical Methods: A Primer*. 1994, London: Chapman and Hall.
223. Krzanowski, W.J., *Principles of multivariate analysis : a user's perspective*. Oxford statistical science series. 1988, New York, USA: Oxford University Press. xxi, 563 p.
224. Martens, H. and Naes, T., *Multivariate calibration*. 1989, Chichester: John Wiley & Sons.

225. Adams, M.J., *Chemometrics in analytical spectroscopy*. RSC analytical spectroscopy monographs. 1995, Cambridge, UK: Royal Society of Chemistry. viii, 216 p.